REGULATION OF NEURONAL L-TYPE Ca^{2+} CHANNEL SIGNALING TO THE NUCLEUS THROUGH AUTISM-LINKED PROTEINS SHANK3 AND CAMKII

By

Tyler Perfitt

Dissertation

Submitted to the Faculty of the

Graduate School of Vanderbilt University

in partial fulfillment of the requirements

for the degree of

DOCTOR OF PHILOSOPHY

in

Molecular Physiology & Biophysics

May 8, 2020

Nashville, Tennessee

Approved:

David Jacobson, Ph.D.

Brad Grueter, Ph.D.

Teru Nakagawa, M.D. Ph.D.

Brian Wadzinski, Ph.D.

To Murphy and Meera,

my cuddly companions

who now have two theses

in their honor.

ACKNOWLEDGEMENTS

This work, and all the years behind it, would not be possible without the scientific and personal support of the other members of the Colbran Lab. In addition, I would like to thank the members of the Department of Molecular Physiology and Biophysics for making me a well-rounded scientist and colleague.

I would like to thank my advisor and mentor, Dr. Roger Colbran, for his guidance over the years. He has been incredibly patient and understanding during my graduate school career. When experiments weren't working or life kept knocking me down, Roger was always available for support and guidance.

I would like to thank my thesis committee for all their time and input into the successful completion of this project. Specifically, I would like to thank Dr. David Jacobson for his guidance and mentorship as I progressed through the trials of grad school, as well as Dr. Teru Nakagawa for his technical expertise with culturing neurons.

Thank you to all the friends I have made along the way at Vanderbilt and in Nashville, for giving me outlets, like going to the movies and playing rugby, that have kept me sane since 2013. And thank you to my family for their love and support through this unfamiliar process and for always enjoying their visits to Nashville.

Lastly, the following dissertation would not be possible without our funding sources:
National Institute of Mental Health, R01-MH063232 (RJC)
National Institute of Neurological Disorders and Stroke, R01-NS078291 (RJC)
National Institute of Diabetes and Digestive and Kidney Disease, T32-DK07563 (TLP)
American Heart Association, 18PRE33960034 (TLP)

TABLE OF CONTENTS

Page

LIST OF FIGURES

Figure **Page**

LIST OF TABLES

Table **Page**

CHAPTER I

INTRODUCTION

1.1 Introduction Overview

The processes underlying learning and memory, and their dysfunction in neurological disorders, are a major focus of neuroscience research. On a molecular level, the experience of learning occurs as sustained changes in the synaptic connections between neurons. This phenomenon, termed synaptic plasticity, rapidly alters the size and protein composition of the synapse and the electrophysiological properties of the various receptors and channels expressed on the synaptic membrane. In addition, longer-term activity-dependent changes in gene transcription, protein translation and protein degradation are important in consolidating these rapid effects as sustained increases or decreases in synaptic strength that can last a lifetime.

The body of work presented in this dissertation focuses on multiple aspects of these signaling processes and how they are regulated. This introduction will briefly describe the structure and function of the synapse and its plasticity. I will then introduce three major players: Ca^{2+}/calmodulin-dependent protein kinase II (CaMKII), SH3 and ankyrin-rich repeat domains protein 3 (Shank3), and L-type Ca^{2+} channels. Finally, I will highlight work that has been previously published relating these proteins to activity-dependent signaling to the nucleus, and how these are known to be disrupted in various neurological and neurodevelopmental disorders.

1.2 The Synapse

1.2.1 Synaptic Transmission

The human brain contains billions of individual neurons, the majority of which do not make direct cell-cell contact. In order to communicate with each other, neurons use specialized points of contact known as synapses. Neuronal axons form multiple presynaptic terminals containing hundreds of synaptic vesicles filled with cell-specific neurotransmitter molecules. Upon firing of a presynaptic action potential, membrane depolarization and biochemical changes allow for these vesicles to fuse with the plasma membrane, a process known as exocytosis. This releases the neurotransmitter cargo outward into the synaptic cleft, where it binds to the extracellular domains of postsynaptic receptors (Kandel et al., 2013).

At excitatory synapses, the synaptic vesicles contain glutamate, and the synaptic terminals are typically closely opposed to dendritic spines; these spines are small protrusions from dendrites, the large network of branches that extend from the cell soma. Several glutamate receptors are localized to these dendritic spines, precisely positioned to respond very efficiently to any release of glutamate. Glutamate binding to ionotropic glutamate receptors, such as α-amino-3-hydroxy-5-methyl-4-isoxazolepropionic acid (AMPA) and N-methyl-D-aspartic acid (NMDA) receptors, allows for receptors to influx Na^+ and Ca^{2+} into the cell (for review, see (Nakanishi et al., 1998; Traynelis et al., 2010; Zhu and Gouaux, 2016)). As these ions enter the cell, the cell depolarizes and voltage-dependent Na^+ and Ca^{2+} channels are opened (Catterall, 2000a). Together, this influx

generates an action potential in the postsynaptic neuron, thereby transmitting an electrical signal to the soma and the axon, communicating the signal from one neuron to another. In addition, glutamate can bind to metabotropic glutamate (mGlu) receptors. Members of the metabotropic glutamate receptor family do not directly pass ions through the plasma membrane. Instead, they act indirectly by generating a second messenger signaling cascade inside cells to biochemically effect ion channels or intracellular stores of Ca^{2+} ions (Niswender and Conn, 2010).

Synaptic transmission is critical for all aspects of neuronal function in the central nervous system. Specialized pre- and post-synaptic proteins regulate synaptic structure and function, and mutation of these proteins is associated with various neurological disorders. This dissertation will focus on postsynaptic signaling molecules localized to excitatory glutamatergic synapses, their binding interactions, and the molecular mechanisms required to initiate a downstream signal to the nucleus, which can be up to hundreds of microns away (Terenzio et al., 2017).

1.2.2 The Postsynaptic Density

The postsynaptic density (PSD) is attached to the postsynaptic membrane of the synaptic cleft. The PSD is a three-dimensional, electron-dense complex of both transmembrane and intracellular proteins that allows the neuron to biochemically respond to synaptic signals (Figure 1.1A) (Sheng and Hoogenraad, 2007). This tightly bound structure includes the AMPA and NMDA receptors that allow for initial Na^{+} and Ca^{2+} influx upon glutamate binding, while mGlu receptors are localized to the PSD periphery. Beneath the

core of the PSD lies the pallidum layer, which contains PSD-associated proteins that are incorporated in an activity-dependent manner (Dosemeci et al., 2016). The major categories of PSD proteins include scaffolding proteins, cell adhesion molecules, and regulators of the actin cytoskeleton (Figure 1.1B).

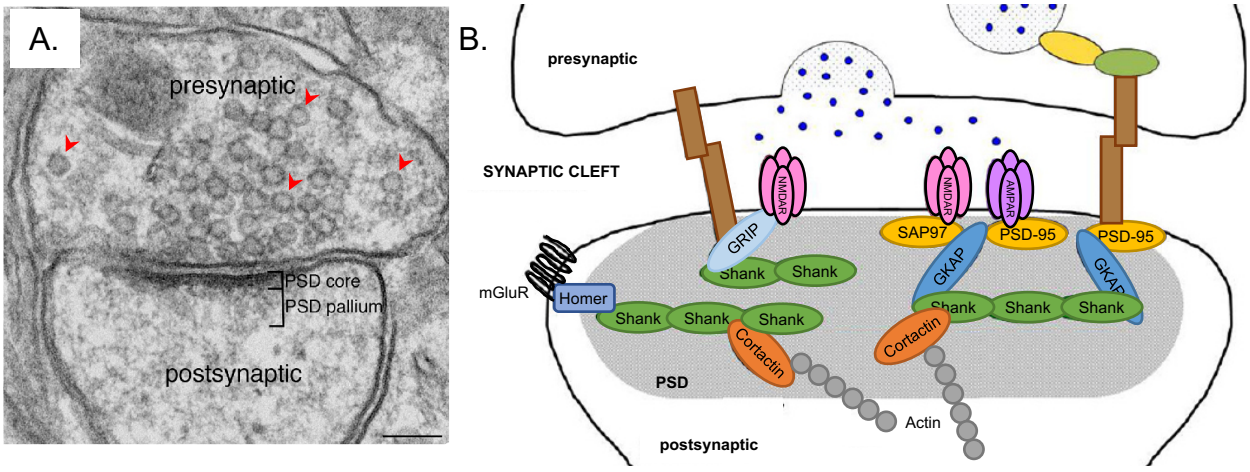

Figure 1.1: Overview of the synapse and postsynaptic density.

A. Electron micrograph image of an excitatory synapse. The presynaptic terminal is filled with vesicles ready to be released across the synaptic cleft (example vesicles are marked with red arrowheads). The postsynaptic density core and pallium are electron-dense structures beneath the postsynaptic membrane. Scale bar, 0.1 µm. Adapted from (Dosemeci et al., 2016). **B.** Diagram of postsynaptic scaffolding proteins and their interactions. Ionotropic glutamate receptors are shown in pink and purple; metabotropic glutamate receptors in black; scaffolding proteins in yellow, blue, and green; actin-binding proteins in orange; F-actin filaments in grey; and cell adhesion molecules in brown. Adapted from (Vyas and Montgomery, 2016).

Scaffolding proteins play a major role in the formation and stabilization of PSDs. These proteins contain multiple protein binding domains to bring together multi-protein complexes. Scaffolding proteins can also regulate the various functions of its binding partners. Broadly, PSD scaffolding proteins keep receptors and signaling molecules from diffusing away from the synaptic cleft. One of the most-well-characterized neuronal

scaffolding proteins is PSD-95 (postsynaptic density protein, 95 kDa) (Cho et al., 1992). Its specific localization to PSDs makes it a useful postsynaptic marker in immunohistochemistry and biochemical studies (for example, see (Gustin et al., 2011; Verpelli et al., 2011)). PSD-95 contains 3 distinct PDZ (PSD-95/DLG tumor suppressor protein/ZO-1) domain repeats, which can bind to the very C-terminal tail of NMDA receptors to directly localize these receptors in the PSD (Kornau et al., 1995). Therefore, NMDA receptor signaling is not only regulated by changes in the receptor itself, but can also be modulated by changes to PSD-95 and its binding partners. Other scaffolding proteins found in the PSD, such as Shanks, GKAP, and Homer, are described in Section 1.3.

Cell adhesion molecules (CAMs) ensure that PSDs are formed opposite excitatory presynaptic terminals and retain this opposition throughout the lifespan of a synapse. They play a critical role in axonal migration, neural pathfinding, and ultimately the establishment of a synapse (Sudhof, 2017). Multiple families of pre- and post-synaptic CAMs form trans-synaptic interactions. Conversely, CAMs are also involved in the elimination of unnecessary connections during synapse pruning. CAMs also contain intracellular domains that are known to bind to scaffolding proteins, such as PSD-95 binding to the CAM neuroligin. These intracellular domains may also function in signal transduction, though this has not been fully characterized (Sudhof, 2018).

The actin cytoskeleton is the primary structural element of both the PSD and the larger dendritic spines. As such, it dictates the overall morphology of the spine, which is a key

feature in dendritic spine function and is often dysregulated in neurological disorders (Yan et al., 2016). Actin accumulates in dendritic spines at higher levels than in dendrites, especially at the PSD (Matus, 2000). Microtubules are the primary cytoskeletal filament in dendrites, and only influence spine morphology under specific conditions (Shirao and Gonzalez-Billault, 2013). Therefore, actin dynamics primarily regulate the overall morphology and function of a dendritic spine and PSD by providing the underlying molecular framework.

To interact with the PSD, actin filaments form complexes with actin-binding proteins. These proteins function to dynamically remodel the cytoskeleton in response to changes in intracellular signaling. For example, the protein complex Arp2/3 induces nucleation and branching of actin filaments and alterations in spine size in an activity-dependent manner (Pollard, 2007). Arp2/3 is activated by the WAVE Complex, a multiprotein that is sensitive to members of the Rho family of GTPase signaling molecules (Soderling and Scott, 2006). ABI1, a vital subunit of the WAVE Complex, is described in Section 1.4.2.

1.2 Mechanisms of Synaptic Plasticity

The strength of synaptic transmission can be enhanced or reduced based on internal cellular activity. These activity-dependent changes in synaptic transmission are thought to underlie learning and memory consolidation. This activity can remodel one or both sides of the synapse, by altering the release of neurotransmitters from the presynaptic terminal, or by adjusting the response to neurotransmitters on the postsynaptic side. This dissertation will focus on postsynaptic mechanisms of plasticity, which can alter the protein composition of the PSD or the surrounding space, resulting in larger

morphological changes to the dendritic spine, as well as sustained changes in the activities of various glutamate receptors. Deficits in synaptic plasticity in a specific brain region correlate with similar disruption of behaviors related to that region. These mechanisms have been studied extensively *in vitro* and *in vivo*, establishing a strong connection between these cellular changes and the larger phenomena of learning and memory (Citri and Malenka, 2007). Typical experiments use electrophysiological recordings in order to capture postsynaptic responses to controlled electrical stimulations (Figure 1.2A).

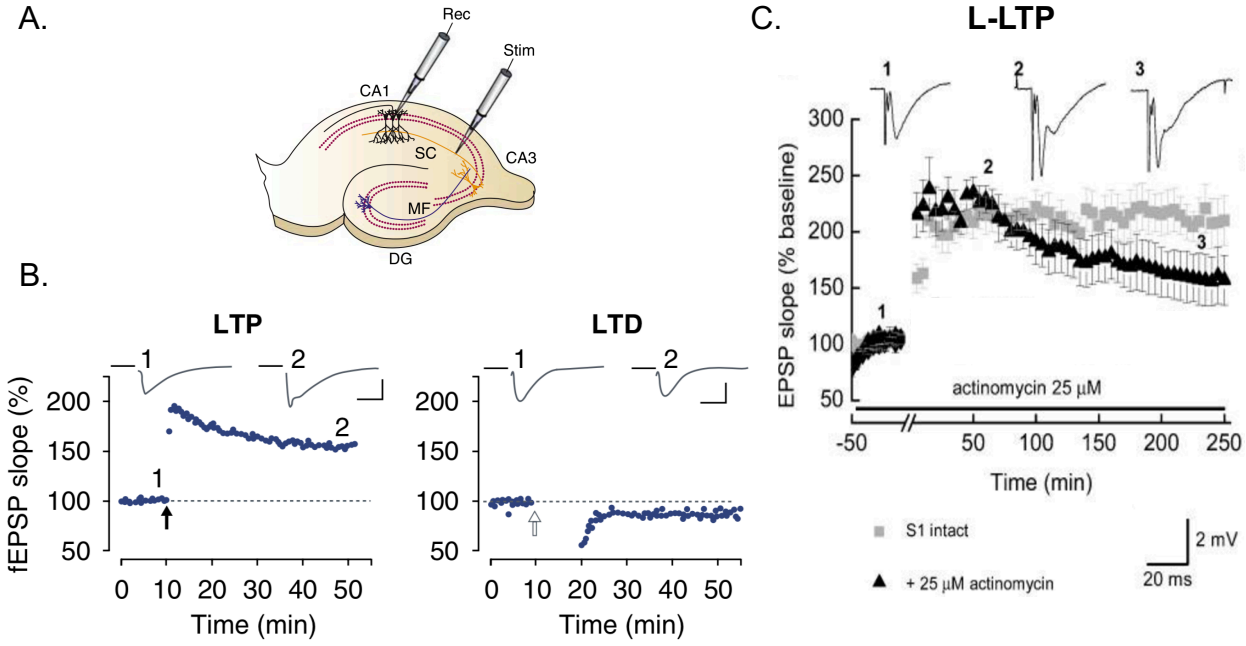

Figure 1.2: Experimental design of hippocampal LTP, LTD, and L-LTP *in vitro*.

A. Drawing of a hippocampal brain slice typically used for electrophysiological experiments. Rec: recording electrode; Stim: stimulating electrode; SC: Schaffer collaterals; MF: Mossy fibers; DG: dentate gyrus. **B.** Example electrophysiological recordings from hippocampal CA1 neurons. *Left*, LTP is induced by high-frequency tetanic stimulation (100 Hz stimulation for 1 s; black arrow). *Right*, LTD is induced by low-frequency stimulation (5 Hz stimulation for 3 min given twice with a 3 min interval; open arrow) A and B, Adapted with permission from Springer Nature (Citri and

Malenka, 2007). C. Measuring L-LTP in hippocampal neurons. Slices were incubated in the absence or presence of mRNA inhibitor actinomycin D before and during stimulation. Note the change in time scale on the X axis between panels B and C. Adapted from (Vickers et al., 2005).

1.2.1 Early Long-Term Potentiation

Since the discovery almost 50 years ago that repetitive stimulation of excitatory hippocampal neurons alters their electrophysiological properties (Bliss and Gardner-Medwin, 1973; Bliss and Lomo, 1973), this enhancement of synaptic strength, termed Long-Term Potentiation (LTP), has been shown to occur in numerous brain regions in different forms (Malenka and Bear, 2004).

The most studied form of LTP occurs in the CA1 region of the hippocampus and is mediated by NMDA receptors and occurs concurrently with membrane depolarization (Figure 1.2B) (Lüscher and Malenka, 2012). Along with depolarization, intracellular Ca^{2+} influx is also required for proper LTP induction (Lynch, 1989). This form of hippocampal LTP is input-specific: potentiation of a single dendritic spine, and the resulting changes, are contained and do not immediately affect adjacent spines (Matsuzaki et al., 2004). This potentiation can be increased with repetitive stimulation, and occurs on a rapid timescale, and is able to be maintained for up to an hour. Along with electrophysiological changes, potentiated spines also undergo structural and biochemical changes. Spine enlargement occurs through actin remodeling pathways, while the protein composition of the PSD, including the total number of ionotropic glutamate receptors as well as CaMKII holoenzymes, is increased (for comprehensive reviews, see (Hell, 2014; Shonesy et al., 2014)). For instance, increased AMPA receptor expression at the plasma membrane is essential for LTP (Lu et al., 2010). Changes in receptor function and targeting result in

increased excitatory postsynaptic currents (EPSCs) that translate to an increase in the likelihood of an action potential firing (EPSP, excitatory postsynaptic potential, graphed in Figure 1.2B, C). The potentiation of NMDA receptor currents can also occur through Group I mGlu receptor activation. Under experimental conditions with a sub-threshold stimulus that does not result in LTP, the addition of a positive modulator of mGlu5 can generate LTP (Rosenbrock et al., 2010). Complementary studies have shown that mGlu5 knockout mice have impaired hippocampal LTP (Lu et al., 1997). In addition, there are NMDA receptor-independent forms of LTP that require voltage-gated Ca^{2+} channels (Morgan and Teyler, 1999). The function of these Ca^{2+} channels will be discussed in depth in Section 1.5.

1.2.2 Long-Term Depression

LTP is not the only outcome of repetitive synaptic stimulation. Synaptic plasticity is bidirectional, allowing for both the enhancement and diminishment of signaling. The diminishment of synaptic strength, termed Long-Term Depression (LTD), is an important component of synaptic physiology as it can counterbalance potentiated neurons to fine-tune synaptic strength (for review, see (Ito, 1989)). LTD can be produced by weaker or low-frequency stimulation of the presynaptic terminal over a prolonged period of time relative to hippocampal LTP (Lüscher and Malenka, 2012). Some forms of LTD also require NMDA receptors, highlighting some similarities in the mechanisms of LTP and LTD (Dudek and Bear, 1992). Similarly, one of the most well-studied forms of LTD at excitatory synapses requires group I mGlu receptors, which are also are involved in LTP (mGlu-LTD). This form of LTD requires novel protein synthesis in order for LTD to persist

(Snyder et al., 2001). In addition, both NMDA receptor-dependent and mGlu-dependent LTD require the internalization of AMPA receptors (Carroll et al., 1999; Oliet et al., 1997). This internalization of AMPA receptors results in decreased surface expression, and thus less current can be generated in the postsynaptic neuron. However, the literature presents conflicting evidence on whether this form of LTD requires intracellular Ca^{2+} or not (Fitzjohn et al., 2001; Holbro et al., 2009).

1.2.3 Late Long-Term Potentiation

Long-term changes in synaptic plasticity are critical for normal brain development and learning. Therefore, neurons must have a mechanism to convert short-term, labile changes, such as transient Ca^{2+} influx and protein phosphorylation, into longer-lasting alterations. These mechanisms occur during the late phase of LTP, also known as L-LTP (versus E-LTP, early phase long-term potentiation). Though L-LTP follows E-LTP, it requires distinct mechanisms to properly potentiate neurons on a longer timescale (3-24 hr) (Baltaci et al., 2018). Initial studies heavily focused on E-LTP mechanisms due to the technical restraints of maintaining an electrophysiological for the time required to efficiently study L-LTP. Since then, we have made great strides in understanding the importance of L-LTP (Citri and Malenka, 2007) and have shown that this phenomenon can lasts for months and up to a year in animal models (Abraham et al., 2002).

L-LTP requires local protein translation within potentiated spines. A variety of mRNA species are present within dendritic spines, including mRNA encoding AMPA receptor subunits, CaMKIIα, and other key postsynaptic proteins (Grooms et al., 2006; Mayford et

al., 1996). This pre-existing mRNA is translated in an activity-dependent manner in order to increase the amount of key synaptic proteins directly in spines. However, *de novo* gene transcription to express additional mRNAs is another mechanism critical for L-LTP (Pittenger and Kandel, 2003). The encoding of many longer-lasting forms of synaptic plasticity may require remodeling of epigenetic factors in the nucleus (Kandel et al., 2013). Epigenetic factors are covalent alterations in chromatin structure that do not change the underlying DNA sequence, but rather alter how it is expressed. Epigenetic alterations, such as histone acetylation and DNA methylation, occur in brain region-specific forms of LTP and memory.

Importantly, inhibition of RNA synthesis and *de novo* gene transcription during critical periods of LTP induction results in an eventual loss of L-LTP, even if E-LTP is achieved (Figure 1.6C) (Nguyen et al., 1994; Vickers et al., 2005). This *de novo* gene transcription and mRNA translation increases the expression of synaptic proteins, transcription factors, and growth signaling molecules that promote synaptic strength and neuronal survival (Flavell and Greenberg, 2008). The following chapters will focus on one pathway that alters gene expression in an activity-dependent manner: L-type Ca^{2+} channels and their signaling to the nucleus.

1.3 Overview of Ca^{2+}/Calmodulin-dependent Protein Kinase II (CaMKII)

In addition to the various components of the PSD described in Section 1.2.2, the PSD also contains a variety of signaling proteins, such as those involved in transducing glutamate receptor activation into second messenger cascades, post-translational

modifications, and lipid signaling. These molecules are vital for turning transient Ca^{2+} increases into downstream biochemical changes. Here, I discuss one of the major signaling molecules present in dendritic spines and PSDs, CaMKII.

1.3.1 CaMKII Structure and Function

The influx of Ca^{2+} into neurons upon stimulation allows for Ca^{2+} ions to interact with calmodulin (CaM), a ubiquitous Ca^{2+} sensor protein. Although Ca^{2+} on its own can activate some signaling molecules (Villalobo et al., 2019), Ca^{2+} binding to CaM, a 17 kDa protein, alters the conformation of CaM to expose hydrophobic residues and promote binding to over 100 other proteins in a Ca^{2+}-dependent manner (Shen et al., 2005). The Ca^{2+}/CaM complex can then trigger downstream signaling processes through direct protein interactions (Hoeflich and Ikura, 2002). One major effector of Ca^{2+}/CaM is the aptly named Ca^{2+}/CaM-dependent protein kinase II (CaMKII) (Kennedy and Greengard, 1981). CaMKII, a member of the CaM kinase family (CaMKs), phosphorylates serine or threonine residues on target substrates to propagate downstream signals (Swulius and Waxham, 2008). In the forebrain, CaMKII can comprise as much as 1% of total protein (Erondu and Kennedy, 1985). CaMKII activity is tightly regulated by Ca^{2+}/CaM binding, though CaMKII is capable of becoming Ca^{2+}/CaM-independent through further modifications (see below).

Each individual molecule of CaMKII consists of three distinct structural domains: an N-terminal catalytic domain, a central regulatory domain that can be further divided into autoinhibitory and CaM-binding regions, and a C-terminal association domain (Figure

1.3A). At basal concentrations of Ca^{2+} in the cell, interaction between the autoinhibitory domain and the catalytic domain of each subunit inhibits substrate binding (Figure 1.3B). Interactions between the association domains of multiple CaMKII subunits mediate the formation of large holoenzymes, typically containing twelve subunits, arranged in two stacked hexameric rings. Single hexameric rings are depicted in Figure 1.3C and D, while the full dodecameric holoenzyme is depicted in Figure 1.3E.

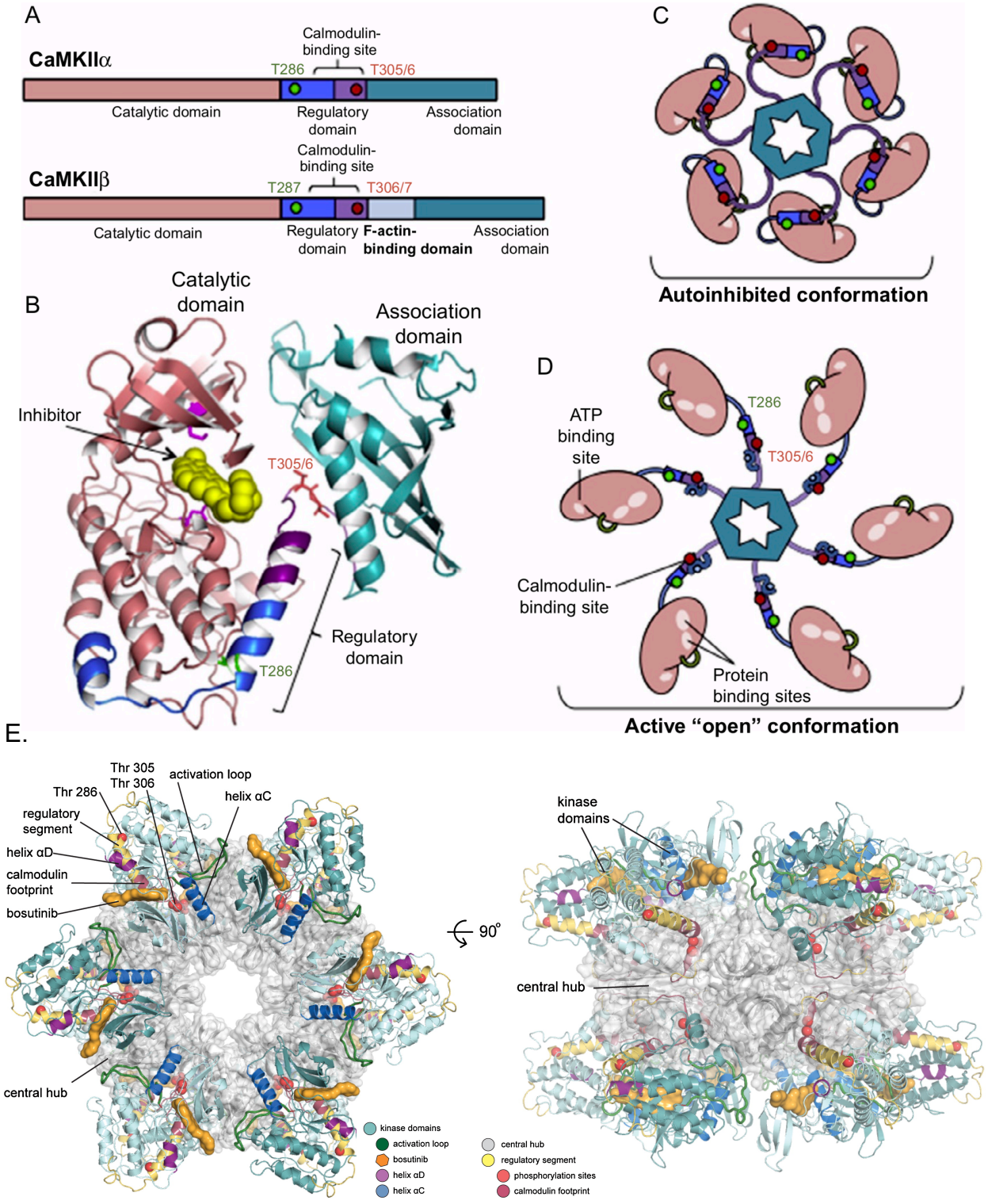

Figure 1.3: Structure and organization of CaMKII.

A. Diagram of CaMKIIα and CaMKIIβ domains, with an N-terminal catalytic domain (pink), regulatory domain (blue/purple), CaMKIIβ-specific F-actin binding domain (grey), and C-terminal

association domain (teal). Important phosphorylation sites and CaM-binding site are also highlighted. **B.** Structure of a single CaMKII subunit in autoinhibited conformation. This individual subunit structure was "excised" from a structure (PDB:3SOA) of an intact inactive CaMKIIα holoenzyme structure using PyMol (DeLano Scientific). Domains and key residues in CaMKII were colored as in A. The yellow structure in the center is a CaMKII inhibitor bound in the kinase active site in this structure. **C.** Cartoon of the compact inactive CaMKII holoenzyme structure. The kinase catalytic domains (pink) decorate the outside of a hexameric central hub formed by the association domains (teal), linked by the regulatory domains. Autoinhibitory interactions of the regulatory and catalytic domains hold the kinase domains in a compact closed con- formation. For clarity, the illustration includes a single ring, whereas the intact dodecameric holoenzyme consists of a stacked pair of rings. **D.** Cartoon illustrating conformational changes associated with CaMKII activation. Binding of Ca^{2+}/CaM disrupts interactions of the regulatory (blue) and catalytic (pink) domains (see B); the kinase domains swing away from the hub of the holoenzyme in an open conformation such that the active site is accessible to ATP and protein substrates. **E.** Crystal structure of the human CaMKII holoenzyme in an autoinhibited state at 4.0 Å. Kinase and regulatory domains are colored, while the association domain is greyed out. *A-D*, adapted from (Shonesy et al., 2014) with permission from Elsevier. *E*, adapted from (Chao et al., 2011) with permission from Elsevier.

The CaMKII family consists of isoforms transcribed by four distinct genes; CaMKIIα, CaMKIIβ, CaMKIIγ, and CaMKIIδ. Ubiquitously expressed throughout the body, these protein kinases play important roles in the brain, heart, and pancreas (Hell, 2014; Norling et al., 1994; Wu and Anderson, 2014). The catalytic and regulatory domains are highly conserved between the four isoforms but the association domains are more variable (Hudmon and Schulman, 2002). Moreover, alternative mRNA splicing introduces a linker domain of variable length that can confer unique features, such as the packing of subunits in the holoenzyme or subcellular targeting. For example, among the >25 total spice variants that have been identified to date, some CaMKIIβ variants of the linker domain encode an F-actin-binding domain, whereas some CaMKIIα/γ/δ splice inserts contain a

nuclear localization signal (Cook et al., 2018). In the mammalian forebrain, CaMKIIα is the most abundantly expressed, followed by CaMKIIβ (Gaertner et al., 2004) (Figure 1.3A). The function of neuronal CaMKIIγ as a shuttle to the nucleus has become more prominent in recent literature (Cohen et al., 2018; Malik et al., 2014). While CaMKIIδ is expressed in the cerebellum, it is primarily studied for its role in cardiac physiology (Grueter et al., 2007).

1.3.2 CaMKII Autophosphorylation and Activation in Neurons

CaMKII possesses a unique activation process that involves conformational changes as a response to changes in Ca^{2+} concentration. As mentioned above, the autoinhibitory domain prevents substrate binding and phosphorylation by the catalytic domain at basal levels of intracellular Ca^{2+} (Chao et al., 2011) (Figure 1.3C). Ca^{2+}-bound CaM releases this inhibition by binding to the nearby CaM-binding domain, releasing the catalytic domain to pivot outward from the hub of the CaMKII holoenzyme. In this 'open' conformation, ATP, CaMKII substrates, and binding partners can all interact with the catalytic domain (Figure 1.3D). When two adjacent subunits bind Ca^{2+}/CaM and are in the 'open' activated conformation, the catalytic domain of one subunit can autophosphorylate Thr286 in the regulatory domain of the adjacent activated subunit. Since Thr286 autophosphorylation prevents the regulatory domain from re-binding to the catalytic domain once Ca^{2+}/CaM has dissociated, this mechanism generates a Ca^{2+}/CaM-independent form of CaMKII that prolongs physiological responses to transient increases of Ca^{2+} (Miller and Kennedy, 1986), leading to its nickname as a "memory molecule" (Lisman, 1985), for review, see (Lisman et al., 2002). However, because this mechanism requires coincident binding of Ca^{2+}/CaM to neighboring subunits, the holoenzyme

structure is essential in allowing CaMKII to generate different biochemical outputs based on the frequency, duration and amplitude of intracellular Ca^{2+} transients (De Koninck and Schulman, 1998).

CaMKII regulation by autophosphorylation at Thr286 is critical for normal kinase activity as well as large-scale neurological functions. Mice with a knock-in mutation of Thr286 to a phospho-null Ala display reduced targeting of CaMKII to PSD (Gustin et al., 2011). Furthermore, these mice show synaptic impairments in the hippocampal LTP as well as cognitive impairments with novel object recognition and learning and memory tasks (Giese et al., 1998). Interestingly, these knock-in mice are still able to form memory after 'intense' behavioral training, suggesting separate roles for CaMKII in the processes of contextual learning and memory (Irvine et al., 2011). Therefore, CaMKII autophosphorylation may be differentially regulated between learning states, adding another layer of complexity to how CaMKII transduces Ca^{2+} signals.

Autophosphorylation not only plays a role in CaMKII activation, but also inhibits activity. CaMKII is autophosphorylated at multiple residues *in vitro* and *in vivo* in addition to Thr286 (Baucum et al., 2015), including Thr305 and Thr306 which functionally reduce CaMKII activity (Colbran and Soderling, 1990). Thr305 and Thr306 are within the CaM-binding domain, and their autophosphorylation prevents Ca^{2+}/CaM binding (Colbran, 1993). Prior autophosphorylation at Thr286 greatly enhances Thr305/306 autophosphorylation, producing a constitutively active form of CaMKII that is unable to bind Ca^{2+}/CaM. In this state, CaMKII must be dephosphorylated at Thr286 to be inactivated (Hashimoto et al.,

1987). Thus, the autophosphorylation of CaMKII at multiple sites allows for complex CaMKII regulation by dynamic changes in intracellular Ca^{2+} concentrations, in addition to the opposing protein phosphatases.

1.3.3 Dual Roles of CaMKII in LTP and LTD

Due to its important function in the transduction of Ca^{2+} signals, CaMKII has been well-studied in the context of multiple forms of synaptic plasticity. CaMKII plays an important role in hippocampal LTP induction. Genetic mutations that disrupt CaMKII activation or kinase activity disrupt hippocampal LTP (ex: (Giese et al., 1998; Mayford et al., 1995; Silva et al., 1992), for review, see (Elgersma et al., 2004)). Moreover, expression of constitutively active CaMKII in postsynaptic neurons increases synaptic strength (Lledo et al., 1995; Pettit et al., 1994). Interestingly, recent experiments with better temporal resolution indicate that CaMKII kinase activity is important for the induction of LTP, but not maintenance (Murakoshi et al., 2017).

CaMKII is also an important signaling molecule in hippocampal LTD as well. Hippocampal LTD that occurs through NMDA receptors or through activation of Group I mGlu receptors require CaMKII activation, and that acute inhibition of CaMKII disrupts LTD (Marsden et al., 2010; Mockett et al., 2011). CaMKII inhibition also prevented mGlu-mediated protein synthesis after a LTD-inducing stimulus (Mockett et al., 2011). The role of CaMKII in LTD, at least in the cerebellum, is isoform-specific. CaMKIIβ knockout mice, when given a stimulation to invoke LTP at Purkinje cell synapses, instead display LTD, while LTD protocols produce LTP (van Woerden et al., 2009).

As mentioned in Section 1.2.2, many proteins in the PSD function in synaptic plasticity under conditions that favor both LTP and LTD. The unique properties of CaMKII activation and autophosphorylation allow for tight regulation of activity within neurons upon stimulation. As CaMKII is sensitive to the frequency and amplitude of Ca^{2+} influx during stimulation (De Koninck and Schulman, 1998; Hanson et al., 1994) (see Section 1.3.2), it may decode these stimulations for targeting and signaling to different receptors. Therefore, it is hypothesized that autophosphorylated CaMKII responds to different kinds of Ca^{2+} influx and synaptic activity in order to properly promote LTP or LTD.

1.3.4 CaMKII Phosphorylation of Other Substrates

Once the catalytic domain of CaMKII has been exposed, ATP and substrate binding allow for CaMKII to phosphorylate a number of different proteins besides other CaMKII molecules. The general consensus sequence for CaMKII phosphorylation is R-X-X-S/T, where R is arginine, X is any amino acid, and S/T is the serine/threonine being phosphorylated. However, CaMKII can phosphorylate sites that do not follow this sequence (White et al., 1998). CaMKII phosphorylation sites have been identified on multiple postsynaptic proteins, altering their function and localization. I will briefly discuss two well-studied CaMKII phosphorylation sites: Ser831 of the AMPA receptor subunit GluA1 and Ser1303 of the NMDA receptor subunit GluN2B.

Phosphorylation of the intracellular regions of AMPA receptor subunit GluA1, especially in its C-tail, regulate multiple channel properties (Carvalho et al., 2000). CaMKII

phosphorylates Ser831 (Barria et al., 1998; Barria et al., 1997; Roche et al., 1996), increasing the channel conductance in an activity-dependent manner (Benke et al., 1998). Phosphorylation also promotes opening of receptors to regulate channel gating (Kristensen et al., 2011). Recent evidence suggests that the C-tail of AMPA receptors, and subsequent regulation by phosphorylation, may not be as physiologically important as initial studies claimed (Herring and Nicoll, 2016). Neurons lacking the entire C-tail of GluA1 undergo LTP the same as unaltered neurons (Granger et al., 2012). Indeed, the relative amount of phosphorylated GluA1 is almost negligible in the adult mouse hippocampus (Hosokawa et al., 2014). However, the specific context and form of LTP induced, as well as slight variations in experimental design, may dictate the overall importance of this phosphorylation site (Huganir and Nicoll, 2013). As a result, the idea that the C-terminal domain of GluA1 AMPA receptors is not involved in synaptic plasticity is still controversial.

Another CaMKII phosphorylation site on GluA1 is Ser567 (Lu et al., 2010). Unlike Ser831, which is located in the long intracellular C-tail of GluA1, Ser567 is located in a smaller intracellular loop. This region is phosphorylated by CaMKII but not PKA or PKC, the other major kinases that phosphorylate the GluA1 C-tail. This provides a CaMKII-specific regulation of GluA1 in this region. Phosphorylation of this residue increases after hippocampal LTD in acute brain slices, in contrast to GluA1 Ser831 phosphorylation (Coultrap et al., 2014). Regulation of GluA1 by phosphorylation at a site outside the GluA1 C-tail may explain why neurons may behave normally when the GluA1 C-tail is deleted (Granger et al., 2012).

CaMKII phosphorylation of the NMDA receptor subunit GluN2B occurs at Ser1303 within the intracellular C-tail (Omkumar et al., 1996). Phosphorylation of this residue reduces the desensitization of the channel under physiological conditions, again demonstrating how CaMKII can regulate channel properties (Tavalin and Colbran, 2016). CaMKII phosphorylation of GluN2B also regulates its binding interaction with the C-tail, as discussed in the following section.

1.3.5 CaMKII-Associated Proteins (CaMKAPs) and Binding Interactions

Our lab pioneered the concept that physiological functions of CaMKII are directed through interactions with CaMKII-Associated Proteins (CaMKAPs). We found that a number of cellular processes are regulated by CaMKII activity, binding interactions, and/or phosphorylation. The most well-studied CaMKAP is the GluN2B subunit of the NMDA receptor; Thr286-autophosphorylated CaMKII binds to residues 1290-1309 in GluN2B, which include the CaMKII phosphorylation site at Ser1303 (Omkumar et al., 1996; Strack and Colbran, 1998; Strack et al., 2000a). This binding region plays a large role in targeting CaMKII from extra-synaptic space to the PSD upon NMDA receptor activation and Ca^{2+} influx. For instance, activity-dependent translocation of CaMKII to the PSD is disrupted in mutant mice harboring two point mutations in the CaMKII-binding region of GluN2B that specifically prevent CaMKII binding (Halt et al., 2012a). Intriguingly, phosphorylation of Ser1303 may promote CaMKII dissociation from GluN2B (Raveendran et al., 2009; Strack et al., 2000a). However, formation of the CaMKII-NMDA complex also increases the affinity of CaMKII to ATP and ‘locks’ the kinase in an open conformation (Bayer et al.,

2001; Bayer et al., 2006). This interaction keeps CaMKII translocated to the PSD and promotes longer-lasting autonomous CaMKII activity, a function critical for synaptic remodeling and plasticity.

While GluN2B plays an important role in anchoring CaMKII to the PSD, the number of CaMKII holoenzymes in a dendritic spine greatly outnumbers GluN2B-containing NMDA receptors (Feng et al., 2011). Therefore, other CaMKAPs may target separate pools of CaMKII for distinct postsynaptic functions. CaMKII may play a structural role in the PSD, in part because it binds to many scaffolding proteins, such as GluN2B, α-actinin, densin, spinophilin, and SAP-97 (Hell, 2014; Jalan-Sakrikar et al., 2012; Jiao et al., 2011; Nikandrova et al., 2010; Robison et al., 2005b). Many of these interactions occur in a CaMKII activity-dependent manner; however, CaMKII can bind to some CaMKAPs under non-autophosphorylated conditions. For example, the interaction between the C-terminal domain of densin and the association domain of CaMKII does not require CaMKII autophosphorylation (Strack et al., 2000b). In comparison, the interaction between CaMKII and alpha-actinin is actually disrupted by CaMKII phosphorylation at Thr306 (Jalan-Sakrikar et al., 2012).

1.3.6 Shank3 as a novel CaMKAP

Our lab conducted an unbiased shotgun proteomics analysis of immunoprecipitated CaMKII complexes isolated from synaptic fractions of mouse forebrain in order to identify novel CaMKAPs. While several established CaMKAPs were detected, Shank3 was unexpectedly the third-most abundant protein detected using this method (Baucum et al.,

2015). The detection of Shank3 as a prominent component of synaptic CaMKII complexes had potentially exciting implications given the known roles of Shank3, as will be discussed below. Subsequent studies showed that Shank3 and CaMKII can be co-immunoprecipitated when co-expressed in HEK293T cells, a heterologous cell system that does not highly express the previously mentioned neuronal proteins (Stephenson et al., 2017). However, such co-immunoprecipitation data can arise from both direct or indirect interactions of the proteins involved, and several synaptic proteins known to interact directly with both Shank3 and CaMKII might facilitate an indirect association between Shank3 and CaMKII, such as $Ca_V1.3$ (Wang et al., 2017b; Zhang et al., 2005), densin (Quitsch et al., 2005; Strack et al., 2000b), NMDAR/PSD-95/GKAP complexes (Naisbitt et al., 1999; Strack and Colbran, 1998), and Homer/mGlu5 complexes (Marks et al., 2018; Tu et al., 1999). However, I tested the hypothesis that this association is mediated via a direct Shank3-CaMKII interaction, establishing Shank3 as a novel CaMKAP (see Chapter III).

1.4 Shank3, a Master Scaffold of the PSD

1.4.1 Shank3 Structure and Expression

Shank3 (SH3 and multiple ankyrin repeat domains 3) is one major scaffolding protein in the PSD of excitatory synapses (see Section 1.2.2). While Shank3 was initially discovered as a binding partner of the postsynaptic scaffold GKAP (Naisbitt et al., 1999), further analyses identified multiple conserved domains known to mediate protein-protein interactions: six ankyrin repeats, SH3 (SRC Homology 3) and PDZ domains, a large proline-rich region, and a C-terminal SAM (sterile α motif) domain (Figure 1.4A). Other

research groups simultaneously and independently cloned the same gene, giving rise to the use of several other names, including ProSAP2 and Spank, but only the name Shank3 is commonly used today (Boeckers et al., 1999; Sheng and Kim, 2000). Shank3 is heavily studied in the brain, though it is also present in the peripheral nervous system, cardiomyocytes, and perhaps the pancreas (Han et al., 2016; Lim et al., 1999; Redecker et al., 2007).

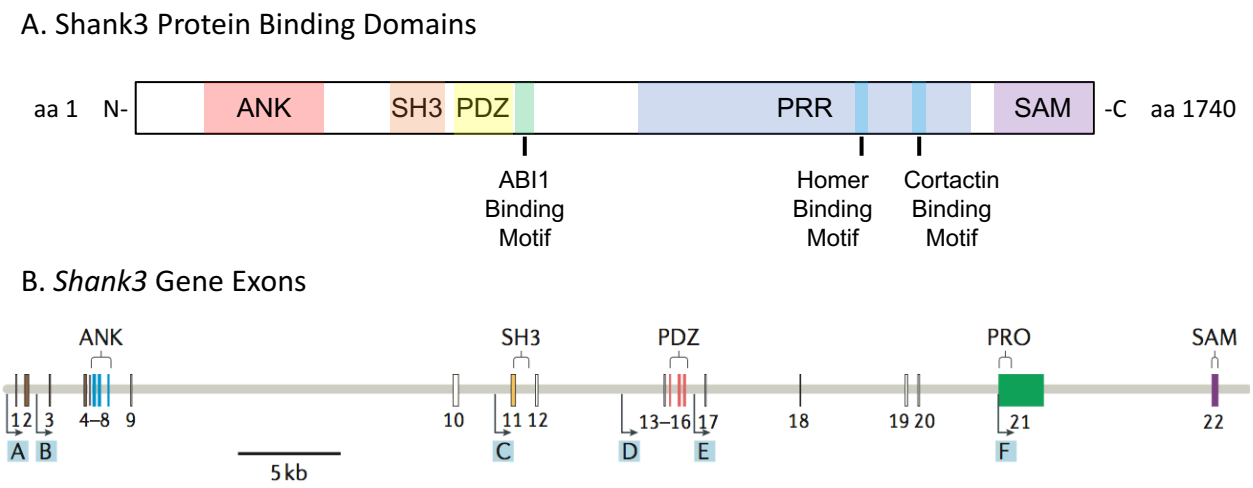

Figure 1.4: Shank3 protein and gene structure.

A. Schematic of canonical Shank3 protein from rat (UniProtKB: Q9JLU4 Isoform 2). Binding domains and amino acid sequence from left to right: ANK, Ankyrin repeat domains, aa 123-313; SH3, Src Homology 3 domain, aa 473-524; PDZ: PSD-95/Dlg tumor suppressor/ZO-1 binding domain, aa 572-663; ABI1 binding motif, aa 677-684; PRR, Proline-rich region, aa 1165-1446; Homer binging motif, aa 1307-1316; Cortactin binging domain motif, aa 1408-1417; SAM, Sterile alpha motif, aa 1647-1737. **B.** Schematic of mouse *Shank3* gene. Exons are numbered 1-22, promoters are labeled A-F. Adapted with permission from Springer Nature (Monteiro and Feng, 2017).

Several variants of Shank3 can be expressed (Waga et al., 2013). The *SHANK3* gene contains one 5' promoter and five separate intragenic promoters, and multiple stop

codons produced by alternative mRNA splicing (Figure 1.4B) (Wang et al., 2014) that together give rise to over 20 protein variants with a wide range of sizes. This splicing occurs in a brain region- and developmental-specific manner and is controlled by epigenetic mechanisms, such as DNA methylation (Beri et al., 2007). These splice variants contain different combinations or truncations of Shank3 and its binding domains. As a result, splice variants are targeted differently within neurons and form distinct macromolecular complexes. Longer splice variants, which contain the C-terminal regions and the SAM domain, are specifically targeted to PSDs, while shorter variants lacking these regions are more cytosolic (Boeckers et al., 2005). In addition, some Shank3 alternative splicing may be regulated by neuronal depolarization, providing an additional layer of complexity to the physiological function of Shank3 (Wang et al., 2014).

Shank3 is a member of the larger Shank3 family of proteins, along with Shank1 and Shank2. All three proteins share an overall similar domain structure and highly homologous sequences within the canonical binding domains. All members of the Shank family can oligomerize with themselves and each other via their SAM domain (Boeckers et al., 2002; Naisbitt et al., 1999). Despite these similarities, the three Shank3 proteins are not functionally redundant. The sequences outside these canonical domains have low similarity, between 35-40% (Lim et al., 1999). Shank1 is a brain-specific isoform, while Shank2 mRNA can be detected in multiple tissues and Shank3 is primarily detected in the heart and brain (Figure 1.5, *left*). In the brain, all three proteins are expressed to some extent in the hippocampus, cortex, and cerebellum (Figure 1.5, *right*). In addition, Shank3

is highly enriched at glutamatergic spines in the striatum, while Shank1 and Shank2 are not detected (Peca et al., 2011).

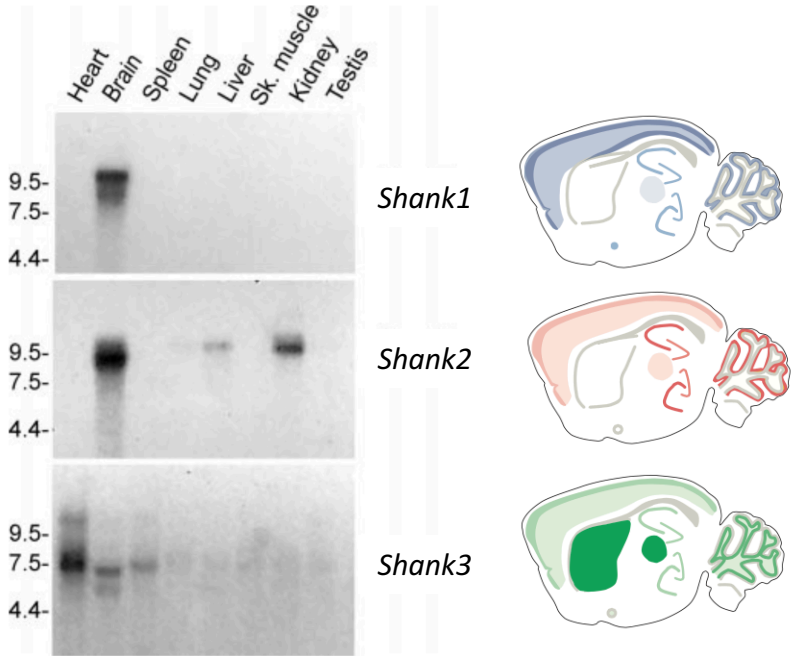

Figure 1.5: mRNA expression of Shank family members.

Left, Northern blot of Shank1, 2, and 3 mRNA from various rat tissues. Adapted from (Lim et al., 1999). *Right*, Diagrams of the mouse brain showing relative mRNA expression of each Shank family member. Darker color indicates stronger expression. Adapted with permission from Springer Nature (Monteiro and Feng, 2017).

1.4.2 Scaffolding Interactions

The primary function of Shank3 is to assemble multi-protein complexes. The modular protein-protein interaction domains described above allow Shank3 to bring together various receptors, channels, signaling molecules, and the actin cytoskeleton in close proximity to signal efficiently. Below, I will briefly describe some of the Shank3 binding partners not yet discussed in this dissertation and their roles in synaptic physiology.

Homer: A companion study to Naisbitt et al., 1999, published in the same issue of *Neuron*, characterized a homer-binding motif in the proline-rich region of Shank3 (Tu et al., 1999). Like Shanks, Homer proteins are scaffolding proteins in the PSD of glutamatergic excitatory synapses. The most studied isoform of Homer in the brain is Homer1, which produces three variants: Homer1a, 1b, and 1c (Shiraishi-Yamaguchi and Furuichi, 2007). An N-terminal EVH1 (Enabled/vasodilator-stimulated phosphoprotein Homology 1) domain in all three Homer variants can interact with Shank3, mGlu1, mGlu5, or the ER-associated IP_3 and ryanodine receptors. Both Homer1b and Homer1c are longer variants and contain C-terminal coiled-coil domains that allow the proteins to multimerize. Homer 1b/c multimers are able to bind multiple proteins simultaneously, bringing Shank3 in close proximity to all the receptors listed above. Homer1a, however, is a truncated version of the protein and does not possess this coiled-coil domain; therefore, it does not multimerize. Homer1a acts as a dominant negative to disrupt signaling complexes by competing with longer Homer variants (Clifton et al., 2019). Homer1b and 1c are constitutively expressed, while Homer1a expression is activity-dependent (Brakeman et al., 1997). As a result, activity-dependent expression of Homer1a uncouples Group I mGlu receptors from some of their binding partners and effectors, such as the NMDA and IP3 receptors and Shank3 (Hu et al., 2010; Kammermeier and Worley, 2007).

Cortactin: The cortactin binding motif on Shank proteins was originally discovered on Shank2, formerly known as CortBP1 (Cortactin-Binding Protein 1) (Du et al., 1998). This same binding motif was also identified in the original characterization of Shank3, and helped to establish CortBP1 as a member of the Shank family (Lim et al., 1999; Naisbitt

et al., 1999). Cortactin promotes actin nucleation through recruitment of Arp2/3 to F-actin filaments (Uruno et al., 2001). Shank3 targets and stabilizes cortactin in dendritic spines, as loss of all three Shank family proteins results in reduced actin and cortactin levels in dendritic spines and more diffuse cortactin expression (MacGillavry et al., 2015). While Shank3 does not directly bind actin, interacting proteins like cortactin place Shank3 at the interface between core, membrane-associated PSD proteins and the actin cytoskeleton of the larger dendritic spine.

GKAP/SAPAP-1: GKAP was identified as one of the first Shank3 binding partners, using a yeast 2-hybrid screen (Naisbitt et al., 1999). GKAP, also known as SAPAP-1, is a member of the SAPAP family of scaffolding proteins and is one of the most abundant scaffolding proteins in the PSD (Sheng and Hoogenraad, 2007; Takeuchi et al., 1997). All members of the SAPAP family bind to PSD-95 at their N-terminus and to Shank3 at their C-terminus (Lee et al., 2018). Therefore, GKAP couples PSD-95/NMDA receptor complexes to Shank3/Homer/mGlu5 receptor complexes. Genetic deletion of SAPAP-3, a striatal-specific member of the GKAP/SAPAP family, results in pronounced anxiety and compulsive behaviors, analogous to human patients with Obsessive Compulsive Disorder. Interestingly, CaMKII phosphorylation of GKAP at Ser54 disrupts the GKAP-PSD-95 interaction, and phosphorylated GKAP is then targeted for ubiquitination and degradation (Shin et al., 2012). Unlike other proteins that interact with the Shank3 PDZ domain, the GKAP-Shank3 interaction involves a non-canonical motif located N-terminal to the Shank3 PDZ domain (Zeng et al., 2016). Work in this dissertation provides evidence

that CaMKII can disrupt GKAP binding to Shank3 by phosphorylation Shank3 at Thr551 in this region, further detailed in Chapter VI.

ABI1: Discovery and characterization of the ABI binding motif in Shank3 occurred later than the other binding regions discussed above (Proepper et al., 2007). ABI1 is an indispensable member of the WAVE Complex, which activates Arp2/3 in a Ras GTPase-dependent manner (Chen et al., 2010). Interestingly, the ABI1 binding motif is conserved between Shank2 and Shank3, but is not present in Shank1 (Lim et al., 1999). Regulation of ABI1 binding to Shank3 via CaMKII and PKA phosphorylation will be discussed in Chapter V.

1.4.3 *SHANK3* as an Autism Spectrum Disorder (ASD) gene

Autism spectrum disorder (ASD) is generally defined by core abnormal behaviors that fall under two broad categories: social and communication deficits, and restrictive and repetitive behaviors, that can both vary in their presentation as well as severity (Bourgeron, 2009). ASD has a high co-morbidity with other neurological disorders, such as abnormal sensory sensitivity (sound, touch, pain), epilepsy and attention deficit hyperactivity disorder (ADHD) (Lukmanji et al., 2019; Zablotsky et al., 2017). ASD also has high co-morbidity with overactive immune systems and gastrointestinal dysfunction, suggesting that the developing immune system or the gut-brain axis are related to ASD etiology (Goyal and Miyan, 2014; Wasilewska and Klukowski, 2015). Just as the behaviors are heterogeneous, so too are the genetics of ASD. In genetic studies, genes

encoding synaptic proteins and proteins involved in neuronal development have become candidate genes for monogenic and syndromic forms of ASD (Carbonetto, 2014).

In humans, haploinsufficiency of the *SHANK3* gene is one of the most prevalent and penetrant causes of monogenic ASD. This is the result of a deletion of the distal end of the long arm of chromosome 22 (Figure 1.6A) (Harony-Nicolas et al., 2015). Known as 22q13.3 deletion syndrome or Phelan-McDermid Syndrome, patients exhibit neonatal hypotonia, facial dysplasia, and developmental delay (Phelan et al., 2001). Comorbidity between Phelan-McDermid Syndrome and ASD is common amongst patients (Soorya et al., 2013). The other genes of the Shank family, *SHANK1* and *SHANK2*, have also been associated as risk genes for ASD (Leblond et al., 2014). Altogether, *SHANK* genes account for a higher percentage of ASD cases compared to almost a thousand other ASD-associated genes (Moessner et al., 2007), highlighting the overall importance of the Shank family in neuronal function.

In addition to large-scale disruptions in the *SHANK3* gene, many missense mutations have been identified in the *SHANK3* gene of patients with neurological disorders (Figure 1.6B) (Arons et al., 2012; Durand et al., 2012; Gauthier et al., 2010). Characterization of these missense mutations has shown that many disrupt specific Shank3 binding interactions, while other functions may remain intact. For instance, a S685I missense mutation in Shank3 was identified in a human patient with ASD (De Rubeis et al., 2014). Ser685 is a PKA phosphorylation site that regulates Shank3 binding to ABI1, and the S685I mutation prevents phosphorylation and disrupts ABI1 binding. I will describe

studies showing that Ser685 can also be phosphorylated by CaMKII in Chapter V. Physiologically, this mutation causes deficits in dendritic morphology and synaptic transmission, a common phenotype in Shank3 mutant studies. A mouse model of the S685I mutation displays some ASD-associated behavior, but not the stereotypic self-grooming seen in most Shank3 mouse lines (Wang et al., 2019b). These studies highlight how mutations in specific regions of Shank3 can result in distinct phenotypes. As a result, different studies have targeted various signaling pathways to reverse or ameliorate ASD-associated phenotypes, including mGlu5, CLK2, PAK, and I_h channels (Bidinosti et al., 2016; Duffney et al., 2015; Vicidomini et al., 2016; Yi et al., 2016). However, these treatments may only benefit a subset of patients based on the specific underlying *SHANK3* gene mutation.

To study various mutations and deletions of the *SHANK3* gene found in humans, researchers have generated over a dozen different *Shank3* mouse models. These different models target the various exons to delete the larger, PSD-associated isoforms of Shank3, while others target the entire gene/protein (Monteiro and Feng, 2017). Other studies have generated mouse models from specific missense mutations identified in humans, such as the S685I mutant mentioned above. However, these different models display distinct phenotypes. While the majority of mutant mice have reduced dendritic spine density, abnormal social behavior and ultrasonic vocalizations, repetitive self-grooming, and disrupted targeting of other synaptic proteins, some mouse models display a subset of phenotypes, or variations, such as allo-grooming versus self-grooming (Jiang and Ehlers, 2013; Wang et al., 2019b).

The clinical heterogeneity in human patients with Shank3 mutations and the varying phenotypes displayed by Shank3 mutant mice could potentially be explained by the complexity of Shank3 alternative slicing (see above) (Jiang and Ehlers, 2013; Zhou et al., 2015). Compensatory increases in different Shank3 splice variants has been reported in some Shank3 mutant mice (Jin et al., 2019). Therefore, comparisons between the various Shank3 mutant mice must acknowledge the caveat that *similar* genetic disruptions may not result in *exact* disruption in Shank3 expression and/or function. Further analysis of Shank3 isoform expression and splicing in these mutant mouse lines, and their distinct synaptic and behavioral phenotypes, will be required to fully understand the physiological function of specific Shank3 isoforms.

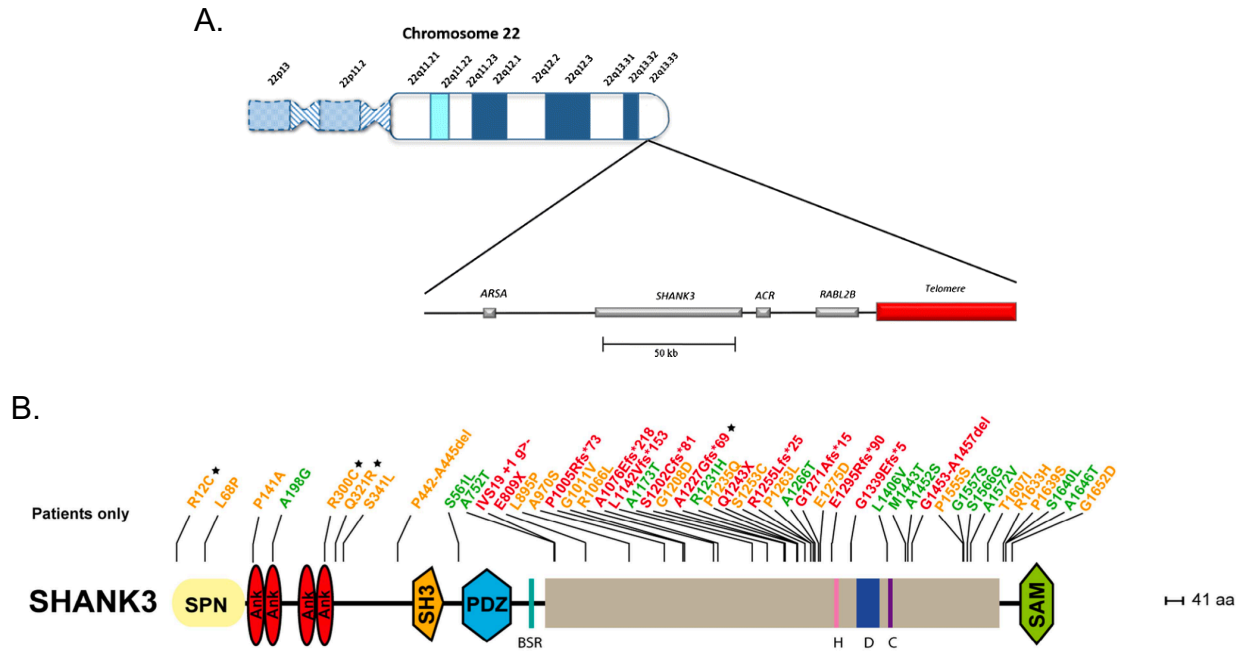

Figure 1.6: Shank3 disruptions in Phelan-McDermid Syndrome and ASD patients.

A. Depiction of human chromosome 22 short arm (p) and long arm (q). The long arm is enlarged to show the distal end, which is further expanded to highlight the genes typically truncated or lost

in Phelan-McDermid Syndrome. Adapted with permission from Springer Nature (Costales and Kolevzon, 2015). **B.** Diagram of Shank3 protein and identified missense mutation from ASD patients, as of 2014. Since then, many more mutations have been uncovered. Green mutation = predicted mild impact on protein function; Orange mutation = moderate; Red = severe. Black stars indicate mutants that have been tested *in vitro* at the time of publication. Adapted from (Leblond et al., 2014).

Both increases and decreases in gene dosage have been linked to various neuropsychiatric disorders (Toro et al., 2010). Intriguingly, there is growing evidence that duplication of the *SHANK3* gene, known as Shank3 Duplication Syndrome, produces a distinct neurodevelopmental disorder from ASD. Duplications in the SHANK3 gene have been identified in human patients with schizophrenia and ADHD (Durand et al., 2006; Failla et al., 2007). Transgenic mice expressing 1.2-fold to 2-fold higher levels of Shank3 protein relative to non-transgenic mice display unique manic-like behaviors, sensitization to amphetamine, and disrupted circadian rhythms (Han et al., 2013). Pharmacological treatment with valproate, but not lithium, reduced mania in Shank3 overexpressing mice. These behavioral phenotypes, along with a resistance to lithium, align more closely with models of bipolar disorder than ASD. (Gitlin, 2006). These data highlight the importance of dose-dependent changes in Shank3 function, as too little or too much Shank3 causes synaptic imbalance and abnormal phenotypes in mice.

1.5 L-Type Ca^{2+} Channel (LTCC) Signaling

1.5.1 Molecular Components of LTCCs

Ca^{2+} influx into cells occurs through numerous different ion channels. Voltage-gated Ca^{2+} channels are a large family of ion channels that are activated upon membrane depolarization. Under basal conditions, typical resting neuronal membrane potentials are

in the range of -90 to -70 mV (Kandel et al., 2013). T-type Ca^{2+} channels are activated by relatively modest membrane depolarizations (e.g., -55 to -20 mV), while L-, P/Q-, N-, and R-type Ca^{2+} channels require stronger depolarization in order to be activated (e.g., -40 to +20 mV) (Nowycky et al., 1985; Xu and Lipscombe, 2001). Therefore, T-type Ca^{2+} channels are referred to as low-voltage activated channels (LVA) while the remainder are referred to as high-voltage activated channels (HVA) (Catterall, 2011). N-, P/Q-, and R-type Ca^{2+} channels play a role in synaptic transmission at the presynaptic terminal, where Ca^{2+} influx initiates synaptic vesicle exocytosis and neurotransmitter release (Stanley, 1997). R-type Ca^{2+} channels are also expressed postsynaptically (Yasuda et al., 2003), but this dissertation will primarily focus on mechanisms of postsynaptic LTCC signaling.

Four members of the voltage-aged Ca^{2+} channel gene family encode LTCCs, numbered $Ca_V1.1$-4 (Ertel et al., 2000). $Ca_V1.1$ is exclusively expressed in skeletal muscle and $Ca_V1.4$ in the retina. $Ca_V1.2$ and $Ca_V1.3$ are expressed in many cell types that are regulated by electrical excitation, such as the brain, endocrine cells, cardiac cells, and auditory cells (Zamponi et al., 2015). The Ca_V1 $\alpha1$ subunits are a single protein composed of four repetitive domains, labeled I-IV. Large intracellular linkers between each domain allow for regulation by protein binding and phosphorylation. Each domain contains six transmembrane helices, with the fifth and sixth helices from each domain forming the channel pore (Wu et al., 2016).

LTCCs must form a multi-protein complex in order to function properly. These complexes are composed of the pore-forming Ca_V1 $\alpha1$ subunit, an intracellular β subunit and a

membrane-associated α2-δ subunit formed by disulfide bonds (Figure 1.7) (Catterall, 2000b). The auxiliary β subunit binds to the intracellular linker that connects domains I and II (I-II linker) of the α1 subunit, at the AID (α-interacting domain). The β subunits modulate Ca^{2+} channel kinetics based on different patterns of localization and expression (Obermair et al., 2009; Schlick et al., 2010). The α2-δ subunit is a unique protein within HVA channels; it is composed of distinct α2 and δ subunits that are linked by disulfide bonds, yet originate from the same gene (De Jongh et al., 1990). The protein is located in the extracellular space, with the δ portion tethered to the membrane. They function to properly traffic Ca^{2+} channels to the plasma membrane and increased expression of these subunits also increases channel current (Davies et al., 2007).

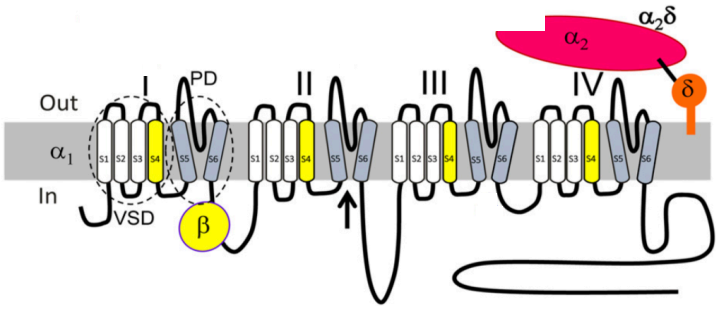

Figure 1.7: Structure and subunits of L-type Ca^{2+} channels.

The α1 subunit is depicted as black lines and cylinders representing transmembrane helices. In and Out refer to inside and outside the plasma membrane, respectively. The four domain repeats of the are numbered I-IV. VSD: voltage-sensing domain, voltage sensor V4 highlighted in yellow. PD: pore domain. Auxiliary β and α2-δ subunits are pictured in yellow and magenta/orange, respectively. Adapted from (Zamponi et al., 2015).

1.5.2 LTCCs and Excitation-Transcription (E-T) Coupling

The vital function of LTCCs is to transform an electrical input (depolarization) into a Ca^{2+} dependent physiological output that alters cell function. In muscle cells, LTCC current causes contraction of muscle cells upon membrane depolarization, known as excitation-contraction coupling (Bers, 2002). LTCC activation in the pancreatic β cell is a critical step in the secretion of insulin, and this excitation-secretion coupling is vital in maintaining glucose homeostasis (Braun et al., 2008; Rorsman et al., 2012). Finally, LTCC activation in neurons can induce synaptic plasticity and downstream activation of gene transcription in the nucleus (Moosmang et al., 2005; Zhang et al., 2006). This process is known as excitation-transcription (E-T) coupling (Hardingham et al., 2017).

Broadly, E-T coupling can occur through a variety of different receptors and pathways, but these signaling cascades converge on a small number of nuclear transcription factors. The best-studied transcription factor is cyclic AMP-dependent responsive element binding protein (CREB). CREB is activated not only by cAMP/PKA-dependent pathways, but also MAPK cascades and Ca^{2+} influx (Figure 1.8) (Kandel, 2012). This allows for multiple forms of neuronal excitation to signal downstream to CREB. Under basal conditions, CREB exists as a monomer in the nucleus. Neuronal stimulation can initiate numerous signaling cascades that lead to the phosphorylation of CREB at Ser133 (Puri, 2019). This phosphorylation occurs through the activation of the nuclear kinase CAMKIV which can be activated directly by Ca^{2+}/CaM or indirectly through upstream activation of nuclear CaMKK (Soderling, 1999). Phosphorylated CREB (pCREB) homo-dimerizes and binds to regions of DNA known as cyclic AMP/Ca^{2+}-dependent responsive elements

(CREs) (Carlezon et al., 2005). When bound to DNA, pCREB promotes histone deacetylation and chromatin remodeling, recruitment of RNA polymerase II, and initiation of gene transcription.

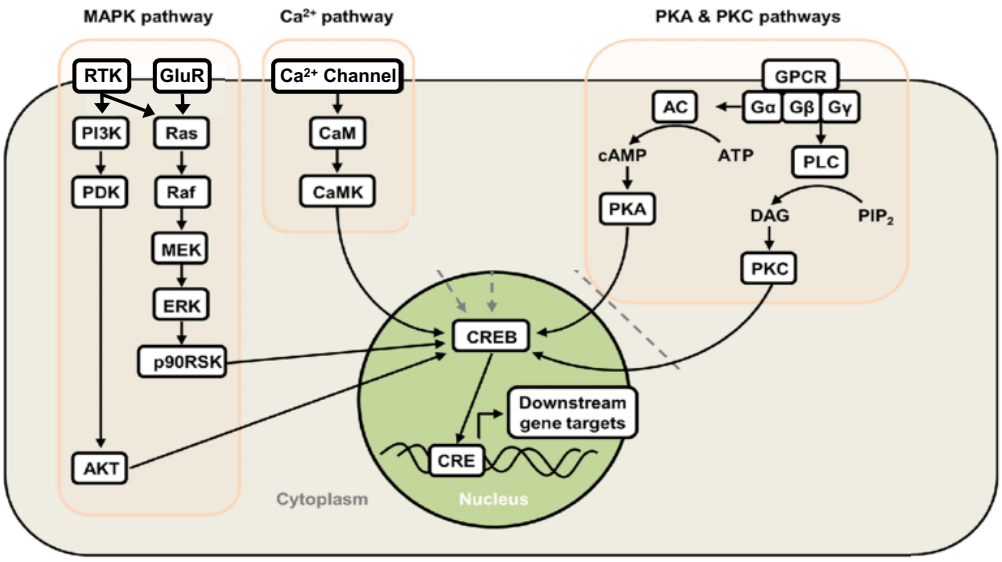

Figure 1.8: Activity-dependent signaling to phosphorylate nuclear CREB.

Diagram of a cell and the many pathways that lead to CREB phosphorylation in the nucleus: the MAPK/ERK pathway, the Ca^{2+} pathway, and the PKA/PKC/GPCR pathways. All pathways converge downstream to phosphorylate the transcription factor CREB at Ser133. Phosphorylated CREB then dimerizes and binds to CRE in DNA to initiate gene expression. Adapted from (Chowanadisai et al., 2014).

Activation of CREB and other activity-dependent transcription factors results in the expression of a specific set of genes, termed *immediate early genes*. These genes are translated into a number of vital neuronal proteins, such as BDNF (brain-derived neurotrophic factor), Homer1a, and c-Fos (Bading, 2013; Benito et al., 2011; Dolmetsch, 2003; Flavell and Greenberg, 2008). Gene expression of *c-Fos* is a widely-used marker

of neuronal activity, due to its low basal expression and relatively short half-life (Gall et al., 1998). These activity-dependent changes in gene expression and protein translation can affect whole cell physiology and alter the function of larger neural circuits.

Other transcription factors work to suppress excitatory transmission, such as MEF2. MEF2 is dephosphorylated by the Ca^{2+}-responsive Ser/Thr phosphatase calcineurin upon neuronal stimulation, which increases expression of Arc to restrict the total number of synapses on a neuron (Flavell et al., 2006). Therefore, E-T coupling is tightly regulated to ensure that different stimuli have specific effects on overall neuronal physiology.

In neurons, E-T coupling can occur through both LTCCs $Ca_V1.2$ and $Ca_V1.3$, as well as Ca_V2 (N-, P/Q-, and R-type) channels (Wheeler et al., 2012). However, this signaling occurs through two very different mechanisms. LTCCs act locally, while Ca_V2 channels broadly contribute to a global increase in Ca^{2+} levels inside the cell. Under conditions that result in robust CREB signaling through Ca_V1 channels, signaling to CREB through Ca_V2 channels is about ~70-fold weaker, demonstrating the overall contribution of Ca_V1 channel signaling is much greater than Ca_V2 channels.

1.6 Mechanisms of LTCC-Dependent Signaling to the Nucleus

E-T coupling can occur through multiple pathways that increase intracellular Ca^{2+} levels. However, evidence suggests that a change in global Ca^{2+} is not necessary for LTCC-dependent CREB phosphorylation. As a result, the current model of LTCC signaling to the nucleus revolves around the generation of a Ca^{2+} “nanodomain” located at the LTCC

channel pore. This section will define the Ca^{2+} nanodomain, highlight important interactions for $Ca_V1.3$-specific signaling, and how this model is associated with a number of neurological disorders.

1.6.1 LTCC Nanodomain Signaling

Ca^{2+} influx from LTCCs at the plasma membrane can initiate signaling to the nucleus, which may be hundreds of microns away. If this occurs without a change in global Ca^{2+} levels, then a Ca^{2+}-sensitive mechanism within the Ca^{2+} nanodomain must initiate downstream signaling. CaMKIIα/β are known to cluster in punctae around Ca_V1 channels during E-T coupling (Wheeler et al., 2008; Wheeler et al., 2012). However, a 2014 study revealed that it is CaMKIIγ that is the critical shuttle protein that translocates to the nucleus during E-T coupling (Ma et al., 2014). This translocation occurs under specific circumstances: First, Ca^{2+} influx through LTCCs promotes formation of Ca^{2+}/CaM, activation of CaMKIIα/β, and Thr286/287 autophosphorylation. Second, the autophosphorylated CaMKIIα/β *trans*-phosphorylates Thr287 in a CaMKIIγ subunit in a separate holoenzyme. When Thr287 is phosphorylated, this increases the affinity for Ca^{2+}/CaM ~1000 fold, a phenomenon known as CaM trapping (Meyer et al., 1992). Third, CaMKIIγ is dephosphorylated by the phosphatase calcineurin (CaN) at Ser334 at the cell surface. Once dephosphorylated, this reveals a nuclear localization signal (NLS) on specific splice variants of CaMKIIγ, shuttling CaMKIIγ and Ca^{2+}/CaM to the nucleus. Finally, the Ca^{2+}/CaM appears to be released from CaMKIIγ to activate CaMKK and CaMKIV, ultimately phosphorylating CREB at Ser133 (Figure 1.9).

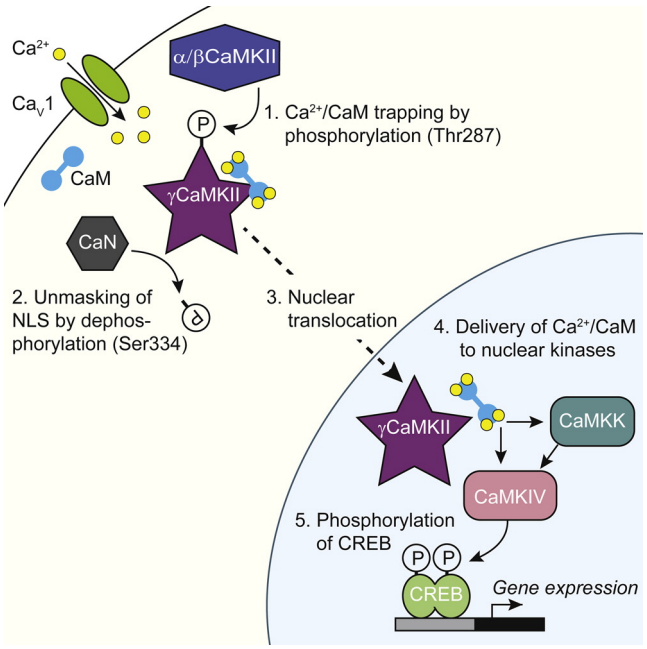

Figure 1.9: A Ca^{2+} nanodomain for LTCC-dependent E-T coupling.

Schematic of the CaMKII pathway for LTCC-dependent signaling to the nucleus. Upon neuronal depolarization, Ca^{2+} influx through Ca_V1 channels generates a Ca^{2+} nanodomain and promotes nearby CaMKII holoenzymes to undergo Thr286/287 autophosphorylation. Activated CaMKIIα/β holoenzymes then *trans*-phosphorylate a CaMKIIγ holoenzyme. Dephosphorylation of CaMKIIγ by calcineurin (CaN) at Ser334 reveals a nuclear localization signal (NLS). Once in the nucleus, Ca2+/CaM activates CaMKK and/or CaMKIV to phosphorylate CREB. Adapted from (Ma et al., 2014) with permission from Elsevier.

Experiments with different Ca^{2+} chelators support the nanodomain model. Neurons loaded with the 'fast' Ca^{2+} chelator BAPTA, which prevents both global and local Ca^{2+} increases, completely disrupted E-T coupling through Ca_V1 channels (Wheeler et al., 2012). In contrast, the 'slow' Ca^{2+} chelator EGTA prevents a rise in global Ca^{2+} while still allowing for Ca^{2+} to influx immediately around the channel pore. Neurons loaded with EGTA were still able to signal to phosphorylate CREB upon depolarization, though the kinetics are slightly slowed (Wheeler et al., 2012). EGTA also did not disrupt the formation

of CaMKII punctae during depolarization, while BAPTA completely prevented puncta formation. Therefore, local Ca^{2+} influx around Ca_V1 channels generates a nanodomain that is necessary for E-T coupling.

Further evidence that CaMKIIγ plays a specific shuttling role comes from studies that generated mice with CaMKIIγ knocked out specifically in excitatory neurons (Cohen et al., 2018). WT and CaMKIIγ-KO mice had similar levels of immediate early genes under basal conditions. After bouts of training in the Morris Water Maze, WT mice had significantly increased levels of nuclear CaM and c-Fos, while CaMKIIγ-KO mice had neither. Complementary studies showed that E-T coupling is disrupted by a CaMKIIγ mutation that is linked to intellectual disability. These studies highlight that multiple CaMKII isoforms play important roles within the Ca^{2+} nanodomain.

Membrane depolarization during E-T coupling causes a conformational change within the transmembrane regions of the Ca_V1 $\alpha1$ subunit, at the S4 voltage sensor (Wu et al., 2015). However, intracellular conformational changes also occur, and can influence LTCC signaling (Kobrinsky et al., 2002). Recent studies show that these intracellular conformational changes, independent of Ca^{2+} influx, are necessary for LTCC-dependent CREB phosphorylation (Li et al., 2016). However, the exact molecular mechanisms underlying these changes in the LTCC nanodomain, such as specific protein binding interactions, remain incompletely understood. There may be cooperation between these conformational changes and intracellular protein-protein interactions, such as CaMKII clustering mentioned above, that regulate the precise localization of all the signaling

proteins within such a small Ca^{2+} nanodomain. This nanodomain model applies to both CaV1.2 and CaV1.3 signaling, as CaMKII interacts with both channels in a similar manner (Wang et al., 2017b). However, the majority of this dissertation will focus on E-T coupling from CaV1.3 channels because Shank3 specifically interacts with CaV1.3 and not 1.2 (see below) (Zhang et al., 2005).

1.6.2 $Ca_V1.3$-Shank3 and $Ca_V1.3$-CaMKII Interactions in LTCC Signaling

Both CaMKII and Shank3 play a role in multiple signaling pathways in the PSD. This dissertation focuses on their coordinated regulation of E-T coupling through LTCCs. Previous studies primary focused on the importance of the CaMKII-$Ca_V1.3$ or Shank3-$Ca_V1.3$ interactions, which I will summarize below.

An association between the LTCC $Ca_V1.3$ and Shank3 has been previous characterized in the literature (Zhang et al., 2005). The four C-terminal amino acids of $Ca_V1.3$, ^{2161}Ile-Thr-Thr-Leu^{2164}, form a PDZ-binding motif that interacts with theShank1 or Shank3 PDZ domains. Interestingly, this interaction is specific to $Ca_V1.3$, as the C-terminus PDZ binding motif of $Ca_V1.2$, ^{2168}Val-Ser-Ser-Leu^{2171}, does not interact with Shank1 or Shank3 PDZ domains. Additionally, only the longest splice variant of the $Ca_V1.3$ C-terminus contains this PDZ-binding motif (Stanika et al., 2016; Zhang et al., 2005).

In the characterization of the $Ca_V1.3$-Shank3 interaction, a secondary binding interaction was identified between the Shank3 SH3 domain and a –PxxP– binding motif located in the $Ca_V1.3$ CTD (Zhang et al., 2005). This binding interaction was able to support $Ca_V1.3$-

Shank3 binding by itself, but was strengthened by the presence of the Shank3 PDZ domain. Our unpublished data suggest this interaction, if present, is not sufficient to support $Ca_V1.3$-Shank3 binding and are discussed more in-depth in Appendix C.

The role of the $Ca_V1.3$-Shank3 interaction in E-T coupling was tested in primary neuronal cultures expressing a recombinant $Ca_V1.3$ with a deletion of the last five amino acid residues, encompassing the ITTL PDZ binding motif (Zhang et al., 2005). A 90 second depolarization of neurons with 20 mM KCl induced CREB phosphorylation in neurons transfected with the full-length channel, but not in neurons expressing the mutant channel. Intriguingly, no difference in CREB phosphorylation was observed in neurons expressing the two channels when using a stronger depolarization of 45 mM KCl, suggesting other mechanisms might come into play when using stronger depolarizations.

More recently, a novel interaction between the $Ca_V1.3$ N-terminal domain (NTD) and CaMKII was identified (Wang et al., 2017b). This interaction requires CaMKII activation by Thr286 autophosphorylation or by Ca/CaM binding. Deletion of $Ca_V1.3$ residues 69-93 or mutation of $Ca_V1.3$ residues ^{83}RKR^{85} to Ala (AAA mutant) completely disrupted binding. While deletion of residues 69-93 did not affect $Ca_V1.3$ Ca^{2+} influx, it did disrupt nuclear signaling to phosphorylate CREB. A mutation of CaMKIIα Val102 to Glu (V102E) selectively disrupts CaMKII binding to $Ca_V1.3$, but not Densin-IN, Densin-CTD, or β_{2a} binding domains. Knockdown of endogenous CaMKIIα/β and re-expression of CaMKII-V102E failed to rescue CREB phosphorylation compared to knockdown alone. Taken

together, these observations indicate that direct interaction of activated CaMKII with the NTD of $Ca_V1.3$ is required for efficient E-T coupling.

In summary, individual protein-protein interactions between $Ca_V1.3$-Shank3 and $Ca_V1.3$-CaMKII are required for proper signaling to the nucleus. Based on the knowledge that CaMKII holoenzymes can bind multiple proteins simultaneously (Robison et al., 2005b) and our preliminary data that Shank3 is a novel CaMKAP, we hypothesized that $Ca_V1.3$, CaMKII, and Shank3 are part of a larger tri-partite protein complex where each protein is bound to the other two proteins (Figure 1.10).

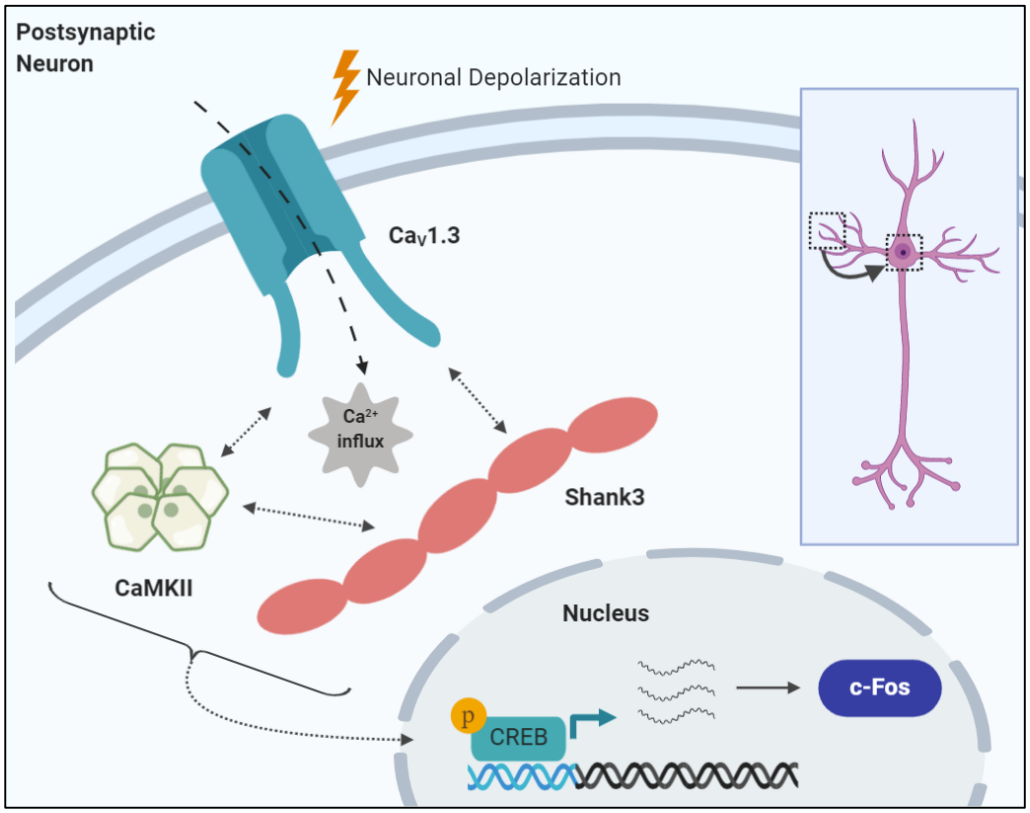

Figure 1.10: CaMKII-$Ca_V1.3$-Shank3 complex in LTCC E-T coupling.

Schematic of LTCC/Ca^{2+} nanodomain. We hypothesize the protein-protein interactions between CaMKII, $Ca_V1.3$, and Shank3 all play a role to increase CREB phosphorylation in the nucleus.

Phosphorylated CREB enhances gene expression and ultimately protein translation of immediate early genes, such as c-Fos. *Insert*, E-T coupling can occur in dendritic spines, hundreds of microns away from the nucleus.

1.6.3 Disruptions of E-T Coupling in Neurological Disorders

Disruptions in activity-dependent gene expression are associated with multiple neuropsychiatric disorders (Ebert and Greenberg, 2013; Gallo et al., 2018) that have been linked to mutations in Ca^{2+} signaling proteins, including L-type calcium channels (LTCCs) and CaMKII (Table 1.1) (Akita et al., 2018; Chia et al., 2018; Cohen et al., 2018; Dick et al., 2016; Hofer et al., 2020; Kury et al., 2017; Limpitikul et al., 2016; Moon et al., 2018; Nyegaard et al., 2010; Pinggera et al., 2015; Pinggera et al., 2017; Pinggera and Striessnig, 2016; Proietti Onori et al., 2018; Stephenson et al., 2017). For example, Timothy Syndrome is caused by mutations in the $Ca_V1.2$ LTCC $\alpha1$ subunit that can disrupt neuronal E-T coupling (Li et al., 2016), contributing to neurobehavioral symptoms of this complex disorder, including ASD. Proper activity-dependent gene expression of the immediate early gene c-Fos is also dysregulated in multiple rodent models of autism (Dubiel and Kulesza, 2015; Orlandini et al., 1996; Williams and Umemori, 2014). Recent studies have shown that initiation of this LTCC-dependent E-T coupling requires recruitment of multiple CaMKII holoenzymes to a nanodomain close to LTCCs (Ma et al., 2014; Wang et al., 2017b; Wheeler et al., 2008), and that E-T coupling is disrupted by a CaMKII mutation linked to intellectual disability (Cohen et al., 2018). Therefore, we hypothesized that these proteins, and their interactions, are all required for the normal E-T coupling within the LTCC/Ca^{2+} nanodomain, and that proper binding and function of all

three proteins – CaMKII, $Ca_V1.3$, and Shank3 – are required for LTCC-dependent signaling to the nucleus and subsequent activity-dependent gene expression.

Protein	Gene	Mutations
CaMKIIα	*CAMK2A*	F98S, E109D, A112V, P212L, H282R, T286P, H477Y (ID), E183V (ASD/ID)
CaMKIIβ	*CAMK2B*	R29X, E110K, P139L, E237K, K301E (ID)
CaMKIIγ	*CAMK2G*	R292P (ID)
$Ca_V1.3$	*CACNA1D*	G403D, I750M (PASNA), G407R, A749G (ASD/ID), V401L, V584I, A760G (ASD), S625L (UND)
Shank3	*SHANK3*	Haploinsufficiency (Phelan-McDermid Syndrome), Duplication (22q13 Duplication Syndrome)
ASD: autism spectrum disorder; ID: intellectual disability; PASNA: primary aldosteronism with seizures and neurological abnormalities; UND: undiagnosed neurodevelopmental disorder		

Table 1.1. Mutations in LTCC nanodomain proteins linked to neurological disorders.

1.7 Overview of Work to be Presented in this Thesis

I hypothesize that CaMKII can directly interact with the scaffolding protein Shank3. I also hypothesize that CaMKII can phosphorylate Shank3, which can occur regardless of a direct CaMKII-Shank3 interaction. Finally, I hypothesize that the formation of a complex containing LTCC $Ca_V1.3$, CaMKII, and Shank3 is necessary for LTCC-dependent signaling to the nucleus to phosphorylate the transcription factor CREB and initiate activity-dependent *de novo* expression of immediate early genes, such as c-Fos.

In the following chapters, I will present data that supports the hypotheses generated above. To begin, Chapter II provides the methodology and describes the materials used to conduct these studies.

Chapter III tests the hypothesis that Shank3 and CaMKII bind directly. I show that this interaction is regulated by CaMKII autophosphorylation at Thr286 and only partially supported by Ca/CaM binding. The CaMKII binding motif in Shank3 is found in a central, uncharacterized region of Shank3 that has some homology to the CaMKII binding motifs identified in $Ca_V1.3$ and mGlu5. Like these other motifs, mutation of three basic residues in this binding motif disrupts CaMKII binding *in vitro* in a selective and specific manner. This mutation also disrupts co-localization of Shank3 and CaMKII in striatal progenitor cells, complementing our biochemical studies.

Chapter IV tests the hypothesis that Shank3 is a substrate of CaMKII phosphorylation. Analysis by mass spectrometry identifies a number of residues phosphorylated by CaMKII *in vitro*. I then validate four putative CaMKII phosphorylation sites on Shank3 using purified protein and phospho-null Ala mutations.

Chapter V focuses on a phosphorylation site identified in Chapter IV, Ser685, that was previously identified as a PKA phosphorylation site. I confirm that this residue is phosphorylated by both CaMKII and PKA using a phospho-null mutation of Ser685 to Ala. Finally, I demonstrate that CaMKII phosphorylation of Shank3 at Ser685 enhances binding between ABI1 and Shank3.

Chapter VI expands upon the phosphorylation data in Chapter IV to test the hypothesis that CaMKII phosphorylation of Shank3 Thr551 disrupts binding between GKAP and

Shank3. I demonstrate that Thr551 is phosphorylated by CaMKII *in vitro*. Phospho-mimetic mutation of Thr551 to Asp reduces GKAP co-immunoprecipitation in heterologous cells, as does co-expression with constitutively active CaMKII. This phosphorylation site may be a novel mechanism for selectively targeting the GKAP-Shank3 interaction without disrupting other PDZ binding partners.

Finally, Chapter VII tests the hypothesis that Shank3 expression, as well as the interactions of Shank3 with CaMKII and $Ca_V1.3$, are both required for proper signaling to the nucleus and subsequent activity-dependent gene expression.

Taken together, the data reported in this thesis significantly advance our understanding of the of molecular signaling mechanisms in the PSD that allow for efficient signaling to the nucleus.

CHAPTER II

MATERIALS AND METHODS

2.1 Molecular Biology and Biochemistry

2.1.1 DNA Constructs

A construct encoding GFP-Shank3 was a generous gift from Dr. Craig Garner (Stanford University). The construct expressing shRNA (pLL3.7) was a gift from Dr. Luk Van Parijs (Massachusetts Institute of Technology). This plasmid was modified to replace the CMV promoter with a 0.4kb fragment of the mouse CaMKII promoter (designated as pLLCK) that is primarily active only in excitatory neurons (Dittgen et al., 2004). Control shRNA (5'-TCGCTTGGGCGAGAGTAAG-3') was designed following Boudkkazi *et al*. (Boudkkazi et al., 2014). Shank3 shRNA (5'-GGAAGTCACCAGAGGACAAGA-3') was designed following Verpelli *et al.* (Verpelli et al., 2011). Sequences encoding shRNA were inserted into pLLCK at HpaI and XhoI restriction sites. The Shank3 shRNA-resistant construct ($Shank3^{R}$) was designed by introducing 6 "silent" nucleotide mutations in the target site that do not alter amino acid sequence at Arg^{1187}, Lys^{1188}, Ser^{1189}, and Pro^{1190}. Knockdown and shRNA-resistance were confirmed by immunoblot and immunostaining.

The mAp-Shank3 construct was generated by inserting Shank3 cDNA into pmApple-C1 construct at BglII and EcoRI restriction sites. The Shank3 shRNA-resistant construct containing a deletion of the PDZ domain (mAp-$Shank3^{R-}\Delta PDZ$) was generated by in-frame PCR deletion of the entire 270bp region encoding ^{572}Iso-Val^{661} from mAp-$Shank3^{R}$.

GST-Shank3 constructs were created by PCR amplification of the relevant cDNA fragments for insertion between EcoR1 and BamH1 restriction sites in pGEX6P-1; the numbering of Shank3 residues is from the canonical rat sequence (UniProtKB: Q9JLU4 Isoform 2). The Shank3 truncation and mutagenesis primers are listed in Table. 2.1. GST-GluA1 and GST-GluN2B were described previously (Barria et al., 1998; Strack et al., 2000a).

Rat $Ca_V1.3$ complete coding sequence (Genbank accession number AF370010) was a gift from Dr. Diane Lipscombe (Brown University). A plasmid encoding $Ca_V1.3$-CTD with an N-terminal HA-tag (HA-$Ca_V1.3$-CTD, for co-immunoprecipitation) was made by inserting rat $Ca_V1.3$ cDNA encoding ^{1469}Met-Leu^{2164} into the pCGNh vector between Xba1 and BamHI restriction sites, a gift from Dr. Winship Herr (Université de Lausanne). A truncation of this plasmid lacking the PDZ binding motif (HA-$Ca_V1.3$-CTD-ΔPDZ) was generated by in-frame PCR deletion of ^{2161}Ile–Leu^{2164} from HA-$Ca_V1.3$-CTD. Rabbit $Ca_V1.2$ cDNA (Genbank accession number X15539) was a gift from Dr. William Thiel (University of Iowa). A plasmid encoding $Ca_V1.2$-CTD with an N-terminal HA-tag (HA-$Ca_V1.2$-CTD) was made by inserting rabbit $Ca_V1.2$ cDNA encoding ^{1507}Asp–Leu^{2171} into the pCGNh vector between Xba1 and BamHI restriction sites.

Rat GKAP cDNA was a generous gift from Dr. Terunaga Nakagawa (Vanderbilt University). Full-length GKAP was PCR amplified and inserted into the pCGNh vector between Xba1 and BamHI restriction sites to generate HA-tagged GKAP. The eGFP-ABI1 vector was purchased from Addgene (#74905). DNA encoding full-length ABI1 was

PCR amplified and inserted into the pCGNh vector between Xba1 and BamHI restriction sites to generate N-terminal HA-tagged ABI1. All constructs were confirmed by DNA sequencing.

Primer	5' to 3' Sequence
GST-Shank3 (1-324) Fw	CTGGAAGTTCTGTTCCAGGGGCCCCTGGGATCCATGGACGGCCCCGGG
GST-Shank3 (1-324) Rv	GATGCGGCCGCTCGAGTCGACCCGGGAATCCAATGGCCACCTGGAAGGC
GST-Shank3 (325-536) Fw	CTGGAAGTTCTGTTCCAGGGGCCCCTGGGATCCATTGCAGGGAACTTTGAGC
GST-Shank3 (325-536) Rv	GATGCGGCCGCTCGAGTCGACCCGGGAATCCTTAATGCCGTGTGTCATACTGTCGC
GST-Shank3 (537-828) Fw	CTGGAAGTTCTGTTCCAGGGGCCCCTGGGATCCGAAACTCGAGAGGACCGG
GST-Shank3 (537-828) Rv	GATGCGGCCGCTCGAGTCGACCCGGGAATCCGTAGTAGGGCGCGGGTGGGGGT
GST-Shank3 (829-1130) Fw	CTGGAAGTTCTGTTCCAGGGGCCCCTGGGATCCGACTCCGGGCCACCCCCCACC
GST-Shank3 (829-1130) Rv	GATGCGGCCGCTCGAGTCGACCCGGGAATCCTTAGGGGGACCGGGAAGG
GST-Shank3 (1131-1467) Fw	CTGGAAGTTCTGTTCCAGGGGCCCCTGGGATCCACACCCGTGCACAGTCC
GST-Shank3 (1131-1467) Rv	GATGCGGCCGCTCGAGTCGACCCGGGAATCCTTAGAGGTAGCGAGGGCGG
GST-Shank3 (1468-1740) Fw	CTGGAAGTTCTGTTCCAGGGGCCCCTGGGATCCTTCCAGAGAAGGTCCAAGCTGTGGGGGG
GST-Shank3 (1468-1740) Rv	GATGCGGCCGCTCGAGTCGACCCGGGAATCCTCAGCTGCCATCCAGC
GST-Shank3 (829-930) Fw	CTGGAAGTTCTGTTCCAGGGGCCCCTGGGATCCTTCGACTCCGGGCCA
GST-Shank3 (829-930) Rv	GATGCGGCCGCTCGAGTCGACCCGGGAATCCTTAGGGACTATCAGGGCCTGA
GST-Shank3 (931-1014) Fw	CTGGAAGTTCTGTTCCAGGGGCCCCTGGGATCCGCCAACCTGGGCGCCTT
GST-Shank3 (931-1014) Rv	GATGCGGCCGCTCGAGTCGACCCGGGAATCCTTAAGGGCTAGGGCCGCC
GST-Shank3 (1015-1130) Fw	CTGGAAGTTCTGTTCCAGGGGCCCCTGGGATCCGGCCCAGTCAAGGA
GST-Shank3 (1015-1130) Rv	GATGCGGCCGCTCGAGTCGACCCGGGAATCCTTAGGGGGACCGGGAAGGTGTTT
GST-Shank3 (473-571) Fw	TCTGTTCCAGGGGCCCCTGGGATCCCGCAAGTTCATCGCTGTGAAGG
GST-Shank3 (473-571) Rv	TCGACCCGGGAATTCCGGTCAAGCCACCTTATCATCAATGACATAATCA
GST-Shank3 (473-664) Fw	TCTGTTCCAGGGGCCCCTGGGATCCCGCAAGTTCATCGCTGTGAAGG
GST-Shank3 (473-664) Rv	TCGACCCGGGAATTCCGGTCAGGTAACAGACACAACCTTCATGACCA
GST-Shank3 (473-664) ∆543-564 Fw	AGAGGACCGGGTCATTGATGATAAGGTGGCTATCCTGCAAAAACGG
GST-Shank3 (473-664) ∆543-564 Rv	CATCAATGACCCGGTCCTCTCGAGTTTCATGCCGTGTGTCAT

GST-Shank3 (537-663) Fw	TGTGTCTGTTTGACCGGAATTCCCGGGTCGACTCGAG
GST-Shank3 (537-663) Rv	ATTCCGGTCAAACAGACACAACCTTCATGACCAGACGGTTG
GST-Shank3 (566-671) Fw	CTGTTCCAGGGGCCCCTGGGATCCATTGATGATAAGGTGGCTATCCTGC
GST-Shank3 (566-671) Rv	CGAGTCGACCCGGGAATTCCGGTCAACTATCCTCCTCTGGCTTCCTG
GST-Shank3 (572-691) Fw	CTGTTCCAGGGGCCCCTGGGATCCATCCTGCAAAAACGGGAC
GST-Shank3 (572-691) Rv	GATGCGGCCGCTCGAGTCGACCCGGGAATTCCGGTCACCGCAGGGTCAG
Shank3 ^{949}RRK^{951}/AAA Fw	CGAAACCGCAGGCCGCCGCGAGTCCGCTGGTGAAGCAGCTTCAG
Shank3 ^{949}RRK^{951}/AAA Rv	CCAGCGGACTCGCGGCGGCCTGCGGTTTCGACGGAGCAAAGAGG
Shank3 T551A Forward	CTTTTCCGCCACTACGCTGTGGGTTCCTATGACAGCCTC
Shank3 T551A Reverse	GGAACCCACAGCGTAGTGGCGGAAAAGACGCTTCGTC
Shank3 T551D Forward	GCCACTACGATGTGGGTTCCTATGACAGCCTCACTTCACAC
Shank3 T551D Reverse	AACCCACATCGTAGTGGCGGAAAAGACGCTTCGTCCGG
Shank3 S557A Forward	GGGTTCCTATGACGCCCTCACTTCACACAGTGATTATG
Shank3 S557A Forward	GTGTGAAGTGAGGGCGTCATAGGAACCCACAGTGTAG
Shank3 S557D Forward	CCTATGACGACCTCACTTCACACAGTGATTATGTCATTGATGATAAGGTGG
Shank3 S557D Reverse	GAAGTGAGGTCGTCATAGGAACCCACAGTGTAGTGGCG
Shank3 S685A Forward	GCCCCCGCCACCACGCTGACCCTGCGGTCCAAGTCC
Shank3 S685A Reverse	AGCGTGGTGGCGGGGGCCCTCTTGGGAGGTGGTGG
Shank3 S685D Forward	GCCCCCGACACCACGCTGACCCTGCGGTCCAAGTCC
Shank3 S685D Reverse	AGCGTGGTGTCGGGGGCCCTCTTGGGAGGTGGTGG

Table 2.1. Primers used in generating Shank3 truncations and point mutants.

2.1.2 Recombinant Protein Purification

Expression and purification of recombinant mouse CaMKIIα has been described previously (Mcneill and Colbran, 1995). The vectors encoding GST fusion proteins were transformed into BL21 (DE3) pLysS bacteria cells, and proteins were purified as previously described (Robison et al., 2005a). Protein expression was induced at room temperature for ~3 hours to reduce the degradation seen at 37°C. Purified bovine heart

PKA for *in vitro* kinase assays was a generous gift from Dr. Jackie Corbin (Vanderbilt University).

2.1.3 GST Pulldown Assay with Purified CaMKIIα

CaMKIIα (1.25 μM subunit) was incubated on ice for 90 s with 50 mM HEPES, pH 7.5, 10 mM magnesium acetate, 0.5 mM $CaCl_2$, 1 μM CaM, and 1 mM DTT, with or without 400 μM ATP (T286-autophosphorylated or basal, respectively), and reactions were terminated with 45 mM EDTA. Separate reactions incubated CaMKIIα (1.25 μM subunit) with 50 mM HEPES, pH 7.5, 10 mM magnesium acetate, 0.5 mM $CaCl_2$, 1 μM CaM, 1 mM DTT with no EDTA or ATP added (Ca/CaM). The reaction was then diluted 10-fold using 1X GST pulldown buffer (50 mM Tris-HCl pH 7.5; 200 mM NaCl; 1% (v/v) Triton X-100), supplemented with 10 mM magnesium acetate and 0.5 mM $CaCl_2$ for Ca/CaM incubations. CaMKIIα (125 nM subunit) was incubated with GST or GST-fusion protein (125 nM) and Pierce Glutathione Agarose beads (Thermo Fisher Scientific, catalog 16101, 10 μL packed resin). Reactions were rocked for 1 hr at 4°C. Beads were washed three times with GST buffer, supplemented as described above where appropriate. Proteins were eluted with 20 mM glutathione, pH 8.0 for 10 minutes (Sigma, St. Louis, MO).

2.1.4 *In Vitro* Kinase Assay with [γ-^{32}P] ATP

GST fusion proteins were incubated at 30°C for the indicated time in 50 mM HEPES, pH 7.5, 10 mM magnesium acetate, 1 μM dithiothreitol, 400 μM [γ-^{32}P] ATP (700-1,000 c.p.m./pmol) containing either purified CaMKIIα (10 nM), 2 mM $CaCl_2$, and 2 μM

calmodulin or purified PKA (10 or 50 nM). After addition of LDS sample buffer (Invitrogen), samples were heated (70°C, 10 min) and resolved by SDS-PAGE. Gels were stained with Coomassie (InstantBlue, VWR) and then exposed to X-ray film (Phenix) for 2-18 hours at -80°C. In some experiments, gel bands were excised and phosphorylation stoichiometries were determined by quantifying ^{32}P incorporation using a scintillation counter. Phosphorylation (mol/mol) was calculated using total amount of GST-fusion protein loaded into the gel and calculating the specific radioactivity of [γ-^{32}P] ATP used in each experiment.

2.1.5 *In Vitro* Kinase Assay for Mass Spectrometry

CaMKII phosphorylation for mass spectrometry was performed as described above, except with non-radiolabeled ATP. To fully maximize phosphorylation of GST-fusion proteins, reactions were incubated for 25 min at 30°C and stopped with addition of LDS Sample buffer (Invitrogen). Samples were heated (70°C, 10 min) and resolved by SDS-PAGE. Gels were stained with Colloidal Blue (Thermo Fisher Scientific, Cat. LC6025) for three hours and washed with deionized water overnight. The band corresponding to full-length protein was then excised and incubated with 100 mM ammonium bicarbonate, pH 8, reduced with 4 mM DTT or TCEP, alkylated with 8 mM iodoacetamide and finally digested overnight with trypsin (10 ng/µl; 37 °C). Peptides were then analyzed by mass spectrometry at the Vanderbilt University Mass Spectrometry Core Lab.

2.1.6 Immunoblotting and Semi-Quantitative Analysis

Samples were resolved on 10% SDS-PAGE gels and transferred to nitrocellulose membrane (Protran, Camp Hill, PA). The membrane was blocked in blotting buffer containing 5% nonfat dry milk, 0.1% Tween 20, in Tris-buffered saline (20 mM Tris, 136 mM NaCl) at pH 7.4 for 30 min at room temperature. The membrane was incubated with primary antibody (see dilutions below) in blotting buffer for 1 hr at room temperature or overnight at 4°C. After washing, membranes were incubated with HRP-conjugated secondary antibody for 1 hr at room temperature, washed again, and then visualized using enzyme-linked chemi-luminescence using the Western Lightening Plus-ECL, enhanced chemiluminescent substrate (PerkinElmer, Waltham, MA) and visualized using Premium X-ray Film (Phenix Research Products, Candler, NC) exposed to be in the linear response range. Images were quantified using ImageJ software. Signals detected in the negative control lanes were used a background value, and were subtracted from experimental lanes. Secondary antibodies conjugated to infrared dyes (LI-COR Biosciences) were used for development with an Odyssey system (LI-COR Biosciences).

2.1.7 Antibodies

The following antibodies were used for immunoblotting at the indicated dilutions: mouse anti-CaMKIIα 6G9 (Thermo Fisher Scientific, Waltham, MA; catalog MA1– 048, 1:5000), pT286 CaMKIIα (Santa Cruz Biotechnology, Dallas, TX; catalog sc-12886-R, 1:3000), mouse anti-Shank3 (University of California at Davis/National Institutes of Health NeuroMab Facility, Davis, CA; catalog N367/62, 1:2000), rabbit monoclonal anti-Shank3 (D5K6R) (Cell Signaling, Danvers, MA; catalog 64555, 1:3000), goat anti-GST (GE

Healthcare Life Sciences, Marlborough, MA; catalog 27-4577-01, 1:5000), polyclonal goat CaMKII antibody (RRID: AB_2631234, 1:5000) (Mcneill and Colbran, 1995), mouse anti-PSD-95 (NeuroMab, catalog 75-028, 1:50,000), mouse anti-GFP (Vanderbilt Antibody and Protein Resource, Nashville, TN; catalog 1C9A5, 1:3000), mouse anti-HA (Biolegend, San Diego, CA; catalog 901503, 1:3000), HRP-conjugated anti-rabbit (Promega, Madison, WI; catalog W4011, 1:6000), HRP-conjugated anti-mouse (Promega, catalog W4021, 1:6000), HRP-conjugated anti-goat (Abcam, Cambridge, United Kingdom; catalog Ab6741, 1:3000), IR dye-conjugated donkey anti-mouse 800CW (LI-COR Biosciences, Lincoln, NE; catalog 926-32213, 1:10,000), and IR dye-conjugated donkey anti-goat 680LT (LI-COR Biosciences, catalog 926-68022, 1:10,000).

2.2. Heterologous Cell Experiments

2.2.1 HEK293T Cell Culture, Transfection, and Immunoprecipitation

HEK293T cells (ATCC, Manassas, VA; catalog CRL-3216) were cultured and maintained in DMEM containing 10% FBS, L-glutamine, and 1% penicillin/streptomycin at 37°C in 5% CO_2. Cells plated on 10 cm dishes were transfected with 5-10 µg of DNA. After 24-48 hr, cells were rinsed in ice-cold PBS and lysed in ice-cold lysis buffer (150 mM NaCl, 25 mM Tris-HCl, pH 7.5, 1% Triton-X 100, 1 mM DTT, 0.2 mM PMSF, 1 mM benzamidine, 10 µg/ml leupeptin, and 10 µM pepstatin). Where indicated, lysis buffer was supplemented with 2 mM EDTA and 2 mM EGTA.

HEK293T cell lysates were incubated with rabbit anti-GFP (Thermo Fisher Scientific, catalog A-11222) and rocked end-over-end at 4°C for 1 hour with 10 µl prewashed

Dynabeads Protein A (Thermo Fisher Scientific, catalog 10001D). Where indicated, HEK293T lysates were supplemented with 1.5 mM $CaCl_2$ and 1 μM calmodulin (final concentrations) to partially activate CaMKII during immunoprecipitation. The beads were isolated magnetically and washed three times using lysis buffer before eluting proteins using 2X SDS-PAGE sample buffer. Inputs and immune complexes were immunoblotted side by side as indicated.

2.2.2 GST Pulldown Assay with HEK293T Cell Lysates

HEK293T cells were transfected and lysed, as described above, and incubated with GST or GST-fusion protein (250 nM) and Pierce Glutathione Agarose beads (Thermo Fisher Scientific, catalog 16101, 10 μL packed resin). Reactions were rocked for 1 hr at 4°C. Beads were washed three times with GST buffer, supplemented as described above where appropriate. Proteins were eluted with 20 mM glutathione, pH 8.0 for 10 minutes (Sigma).

2.2.3 Pre-Phosphorylated GST Pulldown Assay with HEK293T Cell Lysates

Purified CaMKIIα (10 nM) was incubated with GST fusion protein or GST alone (2.5 μM) in 50 mM HEPES, pH 7.5, 10 mM magnesium acetate, 0.5 mM $CaCl_2$, 1 μM CaM, 1 mM DTT, and 400 μM non-radiolabeled ATP at 30°C for 5-20 min. Control reactions were performed in the absence of CaMKIIα. After addition of EDTA (12 mM final), samples were diluted ten-fold in HEK293T cells soluble fractions, and GST proteins were isolated as described in 2.2.2.

2.2.4 ST Hdh Q7/Q7 Cell Culture and Transfection

ST*Hdh*$^{Q7/Q7}$ cells (Trettel et al., 2000), a gift from Dr. Aaron Bowman (Vanderbilt University), were cultured and maintained in DMEM containing 10% FBS, L-glutamine, 1% penicillin/streptomycin, and 400 µg/ml G418 (Mediatech, Tewksbury, MA) at 33°C in 5% CO_2. Cells were plated onto 15 mm coverslips pre-treated with poly-D-lysine in 12-well plates and transfected with 3 µg of DNA overnight. Media was then removed and cells were incubated in serum-free DMEM containing either 0.49% dimethyl sulfoxide (Pierce) or a differentiation medium (serum-free DMEM supplemented with 10 ng/ml fibroblast growth factor (Promega), 240 µM isobutylmethylxanthine (Sigma), 20 µM 12-*O*-tetradecanoylphorbol-13-acetate (Sigma), 48.6 µM forskolin (Sigma), and 5 µM DA (Sigma). After 8-14 hours, cells were fixed in ice-cold 4% paraformaldehyde-4% sucrose in 0.1 M Phosphate Buffer pH 7.4 for 3 minutes and -20°C methanol for 10 minutes. Coverslips were mounted on microscope slides using ProLong Gold antifade reagent with DAPI (Thermo Fisher Scientific, catalog P36931).

2.2.5 ST Hdh Q7/Q7 Colocalization Studies

Images of differentiated ST*Hdh*$^{Q7/Q7}$ cells were collected using a Zeiss 880 inverted confocal microscope using 63X objective. Thresholding and intensity correlation analysis to compare normalized pixel intensities in each color channel were performed using ImageJ as previous described (Baucum et al., 2010). GFP and mApple channels were automatically thresholded before calculating the intensity correlation quotient (ICQ). This method interprets ICQ values in the following ranges: $0 < ICQ \leq +0.5$, dependent overlap

of fluorescent signals; ICQ = 0, random overlap of fluorescent signals; and 0 > ICQ ≥ -0.5, segregation of fluorescent signals (Li et al., 2004).

2.3 Mouse Experiments

2.3.1 Mice

All mice were housed on a 12 h light-dark cycle with food and water ad libitum. CaMKIIα-KO and Camk2a^{tm2Sva} (CaMKIIα^{T286A}) mice on a C57B/6J background were described previously (Giese et al., 1998; Marks et al., 2018). Wild-type (WT) and homozygous littermates were generated using a HetxHet breeding strategy. Both male and female mice age P28-30 were used for biochemical studies. All animal experiments were approved by the Vanderbilt University Institutional Animal Care and Use Committee and were carried out following the US National Institutes of Health Guide for the Care and Use of Laboratory Animals.

2.3.2 Mouse Forebrain Fractionation and Immunoprecipitation

Forebrains were dissected and fractionated as previously described (Baucum et al., 2015; Stephenson et al., 2017). Briefly, P28-30 mice were anesthetized with isoflurane, decapitated, and forebrains were quickly dissected, cut in half down the midline, and a half forebrain was immediately homogenized in an isotonic buffer (150 mM KCl, 50 mM Tris HCl, pH 7.5, 1 mM DTT, 0.2 mM PMSF, 1 mM benzamidine, 1 μM pepstatin, 10 mg/L leupeptin, 1 μM microcystin). The homogenate (~5 ml) was rotated end-over-end at 4°C for 30 min, at which point an aliquot of the 'whole forebrain' input was collected. Samples were then centrifuged at 100,000 x g for 1 hr. After removing the supernatant (cytosolic

S1 fraction), the pellet was resuspended in the isotonic buffer containing 1% (v/v) Triton X-100, triturated until homogeneous, and then rotated end-over-end at 4°C for 30 min. Homogenates were then centrifuged at 10,000 x g for 10 min, and the supernatant (Triton-soluble membrane S2 fraction) was removed. The second pellet (Triton-insoluble synaptic P2 fraction) was resuspended in isotonic buffer containing 1% Triton X-100 and 1% deoxycholate and then sonicated. The P2 fraction was then mixed with 4X SDS-PAGE sample buffer or used for immunoprecipitation studies.

Mouse forebrains fractions were incubated with either mouse anti-CaMKIIα (Thermo Fisher Scientific, catalog #MA1-048) or rabbit anti-Shank3 (Bethyl, catalog A304-178A) and rocked end-over-end at 4°C for 1 hour with 10 µl prewashed Dynabeads Protein G (Thermo Fisher Scientific, catalog 10002D, for mouse) or Protein A (Thermo Fisher Scientific, catalog 10001D, for rabbit). The beads were isolated magnetically and washed three times using lysis buffer before eluting proteins using 2X SDS-PAGE sample buffer. Inputs and immune complexes were immunoblotted side by side as indicated.

2.4 Neuronal Cultures

2.4.1 Primary Hippocampal Neurons

Dissociated hippocampal neurons were prepared from E18 Sprague Dawley rat embryos, as previously described (Shanks et al., 2010). Sex of the embryos was not determined. Neurons were transfected at 7-9 days *in vitro* (DIV) using Lipofectamine 2000 following the manufacturer's directions (Thermo Fisher Scientific). A total of 1 µg of DNA was

transfected for each well of a 12-well plate for 2-3 hours before switching back to conditioned media.

2.4.2 LTCC-CREB Assay and c-Fos Expression

At DIV 13-14, neurons were pre-incubated for 2 hr with 5K Tyrode's solution (150 mM NaCl, 5 mM KCl, 2 mM $CaCl_2$, 2 mM $MgCl_2$, 10 mM glucose and 10 mM HEPES pH 7.5 (~313 mOsm)) with 1 μM TTX, 10 μM APV and 50 μM CNQX to suppress intrinsic neuronal activity by blocking sodium channels, NMDA receptors and AMPA receptors, respectively. Neurons were then treated with either 5K Tyrode's or 40K Tyrode's solution (adjusted to 40 mM KCl and 115 mM NaCl, with all three inhibitors present) for 90 seconds. For the analysis of pCREB levels, neurons were immediately fixed using ice-cold 4% paraformaldehyde-4% sucrose in 0.1 M Phosphate Buffer pH 7.4 for 3 minutes and -20°C methanol for 10 minutes. For the analysis of c-Fos expression, Tyrode's solution was aspirated after 90 seconds and replaced with conditioned media for 3 hours before fixation. Fixed neurons were washed three times with PBS, permeabilized with PBS+0.2% Triton X-100, and then incubated with blocking solution for one hour (1X PBS, 0.1% Triton X-100 (v/v), 2.5% BSA (w/v), 5% Normal Donkey Serum (w/v), 1% glycerol (v/v)). Neurons were then incubated with blocking solution overnight with primary antibodies: rabbit anti-pCREB (Cell Signaling, catalog 9198, 1:1000) or rabbit anti-c-Fos (EMD Millipore, catalog ABE457, 1:500), and mouse anti-CaMKIIα 6G9 (Thermo Fisher Scientific, catalog MA1–048, 1:1000). The following day, neurons were washed three times in PBS+0.2% Triton X-100, then incubated with blocking solution for 1 hour with secondary antibodies: donkey anti-rabbit 647 Alexa Fluor 647 (Thermo Fisher Scientific,

catalog A-31573) and donkey anti-mouse Alexa Fluor 546 (catalog A-10036). Neurons were washed with PBS three times and mounted on slides using Prolong Gold Antifade Mountant with DAPI.

2.4.3 DHPG-CREB Assay

At DIV 20-21, neurons were pre-incubated for 2 hr with 5K Tyrode's solution (150 mM NaCl, 5 mM KCl, 2 mM $CaCl_2$, 2 mM $MgCl_2$, 10 mM glucose and 10 mM HEPES pH 7.5 (~313 mOsm)) with 1 μM TTX, 10 μM APV and 50 μM CNQX to suppress intrinsic neuronal activity by blocking sodium channels, NMDA receptors and AMPA receptors, respectively. Neurons were then treated with either 5K Tyrode's or 5K Tyrode's solution containing 100 μM DHPG (Tocris) for 30 minutes. For nimodipine treatment, neurons were incubated in 5K Tyrode's solution containing 10 μM nimodipine (plus TTX, APV, and CNQX) for about 5 min before switching to 5K Tyrode's solution plus 10 μM nimodipine, DHPG, TTX, APV, and CNQX. Neurons were immediately fixed using ice-cold 4% paraformaldehyde-4% sucrose in 0.1 M Phosphate Buffer pH 7.4 for 3 minutes and -20°C methanol for 10 minutes. Fixed neurons were washed three times with PBS, permeabilized with PBS+0.2% Triton X-100, and then incubated with blocking solution for one hour (1X PBS, 0.1% Triton X-100 (v/v), 2.5% BSA (w/v), 5% Normal Donkey Serum (w/v), 1% glycerol (v/v)). Neurons were then incubated with blocking solution overnight with primary antibodies: rabbit anti-pCREB (Cell Signaling, catalog 9198, 1:1000) and mouse anti-CaMKIIα 6G9 (Thermo Fisher Scientific, catalog MA1–048, 1:1000). The following day, neurons were washed three times in PBS+0.2% Triton X-100, then incubated with blocking solution for 1 hour with secondary antibodies: donkey anti-rabbit

647 Alexa Fluor 647 (Thermo Fisher Scientific, catalog A-31573) and donkey anti-mouse Alexa Fluor 546 (catalog A-10036). Neurons were washed with PBS three times and mounted on slides using Prolong Gold Antifade Mountant with DAPI.

2.4.4 Neuronal Imaging and Quantification

The experimenter was blinded to the transfection conditions by coding the culture dishes prior to microscopy and image analysis. Images were collected using a Zeiss 880 inverted confocal microscope with a 40x/1.30 Plan-Neofluar oil lens. Non-transfected excitatory neurons were identified by CaMKIIα immunostaining. The binocular lens was used to identify transfected neurons based on EGFP expression from the shRNA construct. In experiments with mAp-Shank3R rescue, mAp expression was also confirmed in EGFP-positive cells. The DAPI channel was then used to focus on the z-plane that yielded the highest DAPI signal (one that presumably runs through the nuclei) for image acquisition. Images were then collected in all channels and MetaMorph Microscope Automation and Image Analysis Software (Molecular Devices, San Jose, CA) was used to quantify pCREB or c-Fos signals. Briefly, nuclei were identified by thresholding the DAPI channel to create and select the nuclear regions of interest (ROIs). The ROIs were then transferred to other channels to measure the average pCREB or c-fos intensity. ROIs were collected from transfected (EGFP-positive) neurons and nearby non-transfected (EGFP-negative) neurons. The relative intensity was calculated as $[(\text{channel}^{x} - \text{channel}^{5K})/(\text{channel}^{40K} - \text{channel}^{5K})]$, where channel^{x} is the signal being calculated, and channel^{5K} and channel^{40K} are the average signals of the 5K and 40K (or 5K+DHPG, when performing DPHG-CREB assays) conditions in that batch of cultured neurons, respectively. Sample size was

calculated based on previous experimental design (Wang et al., 2017b). Data shown were collected from images of the indicated total number of neurons from 3-5 independent cultures.

2.4.5 Ca^{2+} Imaging of Primary Neurons

Dissociated rat hippocampal neurons were cultured in 35-mm glass bottom dishes (Cellvis, catalog D35-10-1.5-N) coated with 2.5 µg/mL laminin (Roche, Basel, Switzerland) and 37.5 µg/mL poly-L-lysine (Sigma), as described previously (Sala et al., 2003). Cultures were transfected with a total of 2.5 µg of DNA/dish after DIV 8, as described above. To allow for Ca^{2+} imaging using Fura-2, shRNA constructs were re-engineered to co-express an mApple fluorescent reporter rather than GFP. Transfected neurons were imaged on DIV 12-14. Cells were incubated for 30 min at 37°C in 5% CO_2 in conditioned culture medium (see above) supplemented with 2 µM Fura-2 acetoxymethyl ester AM (Thermo Fisher Scientific, catalog F1221), then incubated in 5K Tyrode's solution with TTX, APV, and CNQX (see above) for 5 min at 37°C. Cells were incubated in 2.5 mL solution and perifused at a flowrate of 2 mL/min at 32°C with identical buffer for at least 300 seconds then flow was changed to 40K Tyrode's solution with TTX, APV, and CNQX for at least 150 seconds. Intracellular Ca^{2+} was measured every 5 seconds as a ratio of Fura-2 emission (510 nm) by excitation at 340 nm and 380 nm (F_{340}/F_{380}) using a Nikon Eclipse Ti2 microscope equipped with an epifluorescence illuminator (Sutter Instrument, Novato, CA), a Prime 95B equipped with 25 mm CMOS sensors camera (Photometrics Scientific, Tucson, AZ), and Nikon Elements software (Nikon, Melville, NY RRID:SCR_014329). Transfected (mApple positive) cell somas were

selected as regions of interest (ROIs) using Nikon Elements software and Ca^{2+} responses were quantified as a function of time by the change in Fura-2 fluorescence ratio above baseline ($\Delta F = (F_{340}/F_{380}) / (F_{340}/F_{380})_{baseline}$). Daily averages from 12-90 transfected cells for each condition (control/Shank3 shRNA) were generated for 4 independent biological replicates. Areas under the curve (AUC) of the averaged Fura-2 responses during the first 90 seconds of stimulation were quantified as an indicator of the change in intracellular Ca^{2+} for each replicate. Alternatively, we expressed the average ΔF/F0 values in Shank3 shRNA cells as a percentage of average ΔF/F0 values in control cells for each experiment. Averaging normalized data across four experiments revealed a modest 10-20% reduction in Ca^{2+} influx following Shank3 knockdown at each time point following depolarization with p=0.041 for the primary time effect (One-way ANOVA with repeated measures). However, none of the individual time points were significantly different from baseline (Dunnett's multiple comparison test).

CHAPTER III

MOLECULAR DETERMINANTS OF A NOVEL SHANK3-CAMKII BINDING INTERACTION

3.1 Introduction

CaMKII has critical roles in neuronal signaling and plasticity. Ca^{2+}/calmodulin (CaM) binding to 12-subunit CaMKII holoenzymes stimulates inter-subunit autophosphorylation at Thr286 (in CaMKIIα), a key mechanism underlying learning and memory (reviewed in (Hell, 2014; Lisman et al., 2012; Shonesy et al., 2014)). Thr286-autophosphorylated CaMKII can remain autonomously active after the initial Ca^{2+} influx dissipates and Ca^{2+}/CaM dissociates (Lai et al., 1986; Miller and Kennedy, 1986; Miller et al., 1988), leading to sustained phosphorylation of downstream targets. Activated CaMKII also interacts with a number of other synaptic proteins. For example, activated CaMKII binding to NMDA receptor GluN2B subunits is important for CaMKII targeting to dendritic spines and for normal synaptic plasticity (Bayer et al., 2001; Bayer et al., 2006; Halt et al., 2012b; Strack and Colbran, 1998). The neuronal protein densin-180 can bind to both $Ca_V1.3$ LTCCs and CaMKII, thereby suppressing Ca^{2+}-dependent inactivation of $Ca_V1.3$ and facilitating overall Ca^{2+} entry (Jenkins et al., 2010; Jiao et al., 2011). In addition, a recent study showed that CaMKII binding to mGlu5 metabotropic glutamate receptors modulates the mobilization of intracellular Ca^{2+} stores (Marks et al., 2018). This emerging evidence supports the hypothesis that direct interactions of CaMKII with CaMKII-Associated Proteins (CaMKAPs) are important for synaptic signaling.

In a recent proteomics study, we identified Shank3 as one of the most abundant proteins detected in CaMKII complexes isolated from a Triton X-100/deoxycholate-solubilized synapse-enriched subcellular fraction (Baucum et al., 2015). Canonically, the full-length Shank3 protein contains an N-terminal ankyrin repeat domain, SH3 and PDZ domains, a proline-rich region with binding sites for homer and cortactin, and a C-terminal SAM domain that mediates oligomerization (Naisbitt et al., 1999). Diverse mutations in Shank3 are strongly linked to ASD and schizophrenia (Leblond et al., 2014; Soler et al., 2018), while a chromosomal deletion causes haploinsufficiency of the *SHANK3* gene in 22q13 deletion syndrome (Phelan-McDermid Syndrome), another neurodevelopmental disorder associated with ASD (Harony-Nicolas et al., 2015). Indeed, knockdown of Shank3 expression in cultured hippocampal neurons reduces dendritic spine formation and mEPSC frequency (Verpelli et al., 2011), and several unique *Shank3* mutant mouse lines display different combinations of deficits in synaptic transmission, social behavior, and learning (reviewed in (Monteiro and Feng, 2017)).

Here we identify a novel binding site for CaMKII in Shank3 and show that CaMKII activation, either by Ca^{2+}/CaM-binding or Thr286 autophosphorylation, is required for this interaction. Using site-directed mutagenesis, we identified three residues in Shank3 that are critical for this interaction. Mutation of these residues in full-length Shank3 disrupts co-immunoprecipitation and colocalization with CaMKII.

3.2 CaMKIIα and Shank3 Interact in the Mouse Forebrain

Our previous proteomics study detected numerous peptides originating from the Shank3 protein in immunoprecipitated CaMKII complexes isolated from solubilized synaptic fractions of mouse forebrain (Baucum et al., 2015). To extend this observation, we first compared the distribution of Shank3 and CaMKII across cytosolic (S1), Triton-soluble membrane (S2), and Triton-insoluble synaptic (P2) fractions isolated from mouse forebrain extracts. The Shank3 antibody detected two major bands in whole mouse forebrain extracts – the expected ~180 kDa band, plus an ~125 kDa band. Both Shank3 bands were undetectable in S1 or S2 fractions and were relatively enriched in the P2 fraction, similar to other synaptic proteins, such as PSD-95 (Figure 3.1A, *left*). Since *Shank3* undergoes complex transcriptional and post-transcriptional regulation through intragenic promoters and alternative splicing (Waga et al., 2013; Wang et al., 2011), the two bands may represent different Shank3 variants. In contrast, similar levels of CaMKII were detected in the S2 and P2 fractions, with lower levels in S1, consistent with our prior studies (Gustin et al., 2011). Thus, a subpopulation of CaMKII and essentially all of the Shank3 are present in mouse forebrain subcellular fractions enriched in synaptic proteins in wild-type mice.

In order to further investigate the association of Shank3 with CaMKIIα, synaptic P2 fractions were isolated in parallel from wild-type or CaMKIIα-KO littermates (as a negative control) and solubilized by sonication in sodium deoxycholate plus Triton X-100 to at least partially disrupt the postsynaptic density (see Methods), were incubated with a control IgG antibody or a CaMKIIα-specific monoclonal antibody. Immunoblotting confirmed that

CaMKIIα-KO mice do not express CaMKIIα, and revealed that the levels of Shank3 in whole forebrain lysates (both major bands) and the distribution of Shank3 between the S1, S2 and P2 fractions were similar in WT and CaMKIIα-KO mice (Figure 3.1A and 3.1B, *left*). Shank3 was readily detected in CaMKIIα complexes isolated from WT mouse forebrain, but not from CaMKIIα-KO mouse forebrain, and not in any samples isolated using a control IgG (Figure 3.1C). Interestingly, the ratio of the higher and lower molecular weight Shank3 bands was consistently higher in CaMKII immune complexes than in the P2 input, perhaps suggesting that CaMKII preferentially interacts with the larger Shank3 protein. Taken together, these data demonstrate that Shank3 is specifically associated with CaMKIIα complexes in mouse brain extracts.

We next tested for reciprocal co-immunoprecipitation of CaMKIIα with complexes isolated using a Shank3 antibody. Since interactions between CaMKII and other proteins are often enhanced by Thr286 autophosphorylation, we compared the association of CaMKIIα with Shank3 in solubilized synaptic P2 fractions isolated from WT mice and CaMKIIα^{T286A} mice with a knock-in mutation of Thr286 to Ala, preventing CaMKII regulation by Thr286 autophosphorylation (Giese et al., 1998). Immunoblotting confirmed that whole forebrain lysates from WT and CaMKIIα^{T286A} mice contain similar total levels of CaMKIIα and Shank3 (both major bands) (Figure 3.1B, *right*). Moreover, the distribution of Shank3 between S1, S2 and P2 fractions was similar in WT and CaMKIIα^{T286A} mice (Figure 3.1A), although CaMKIIα was partially re-distributed from P2 to S2 fractions from CaMKIIα^{T286A} (Figure 3.1A), as previously reported (Gustin et al, 2011). Shank3 immune complexes isolated from WT and CaMKIIα^{T286A} mice contained similar levels of Shank3, but there

was a substantial reduction in levels of co-immunoprecipitated CaMKIIα from CaMKIIα^{T286A} compared to WT tissue (Figure 3.1D, compare CaMKIIα signal in lanes 5 and 6) (93±4% reduced compared to WT, p=0.0008, one sample Student's t-test with equal variance compared to the theoretical normalized WT value of 100, *n* = 3). In combination, these data indicate that Shank3 interacts directly or indirectly with CaMKII in deoxycholate-solubilized synaptic fractions of mouse brain, and that this association is regulated by Thr286 autophosphorylation of CaMKII.

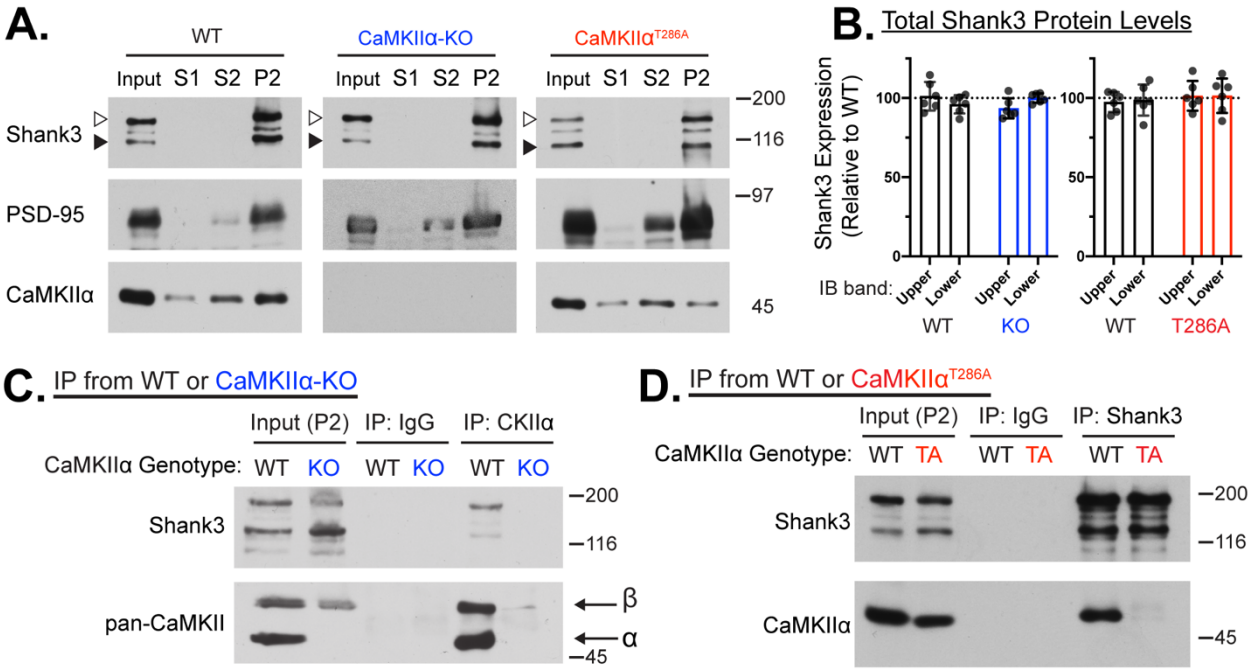

Figure 3.1: Reciprocal co-immunoprecipitation of Shank3 and CaMKIIα from mouse forebrain extracts.

A. Whole forebrain lysates (Input), cytosolic (S1), membrane-associated (S2), and synaptic (P2) subcellular fractions from wild-type, CaMKIIα-KO, and CaMKIIα^{T286A} mice were immunoblotted for localization of Shank3 (Cell Signaling antibody), PSD-95, and CaMKIIα. The Shank3 antibody detected two bands of (open and solid arrowheads) that are primarily localized in P2 fractions, which were also enriched for CaMKIIα. **B**. The upper and lower Shank3 bands in whole forebrain lysates from WT and CaMKIIα-KO mice (left) or WT and CaMKIIα^{T286A} mice (right) were

quantified. Signals were corrected for protein loading based on Ponceau stained membranes and normalized to the levels of the upper Shank3 band in WT samples. **C.** Synaptic (P2) fractions from WT or CaMKIIα-KO mouse forebrains were immunoprecipitated using control IgG or CaMKIIα-specific antibodies, and immunoblotted using Shank3 (Cell Signaling antibody) and pan-CaMKII antibodies. The CaMKIIα and CaMKIIβ bands are indicated by arrows. CaMKIIα and co-immunoprecipitated Shank3 were not detected in samples isolated from CaMKIIα-KO mice. **D.** Synaptic (P2) fractions from WT or CaMKIIα^{T286A} mouse forebrains were immunoprecipitated using control IgG or Shank3 (Bethyl) antibodies, and immunoblotted using Shank3 (Cell Signaling) and CaMKIIα antibodies. The levels of co-precipitated CaMKIIα from CaMKIIα^{T286A} mice were significantly reduced (93±4% reduction in lane 6 compared to lane 5, n=3, $p < 0.001$, one sample Student's t-test with equal variance compared to theoretical value of 100). All immunoblots are representative of ≥3 biological replicates.

3.3 Thr286-Autophosphorylated CaMKIIα Directly Binds to Shank3 (829-1130)

To determine whether CaMKIIα directly interacts with Shank3, we first expressed and purified a series of six non-overlapping GST fusion proteins spanning the full length of Shank3 (Figs. 3.2A, 3.2B). Some of the purified proteins contained proteolytic degradation fragments and the full-length proteins are denoted by asterisks in Figure 3.2B. Since co-immunoprecipitation of CaMKIIα with Shank3 from brain extracts was strongly reduced in the absence of Thr286 autophosphorylation, each purified GST fusion protein was incubated with purified Thr286-autophosphorylated CaMKIIα and complexes were isolated using glutathione agarose. A GST fusion protein containing the CaMKII-binding domain of the NMDA receptor GluN2B subunit (residues 1260-1309), a well-established CaMKAP (Strack and Colbran, 1998), was used as a positive control. Similar amounts of activated CaMKIIα bound to a GST-Shank3 fusion protein containing residues

829-1130 (GST-Shank3 #4 in Figure 3.2) and to GST-GluN2B, but there was no consistently detectable interaction with any other Shank3 fragment (Figure 3.2B).

CaMKII is initially activated by Ca^{2+}/CaM-binding alone followed by Thr286-autophosphorylation, which is sufficient to maintain the activated conformation even following dissociation of Ca^{2+}/CaM. Since CaMKAPs display distinct preferences for binding to various active and inactive conformations of CaMKII, we tested the binding of different CaMKIIα conformations to GST-Shank3 (829-1130) in parallel (Figure 3.2C). Pre-activation of CaMKII is essential for binding to GST-Shank3 (829-1130), because there was no interaction with inactive kinase (Figure 3.2C). Inactive CaMKIIα also did not bind to any other GST-Shank3 proteins compared to GST negative control (data not shown). GST-Shank3 (829-1130) bound to the active conformations of CaMKIIα induced by Ca^{2+}/CaM-binding alone or by Thr286 autophosphorylation, but Ca^{2+}/CaM-binding alone supported substantially reduced binding (23±5%; mean ± SEM). In combination, these data show that activated CaMKIIα can directly bind to a central, poorly characterized domain in the Shank3 protein, and that Thr286 autophosphorylation significantly enhances the interaction.

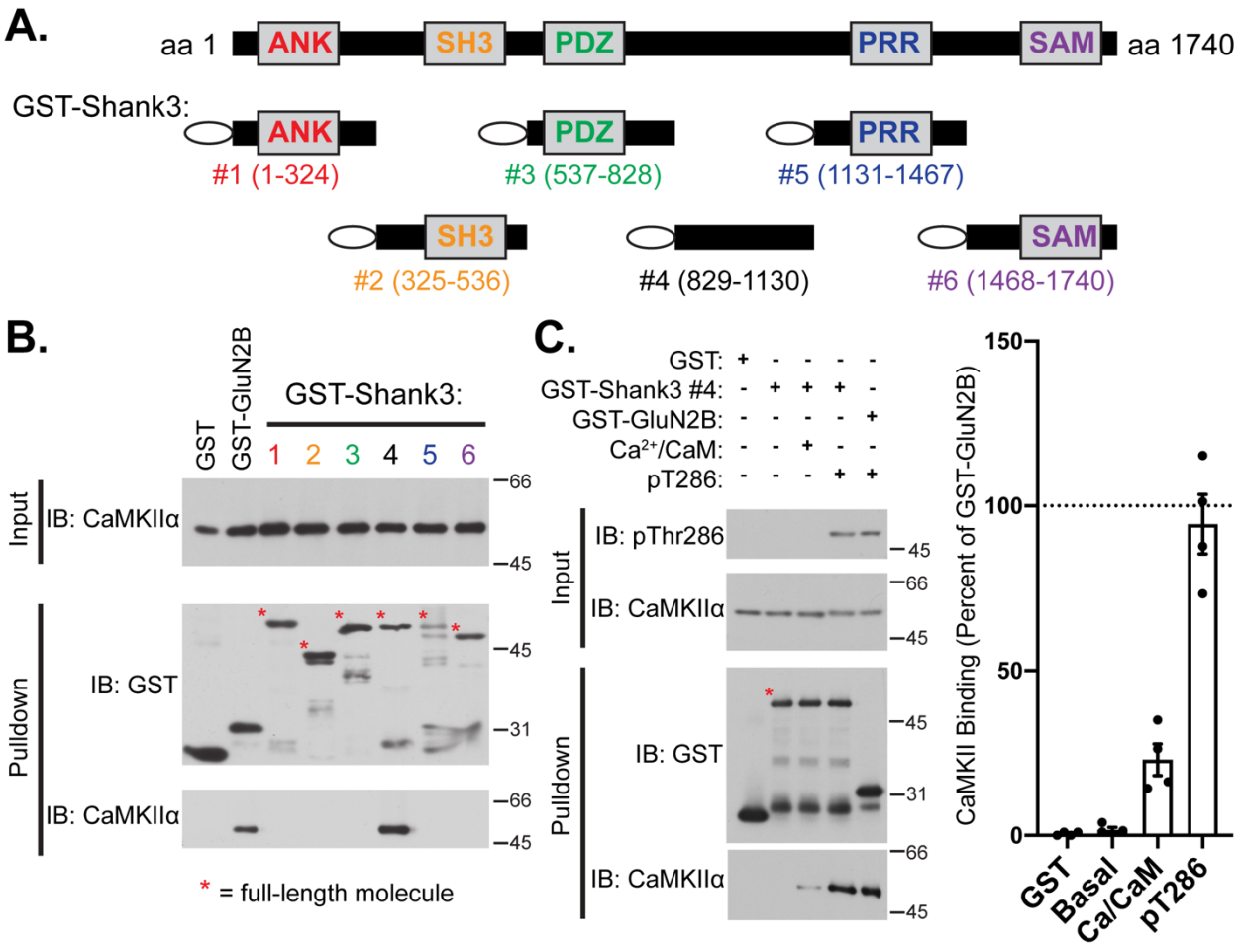

Figure 3.2. T286-phosphorylated CaMKIIα specifically binds to Shank3 (829-1130).

A. Domain structure of full-length Shank3 and the six GST-Shank3 fusion proteins used in these studies that span the entire Shank3 protein. Canonical Shank3 domains are depicted as gray boxes with residue numbers listed in parentheses. ANK = ankyrin-rich repeats, SH3 = Src homology 3 domain, PDZ = PSD95/Dlg1/zo-1 domain, PRR = proline-rich region containing binding sites for Homer and Cortactin, SAM = Sterile alpha motif involved in multimerization of Shank3. **B.** Glutathione agarose co-sedimentation assay shows that pre-activated (Thr286-autophosphorylated) CaMKIIα specifically binds to GST-Shank3 #4 (829-1130) and positive control GST-GluN2B (1260-1309). Full-length GST fusion proteins denoted with asterisks on the GST immunoblot. **C.** Glutathione agarose co-sedimentation assay shows that, in the absence of Ca^{2+}/CaM-binding or Thr286 autophosphorylation, CaMKIIα (Basal) does not bind to GST-Shank3 #4; *in vitro* binding of CaMKIIα is partially supported by Ca^{2+}/CaM-binding (Ca/CaM), and maximally enhanced by pT286-autophosphorylation. The bar graph reports levels of each form of CaMKII bound to GST-Shank3 #4 (or the GST negative control) (mean ± SEM) relative to levels

of pT286-CaMKIIα binding to GST-GluN2B. Immunoblots are representative of 3-4 biological replicates.

3.4 A Shank3 Tri-basic Residue Motif is Required for CaMKII Binding

Residues 829-1130 of Shank3 connect the canonical PDZ domain to the proline rich motif, and the functional role(s) of this region is poorly understood (Naisbitt et al., 1999; Tu et al., 1999). In order to identify CaMKII-binding determinants within this domain, we initially generated and purified three smaller GST-Shank3 fusion proteins (Figure 3.3A). Similar amounts of Thr286-autophosphorylated CaMKII bound to GST-Shank3 (931-1014) (protein 4b in the figure) and GST-Shank3 (829-1130), but there was no detectable interaction with GST-Shank3 proteins containing residues 829-930 (protein 4a) or residues 1015-1130 (protein 4c) (Figure 3.3B). Examination of the amino acid sequence of Shank3 residues 931-1014 revealed a region sharing some similarity with recently-characterized CaMKII binding domains in the N-terminal domain of the LTCC $Ca_V1.3$ α subunit (Wang et al., 2017b) and the C-terminal domain of mGlu5 (Marks et al., 2018) (Figure 3.3A). Since mutation of the tri-basic residue motifs in $Ca_V1.3$ (^{83}Arg-Lys-Arg^{85}) and mGlu5 (^{866}Lys-Arg-Arg^{868}) prevented CaMKIIα binding, we mutated the conserved Shank3 ^{949}Arg-Arg-Lys^{951} motif to Ala residues within GST-Shank3 (829-1130). This RRK/AAA mutation essentially abrogates the binding of Thr286-autophosphorylated CaMKIIα (Figure 3.3C). These data indicate that ^{949}Arg-Arg-Lys^{951} in Shank3 are essential for the direct binding of Thr286-autophosphorylated CaMKII *in vitro*.

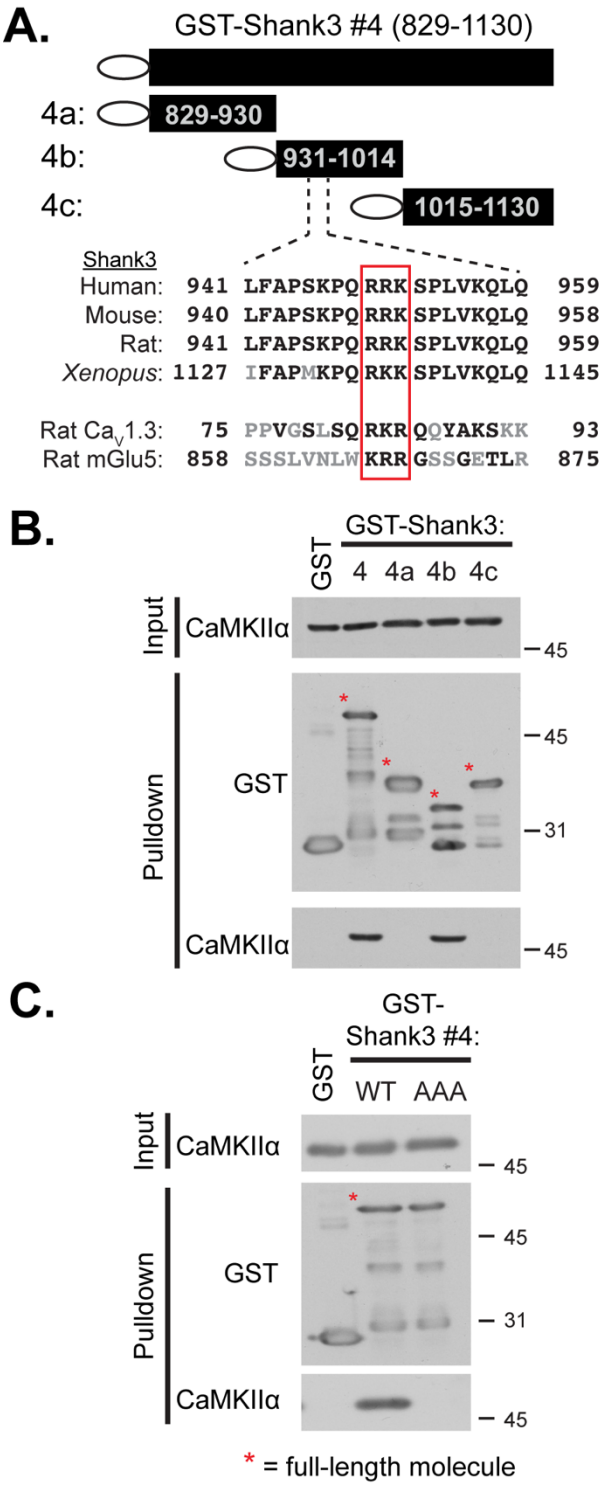

Figure 3.3. Characterization of the CaMKII-binding motif in Shank3.

A. *Top,* Diagram of 3 truncations used to map the CaMKII interaction site within GST-Shank3 #4 (829-1130). *Bottom*, Sequence alignment of human Shank3 residues 941-959 with the corresponding Shank3 residues in other species and the CaMKII-binding domain in the N-terminal

domain of the *Rattus norvegicus* $Ca_V1.3$ $\alpha1$ subunit (Wang et al., 2017b) and the C-terminal tail of the *Rattus norvegicus* mGlu5 (Marks et al., 2018), with conserved residues in black and dissimilar residues in grey. The conserved tri-basic residue motif is highlighted in red box. **B.** Glutathione agarose co-sedimentation assay comparing binding of activated CaMKIIα to GST-Shank3 #4 (829-1130) and 3 non-overlapping fragments (4a, 4b, and 4c). Full-length GST fusion proteins denoted with asterisks. GST-Shank3 #4 (829-1130) and #4b (931-1014) bind similar amounts of pT286-autophosphorylated CaMKIIα, but there is no detectable binding to the other Shank3 fragments. **C.** Mutation of amino acids ^{949}RRK^{951} to AAA in GST-Shank3 #4 (829-1130) blocks CaMKIIα binding in glutathione agarose co-sedimentation assay (98±4% reduced compared to WT, n=3, $p < 0.001$, one sample Student's t-test with equal variance compared to theoretical value of 100). All immunoblots are representative of 3 biological replicates.

3.5 The RRK/AAA Mutation of Full-Length Shank3 Disrupts Binding to CaMKII but not to $Ca_V1.3$

In order to determine whether the ^{949}Arg-Arg-Lys^{951} motif is essential for association of CaMKII with full-length Shank3, we generated the RRK/AAA mutant in GFP-tagged full-length Shank3 (GFP-Shank3-AAA). CaMKIIα was co-expressed with GFP, GFP-Shank3-WT, or GFP-Shank3-AAA in HEK293T cells. Excess Ca^{2+}/CaM was added to the cell lysates to activate CaMKIIα and a GFP antibody was used for immunoprecipitation. Similar robust GFP protein signals were detected in samples immunoprecipitated from each lysate; CaMKIIα was detected in immune complexes containing GFP-Shank3-WT, but not GFP negative control or GFP-Shank3-AAA complexes (Figure 3.4A). Thus, the ^{949}Arg-Arg-Lys^{951} motif in Shank3 is required for CaMKIIα association.

To test whether the RRK/AAA mutation has broader effects on protein binding to Shank3, we performed a similar co-immunoprecipitation experiment using an HA-tagged C-

terminal domain (CTD) of the L-type calcium channel $Ca_V1.3$ α subunit, which can interact with the nearby PDZ domain (residues 572-661) of Shank3 (Zhang et al., 2005). Lysates of HEK293T cells expressing the HA-$Ca_V1.3$-CTD and either GFP, GFP-Shank3-WT, or GFP-Shank3-AAA were immunoprecipitated using a GFP antibody. Similar amounts of the HA-$Ca_V1.3$-CTD co-immunoprecipitated with both GFP-Shank3-WT and GFP-Shank3-AAA immune complexes, but not with GFP alone (Figure 3.4B). Thus, the interaction of $Ca_V1.3$ with Shank3 is not affected by mutation of the ^{949}Arg-Arg-Lys^{951} motif, indicating that this mutation does not have broader (non-specific) effects on the interactions of other proteins with GFP-Shank3.

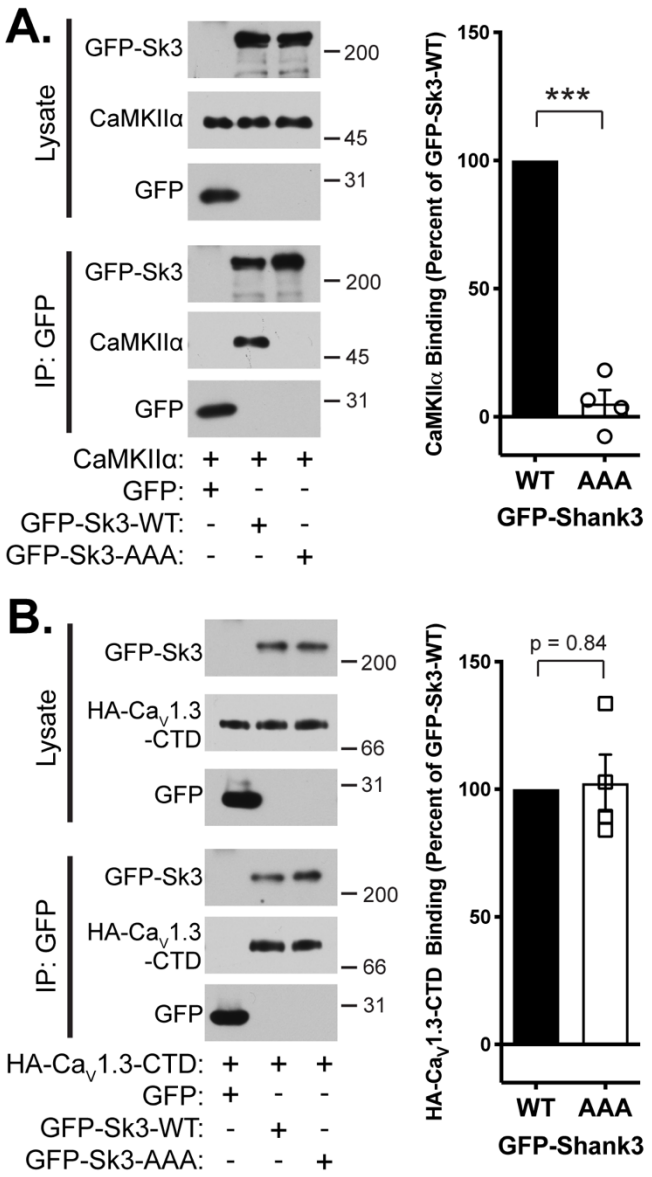

Figure 3.4. A Shank3 ^{949}RRK^{951} to AAA mutation disrupts association with CaMKIIα, but does not with the $Ca_V1.3$ C-terminal domain.

A. Soluble fractions of HEK293T cells expressing CaMKIIα with GFP or GFP-Shank3 (WT or ^{949}RRK^{951} to AAA mutant) were immunoprecipitated using a GFP antibody. Co-precipitation of CaMKIIα with GFP-Shank3-AAA is significantly reduced by 95±10% compared to GFP-Shank3-WT (*** $p < 0.001$, one-sample Student's t-test with equal variance compared to a theoretical value of 100). **B.** Soluble fractions of HEK293T cells expressing GFP or GFP-Shank3 (WT or AAA) with the HA-tagged C-terminal domain of the $Ca_V1.3$ α1 subunit (HA-$Ca_V1.3$-CTD), were immunoprecipitated as in panel A. The AAA mutation has no significant effect on the co-

precipitation of HA-Ca_V1.3-CTD ($p = 0.84$). All immunoblots are representative of 4 biological replicates. Bar graphs show the mean ± SEM.

3.6 Co-localization of Fluorescent CaMKII and Shank3 in Striatal Progenitor Cells

To investigate whether Shank3 interacts with CaMKIIα in intact cells, we performed a series of colocalization experiments in ST*Hdh*$^{+/+}$ cells. This striatal progenitor cell line can be pharmacologically-induced to initiate a neuronal differentiation program (see Methods), extending neurite-like outgrowths containing microtubule-associate protein 2, a dendritic marker (Trettel et al., 2000). However, ST*Hdh*$^{+/+}$ cells do not express detectable levels of endogenous Shank3 or CaMKIIα before or after differentiation (Figure 3.5A, *left* and *center*). Therefore, they represent an excellent heterologous cell model to explore the colocalization of Shank3 and CaMKIIα in a neuron-like environment, without potentially confounding effects of high levels of endogenous CaMKIIα, Shank3 or other CaMKAPs that might compete for the interactions of the expressed proteins.

Since our *in vitro* studies indicate that CaMKII activation and Thr286 autophosphorylation is a critical modulator of Shank3 binding, we first investigated colocalization of GFP-Shank3-WT with either mAp-CaMKIIα-WT, mAp-CaMKIIα-T286D (phospho-mimetic), or mAp-CaMKIIα-T286A (phospho-null) in fixed, differentiated cells. GFP-Shank3-WT (green channel) was concentrated in puncta in the soma and in neurite-like outgrowths (Figure 3.5B), but the appearance of the mApple fluorescence (magenta) varied with the CaMKIIα Thr286 mutation. Signals from mAp-CaMKIIα-WT and CaMKIIα-T286D displayed punctate characteristics in the soma and in neurite-like outgrowths that appeared to partially overlap with GFP-Shank3-WT punctae, whereas the signal from

mAp-CaMKIIα-T286A was generally diffuse throughout the cell and the limited number of visible punctae did not align with GFP-Shank3-WT punctae (Figure 3.5B, see inset images of neurite-like outgrowths). To provide an unbiased assessment of the colocalization of the mApple and GFP signals across multiple cells, we analyzed images of whole transfected cells using image correlation analysis, which quantifies colocalization on an ICQ scale from -0.5 (mutually exclusive signals) to +0.5 (perfect colocalization), with 0 representing random overlap (Li et al., 2004). The ICQ values for overlap of GFP-Shank3-WT with mAp-CaMKIIα-WT, mAp-CaMKIIα-T286D, and mAp-CaMKIIα-T286A were 0.29±0.02, 0.36±0.02, and 0.17±0.02, respectively (Figure 3.5C). These data confirm that mAp-CaMKIIα-WT and mAp-CaMKIIα-T286D significantly colocalized with GFP-Shank3-WT in these cells, whereas the colocalization of mAp-CaMKIIα-T286A with GFP-Shank3-WT was much weaker ($p<0.0001$). The unexpectedly robust colocalization of mAp-CaMKIIα-WT with GFP-Shanks3-WT may be explained by the observation that mAp-CaMKIIα-WT is significantly phosphorylated at Thr286 in ST*Hdh*$^{+/+}$ cells under these conditions (Figure 3.5A, *right*). Taken together, these data show that Shank3 colocalization with CaMKII in intact cells is sensitive to Thr286 modification, commensurate with our biochemical data (Figure 3.2C).

If the colocalization of mAp-CaMKIIα-WT with GFP-Shank3 requires the direct interaction that we identified *in vitro*, the RRK/AAA mutation in the central domain of Shank3 should interfere with colocalization. Therefore, a second series of studies compared the colocalization of mAp-CaMKIIα-WT with GFP-Shank3-WT or GFP-Shank3-AAA; as an additional negative control, we examined the colocalization of soluble mApple with GFP-

Shank3-WT (Figure 3.5D). GFP-Shank3-WT and GFP-Shank3-AAA adopted a punctate localization pattern similar to that observed in Figure 3.5B. However, mAp-CaMKIIα-WT overlapped with GFP-Shank3-WT punctae, but not GFP-Shank3-AAA (Figure 3.5D, compare *top* to *center*). The soluble mApple diffusely filled the cell, with minimal overlap with GFP punctae (Figure 3.5D, *bottom*). This qualitative assessment was confirmed by image correlation analysis, with ICQ values for overlap of 0.31±0.02, 0.07±0.01 and 0.09±0.02. respectively (Figure 3.5E). These data indicate that the colocalization of mAp-CaMKIIα-WT with GFP-Shank3-WT punctae in intact cells is disrupted by the RRK/AAA mutation that we have shown disrupts the direct interaction of CaMKII with Shank3 *in vitro*.

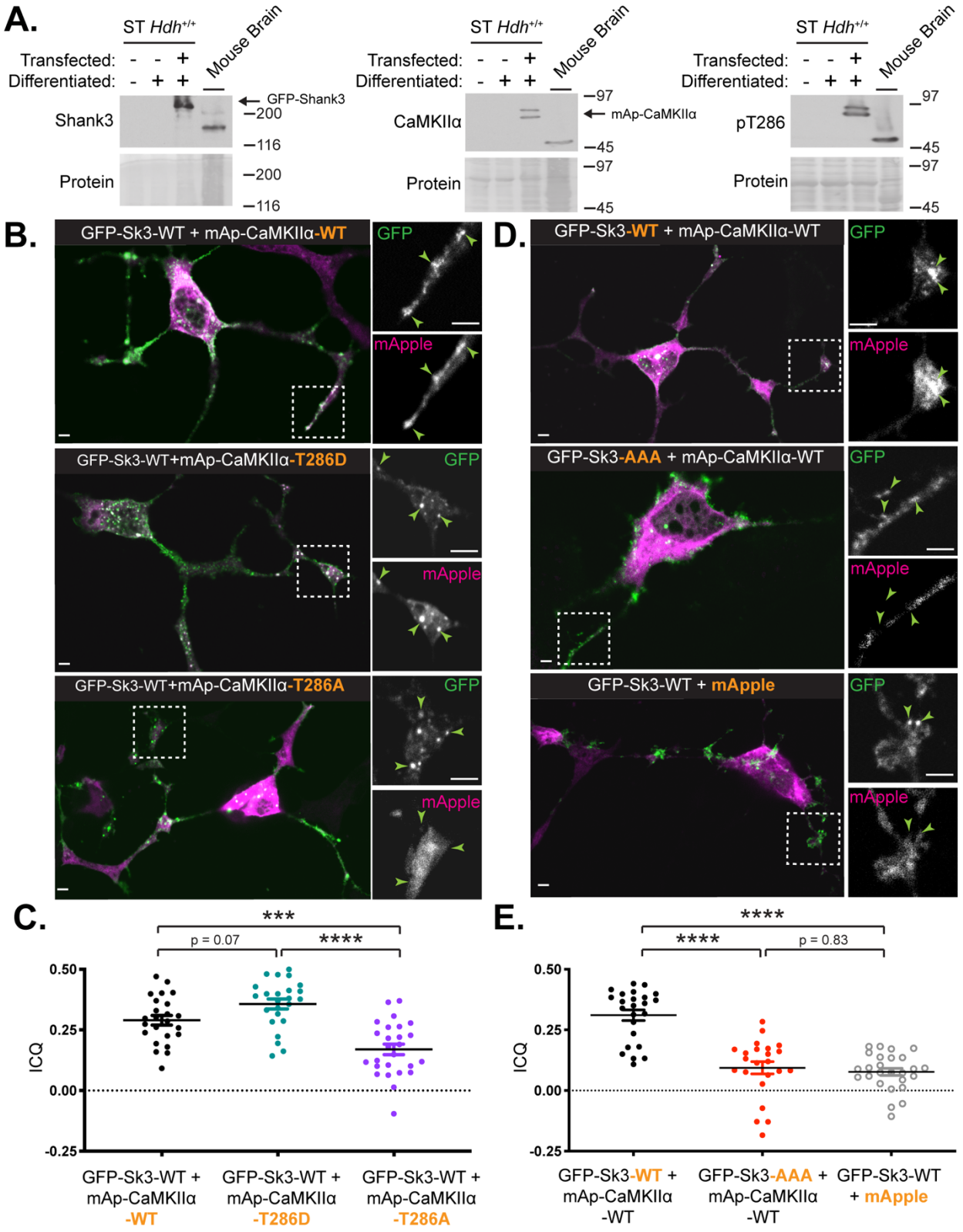

Figure 3.5. Shank3 ^{949}RRK^{951} to AAA mutation disrupts colocalization of activated CaMKIIα.

A. Immunoblots of undifferentiated, differentiated, and transfected/differentiated ST*Hdh*$^{+/+}$ cells, with a wild-type mouse forebrain lysate as positive control. Shank3 and CaMKIIα are not expressed in non-transfected ST*Hdh*$^{+/+}$ cells, and transfected mApple-tagged CaMKIIα (mAp-CaMKIIα) is T286-phosphorylated. **B**. Representative images of differentiated ST*Hdh*$^{+/+}$ cells expressing GFP-Shank3-WT with mAp-CaMKIIα-WT (left), mAp-CaMKIIα-T286D (center), or mAp-CaMKIIα-T286A (right). Inset images show regions (dash-lined box) of the processes containing punctate GFP signals (arrowheads) that overlap with mApple signal from CaMKIIα-WT and -T286D, but not -T286A. **C**. Intensity correlation analysis quantifying the colocalization of GFP and mAp signals in transfected and differentiated ST*Hdh*$^{+/+}$ cells in panel B. Each data point represents an ICQ value from a single cell, with 7-12 cells analyzed from each of 3 independent cultures/transfections. ICQ values for GFP-Shank3-WT and either mAp-CaMKIIα-WT (mean±SEM: 0.29±0.02) or mAp-CaMKIIα-T286D (0.36±0.02) were significantly more colocalized compared to mAp-CaMKIIα-T286A (0.17±0.02) (1-way ANOVA, $F_{(2,71)} = 21.35$, $p < 0.0001$. Tukey's post-hoc test, *** $p < 0.001$, **** $p < 0.0001$). **D**. Representative images of differentiated ST*Hdh*$^{+/+}$ expressing GFP-Shank3-WT or GFP-Shank3-AAA with soluble mAp or mAp-CaMKIIα-WT. Inset images show expanded regions of the processes, as in panel B. **E**. Intensity correlation analysis quantifying the colocalization of GFP and mAp signals in transfected and differentiated ST*Hdh*$^{+/+}$ cells in panel C. GFP-Shank3-WT and mAp-CaMKIIα-WT (0.31±0.02) are significantly more colocalized than GFP-Shank3-WT and mAp (0.07±0.01) or GFP-Shank3-AAA and mAp-CaMKIIα (0.09±0.02) (1-way ANOVA, $F_{(2,70)} = 39.55$, $p < 0.0001$. Tukey's post-hoc test, **** $p < 0.0001$). All scale bars in panels B and D: 2.5 μm.

3.7 Discussion

We recently used a proteomics approach to show that synaptic CaMKII complexes immunoprecipitated from mouse forebrain contain many other proteins, including substantial amounts of Shank3, a synaptic scaffolding protein (Baucum et al., 2015). In addition, we found that complexes containing Shank3 and CaMKII can be co-immunoprecipitated from transfected HEK293T cells (Stephenson et al., 2017). However, the co-immunoprecipitation of two proteins may arise from direct or indirect interactions

of the proteins involved. Here, we explicitly demonstrate a direct interaction between purified Shank3 and purified CaMKII and define its regulation by CaMKII activation. Thr286-autophosphorylated CaMKIIα robustly and directly binds to a central domain in Shank3 with no previously defined biochemical or physiological function, and mutation of three basic residues within this domain to Ala (AAA mutation) largely prevents binding. Moreover, *in vitro*, this Shank3 domain binds weakly to CaMKIIα activated only by Ca^{2+}/calmodulin-binding. The colocalization of CaMKII with Shank3 in intact cells is regulated by CaMKII activation and disrupted by the AAA mutation, concordant with our *in vitro* findings. Moreover, the strong co-immunoprecipitation of CaMKIIα with Shank3 from mouse forebrain extracts is largely abrogated by a knock-in Thr286 to Ala mutation, showing that CaMKIIα Thr286 autophosphorylation is required for robust CaMKII-Shank3 interactions *in vivo*.

CaMKII has diverse physiological functions, in part due to its regulation by different CaMKAP interactions. Like Shank3, most CaMKAPs preferentially bind activated CaMKII conformations, induced by either Ca^{2+}/CaM-binding and/or Thr286 autophosphorylation. Therefore, CaMKII activation acts as a switch to stimulate Shank3 binding. Interestingly, Shank3 selectivity for different activated conformations of CaMKII differs from that of GluN2B subunits of the NMDA receptor. Ca^{2+}/CaM binding alone is insufficient for GluN2B binding but partially supports interactions with Shank3 and densin, relative to Thr286 autophosphorylated CaMKIIα (Jiao et al., 2011; Robison et al., 2005a; Wang et al., 2017b). While the physiological significance of these differences is unclear, they presumably reflect subtle variations in how these CaMKAPs interact with CaMKIIα. In this

regard, it is interesting to note that CaMKII-binding domains of activation-dependent CaMKAPs can be sub-classified based on sequence homology. CaMKII-binding domains in GluN2B subunits and LTCC β1/2 subunits share sequence homology with the auto-regulatory domain surrounding the Thr286 autophosphorylation site of CaMKIIα itself (Grueter et al., 2008; Strack et al., 2000a). However, the sequence of an internal CaMKII-binding domain in densin, another synaptic scaffolding protein, is distinct, resembling that of the naturally-occurring CaMKII inhibitor protein CaMKIIN (Jiao et al., 2011). Furthermore, recently identified CaMKII-binding domains in LTCC $Ca_V1.2$ and $Ca_V1.3$ α1 subunits and the mGlu5 metabotropic glutamate receptor contain critical tri-basic residue motifs (Marks et al., 2018; Wang et al., 2017b), similar to that in Shank3 identified here (Figure 3.3). However, the tri-basic residue motif alone is insufficient for CaMKII binding, because Thr286-autophosphorylated CaMKIIα does not bind two GST-Shank3 proteins (#3 and #4a) that contain tri-basic sequences (^{707}Arg-Arg-Lys^{709} and ^{919}Lys-Arg-Arg^{921}, respectively) (Figs. 3.2B, 3.3B). Further studies will be needed to explore contributions of residues surrounding the tri-basic binding motifs, and perhaps secondary or tertiary structure, to CaMKII binding with Shank3.

It is well established that activated CaMKII and Shank3 are highly enriched in dendritic spines (Boeckers et al., 2005; Shen and Meyer, 1999), and are also found in complexes containing NMDA receptors and other CaMKAPs (Naisbitt et al., 1999). Since dendritic spines contain several CaMKAPs, it can be difficult to discern their individual contributions to modulating CaMKII localization and function. However, knock-in mutations of GluN2B subunits of the NMDA receptor in mice that block CaMKII binding reduce the amount of

CaMKII in postsynaptic densities and impair both synaptic plasticity and memory recall (Halt et al., 2012b). While Shank3 knockdown has been shown to disrupt NMDAR-mediated postsynaptic currents and DHPG-induced long-term depression (Duffney et al., 2013; Verpelli et al., 2011), the roles of specific protein interactions with Shank3 are poorly understood. We posit that one of the functions of Shank3 is to target a subpopulation of CaMKII holoenzymes to specific postsynaptic complexes.

CHAPTER IV

CAMKII PHOSPHORYLATION OF SHANK3: IDENTIFICATION OF PHOSPHORYLATION SITES *IN VITRO*

4.1 Introduction

The scaffolding protein Shank3 interacts directly or indirectly with receptors, ion channels, cytoskeletal proteins, and signaling molecules to regulate their targeting and anchoring to postsynaptic densities and dendritic spines in excitatory neurons (Monteiro and Feng, 2017; Sala et al., 2001). These interactions are mediated by well-defined binding domains in Shank3, including multiple ankyrin repeats, SH3 and PDZ domains, a novel CaMKII binding motif, distinct proline-rich regions for binding to ABI1, homer, and cortactin, and a C-terminal SAM domain (Du et al., 1998; Naisbitt et al., 1999; Perfitt et al., 2019; Proepper et al., 2007; Tu et al., 1999). Mutations in the *SHANK3* gene are often linked to neurodevelopmental and neuropsychiatric disorders, such as autism spectrum disorder (ASD) (Durand et al., 2006). Moreover, disruptions of Shank3 expression in multiple mouse models result in deficits in synaptic transmission, abnormal neuronal morphology, and diverse behavioral phenotypes (Wang et al., 2014; Zhou et al., 2015). Since phenotypes of these mouse models vary with the specific *Shank3* mutation, which often target different exons, understanding physiological signaling mechanisms coupled to different regions of Shank3 will provide better targeted therapy for Shank3-related neuropsychiatric disorders.

Chapter III identified Shank3 as a CaMKAP (CaMKII-Associated Protein). As described in Chapter I, many CaMKAPs are also phosphorylated substrates. Phosphorylation may occur directly at the CaMKII binding site, affecting the protein-protein interaction, or at other residues of the protein to regulate separate functions. As Shank3 is a large protein containing many Ser/Thr residues, we hypothesized that CaMKII might be able to phosphorylate Shank3. Therefore, we sought to generate a list of putative phosphorylation sites using mass spectrometry and validate these findings using phospho-null point mutants.

4.2 CaMKII Phosphorylates Multiple Residues *In Vitro*

To first test for CaMKII phosphorylation of Shank3, we used a library of non-overlapping GST-tagged fusion proteins. These proteins were separately incubated with purified CaMKIIα and radiolabeled [γ-^{32}P] ATP. A GST fusion protein containing residues 1269-1309 of the GluN2B subunit of the NMDA receptor, which is phosphorylated by CaMKII at Ser1303, was included as a positive control. To improve the chance of detecting robust CaMKII substrates that are more likely to be physiologically relevant, proteins were incubated for a relatively short period (2 min) before reactions were stopped. Proteins were run on a gel, stained, and then exposed to film to detect ^{32}P incorporation (Figure 4.1). We detected robust ^{32}P incorporation in GST-Shank3 #2 (325-536) and GST-Shank3 #3 (537-828), which contain the SH3 and PDZ domains, respectively. These proteins had a stronger 32P incorporation than GST-GluN2B, which contains exactly 1 phosphorylation site at Ser1303. Therefore, we hypothesized that these GST-Shank3 fusion proteins contain multiple phosphorylated residues. Weaker signal was observed

with GST-Shank3 #6 (1468-1740), and a weaker and less consistent signal was observed with GST-Shank3 #4 (829-1130) which contains the CaMKII binding motif (see Figure 3.2). No phosphorylation was observed on our GST negative control, GST-Shank3 #1 (1-324), or GST-Shank3 #5 (1131-1467).

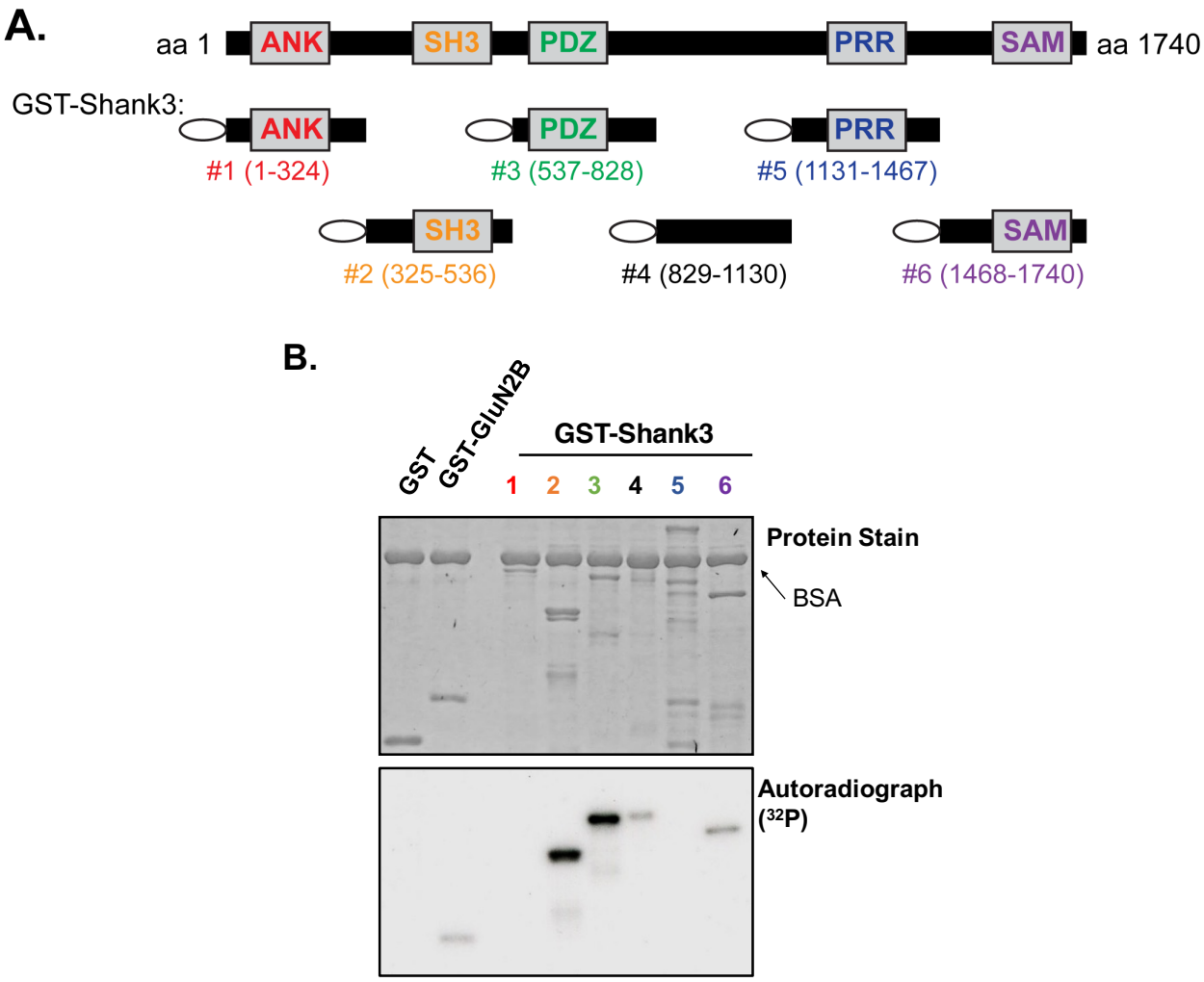

Figure 4.1: CaMKII phosphorylates multiple GST-Shank3 fusion proteins *in vitro*.

A. Diagram of GST-Shank3 fusion proteins used for phosphorylation studies, same as Figure 3.2. **B.** After incubation with CaMKII and [γ-^{32}P] ATP, GST-Shank3 proteins were run on SDS-PAGE gel, stained (top), and exposed to film to determine ^{32}P incorporation (bottom). GST and GST-GluN2B are negative and positive controls, respectively. Robust ^{32}P incorporation is seen in GST-

Shank3 #2 (325-536) and 3 (537-828), with weaker signals in #4 (829-1130) and 6 (1468-1740). Representative of at least 3 replicates.

4.3 Identification of Phosphorylated Residues by Mass Spectrometry

To identify the multiple CaMKII phosphorylation sites detected by autoradiography, we utilized a mass spectrometry approach to generate phospho-proteomics data. GST-Shank3 fusion proteins (325-536), (537-828), (829-1130), and (1468-1740), the four truncations that demonstrated ^{32}P incorporation in Figure 4.1, were heavily phosphorylated by CaMKII with non-radiolabeled ATP for a longer time period (25 min) in an effort to bolster signal from weakly phosphorylated sites. These proteins were then submitted to the Vanderbilt Mass Spectrometry Core for spectral analysis. The findings of this study are summarized in Table 4.1.

GST-Shank3 (325-536)			
45% Sequence Coverage			
Amino Acid	Shank3b Residue	Phosphorylated Spectral Counts	Detected *In Vivo*
Ser	361	18%	-
Ser	373	60%	+
Ser	375	20%	+
Thr	391	1.2%	-
Ser	421	9%	-
Ser	436	10%	+

GST-Shank3 (325-536)			
63% Sequence Coverage			
Amino Acid	Shank3b Residue	Phosphorylated Spectral Counts	Detected *In Vivo*
Thr/Ser	551/557	77%	+ (557)
Ser	685	65%	+
Ser	694	59%	+
Thr	724	2%	-
Thr	779	<1%	+
Ser	781	69%	+
Ser	801	43%	+

GST-Shank3 (829-1130)			
64% Sequence Coverage			
Amino Acid	Shank3b Residue	Phosphorylated Spectral Counts	Detected *In Vivo*
Ser/Thr	873/875	7%	-
Ser	891	60%	+
Ser	898	40%	+
Ser/Ser	938/940	30%	-
Ser	973	1%	-
Ser	980	17%	-
Ser/Ser	1000/1001	8%	+ (1000)
Thr	1008	7%	+

GST-Shank3 (1468-1740)			
87% Sequence Coverage			
Amino Acid	Shank3b Residue	Phosphorylated Spectral Counts	Detected *In Vivo*
Ser	1472	15%	+
Ser	1481	2%	-
Ser	1511	63%	+
Ser	1548	<1%	-
Ser	1549	20%	-
Ser	1554	3%	-
Ser	1555	<1%	-
Ser	1570	3%	-
Ser	1587	<1%	-
Ser	1593	50%	-
Thr	1617	1%	-
Ser	1622	<1%	-
Ser	1623	61%	-
Ser	1654	<1%	-

Table 4.1: Putative CaMKII phosphorylation sites identified by mass spectrometry.

Phosphorylated serine or threonine residues from four GST-Shank3 fusion proteins after incubation with CaMKII. Quantification of phosphorylated spectral counts measures the relative abundance of a phosphorylated peptide compared to the total abundance of the peptide. Rows with two residues listed indicate that the exact phosphorylation site was unable to be identified. Data for *in vivo* mass spectrometry from (Huttlin et al., 2010; Wang et al., 2019b). Data from one technical replicate.

Our proteomics data contained six putative sites on GST-Shank3 #2 (325-536), 7-8 sites on GST-Shank3 #3(537-828), 8-11 sites on GST-Shank3 #4 (829-1130), and 14 sites on GST-Shank3 #6 (1468-1740). Some peptides contained multiple serine/threonine residues and we were unable to precisely define which residue was phosphorylated. In addition, we observed a wide range of relative levels of phosphorylation between residues. To quantify phosphorylated peptides, we calculated the AUC of the extracted ion chromatograms corresponding to an identified phospho-peptide. We then normalized the phospho-peptide AUC as a percentage of the total peptide AUC. Using this method, we identified 22 phosphorylation sites that were moderately or strongly phosphorylated (greater than 5% phosphorylated), and 13 sites that are likely to be non-specifically phosphorylated (less that 5% phosphorylated). The 22 likely phosphorylation sites are shown in Figure 4.2 as well as their general position on Shank3.

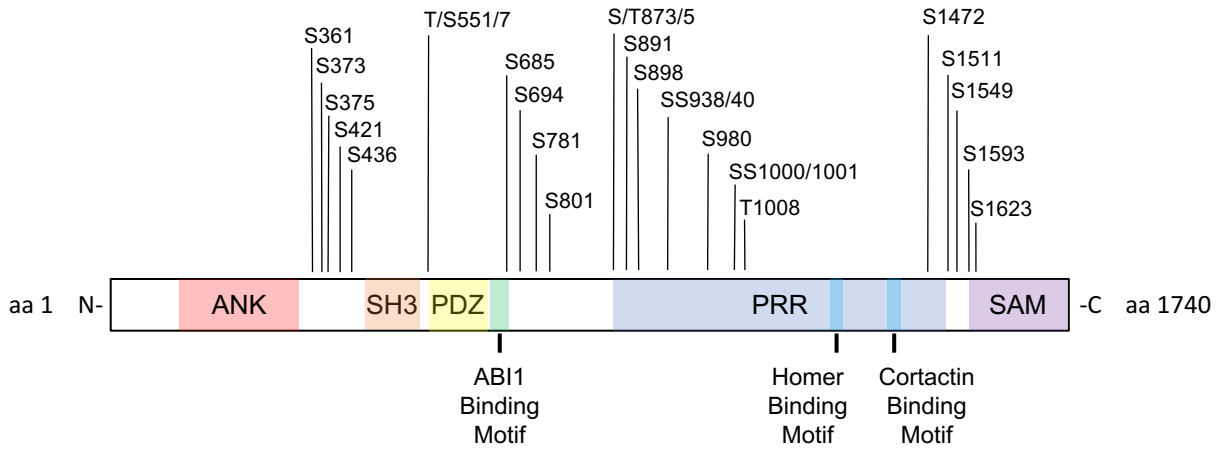

Figure 4.2: Putative CaMKII phosphorylation sites on Shank3.

Diagram of 22 likely CaMKII phosphorylation sites detected on Shank3 *in vitro*. Only those sites detected with >5% phosphorylated spectral counts are shown in this figure.

4.4 Validation of Previously-Identified CaMKII Phosphorylation Sites on Shank3

Two previous phospho-proteomics studies attempted to identify CaMKII phosphorylation sites on PSD associated proteins (Dosemeci and Jaffe, 2010; Jaffe et al., 2004). These studies identified Shank3 Ser694, Ser1511, Ser1587, and Ser1593 as potential CaMKII phosphorylation sites. In our phospho-proteomics study, all four sites were identified, though they were phosphorylated at varying percentages. However, other kinases are present in the PSD, such as PKA, PKC, and MAPK (Carr et al., 1992; Suzuki et al., 1995; Suzuki et al., 1993). Therefore, we sought to directly test whether these sites are phosphorylated by CaMKII *in vitro*.

We generated a GST-Shank3 (537-828) fusion protein with Ser694 mutated to phospho-null Ala (S694A). In addition, we generated three separate GST-Shank3 (1468-1740) fusion proteins that each contained a mutation of Ser1511, Ser1587, and Ser1593 to

phospho-null Ala (S1511A, S1587A, and S1593, respectively). We then directly phosphorylated WT or mutant GST-Shank3 proteins for 2 min with CaMKII and radiolabeled ATP to assess ^{32}P incorporation (Figure 4.3A). As protein loading was slightly uneven between mutants, we also calculated phosphorylation (mol/mol) for each protein (Figure 4.3B). In GST-Shank3 (537-828), the S694A mutation trends towards a significant reduction in phosphorylation. In GST-Shank3 (1468-1740), only the S1511A mutation significantly reduced phosphorylation, while S1587A and S1593A did not (n=4, $p < 0.001$, paired t-test with equal variance).

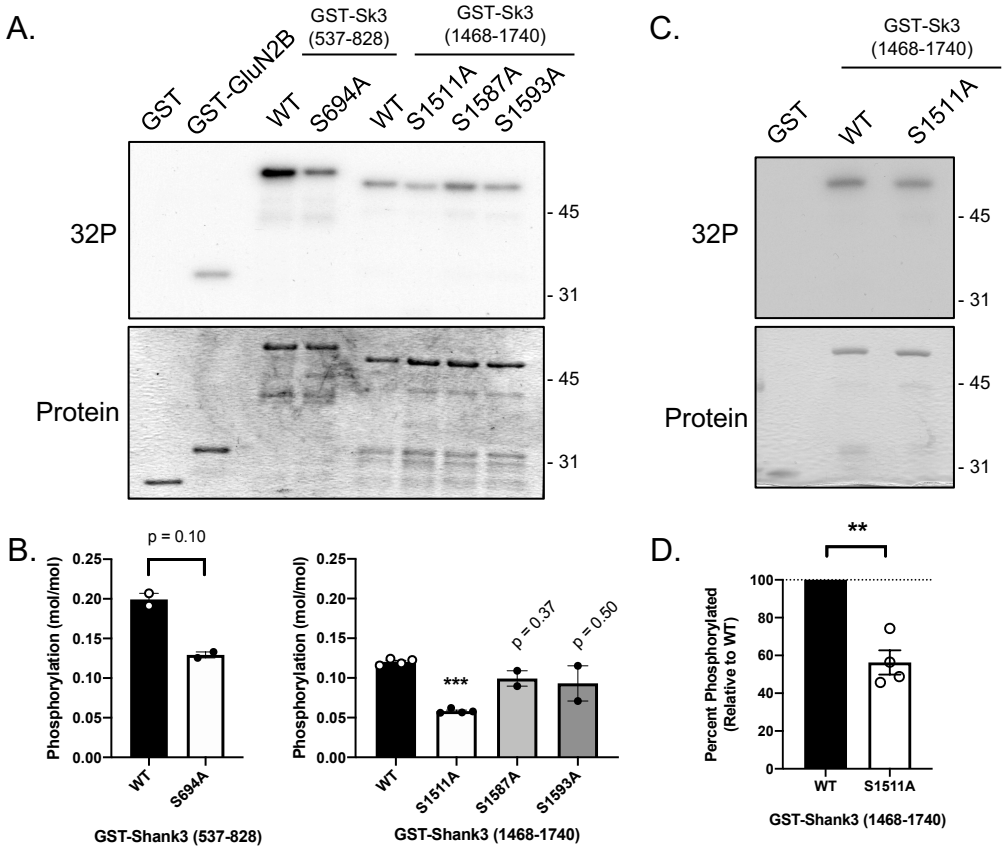

Figure 4.3: Validation of previously identified Shank3 phosphorylation sites.

A. The indicated GST fusion proteins were incubated with 10 nM CaMKII for 2 minutes before being separated by SDS-PAGE and exposed to film. Representative of 2-4 replicates. **B.** Gel bands from A were excised and measured in a liquid scintillation counter. S694A mutation trends

towards a significant reduction in phosphorylation in GST-Shank3 (537-828). S1511A significantly reduces phosphorylation in GST-Shank3 (1468-1740), while S1587A and S1593 do not (paired Student's t test with equal variance, *** p = 0.0002). **C.** The indicated GST fusion proteins were incubated with 10 nM CaMKII for 2 minutes before being separated by SDS-PAGE and exposed to film. **D.** Autoradiograph signals were normalized to protein stain, and S1511A significantly reduces phosphorylation (43.7±6% reduced compared to WT, n=4, ** p = 0.006, one-sample Student's t-test with equal variance compared to a theoretical value of 100). C. and D., representative of 4 replicates.

Mutation of Ser1511 to Ala produced the largest reduction of ^{32}P incorporation. Therefore, we sought to investigate Ser1511 phosphorylation more rigorously. Separate reactions of GST-Shank3 (1468-1740) WT or S1511A were incubated for 2 min with CaMKII and radiolabeled ATP to assess 32P incorporation (Figure 4.3C). With more equal protein loading compared to Figure 4.3A, we were better able to quantify a significant reduction of ^{32}P incorporation in GST-Shank3 (1468-1740) S1511A (44±6% reduction relative to WT, n=4, $p < 0.01$, one sample Student's t-test compared to a theoretical value of 100) (Figure 4.3D).

4.5 Discussion

Although GST-Shank3 #4 (829-1130) and #6 (1468-1740) were weakly phosphorylated relative to the other GST-Shank3 fusion proteins in Figure 4.1, more putative phosphorylation sites were detected in the mass spectrometry study. This may be a result of the mass spectrometry samples being phosphorylated for longer (2 versus 25 min). A longer phosphorylation would allow for more non-specific phosphorylation to occur, as we observed many putative sites that did not meet our somewhat arbitrary >5% threshold on

these proteins. In addition, CaMKII may preferentially phosphorylate other Shank3 residues, such as those near the SH3 and PDZ domains, before phosphorylating those near the CaMKII binding motif and the SAM domain. GST-Shank3 #6 (1468-1740) also had the highest sequence coverage, which may contribute to the higher number of putative phosphorylation sites identified.

Not all Ser/Thr residues within these fusion proteins were recovered, as indicated by the sequence coverage under each protein (Table 4.1). This is likely due to trypsin digest creating peptides that could not be recovered after mass spectrometry, either due to size or other biochemical properties. Other protease digests, such as elastase or endoproteinase AspN, which cleave proteins differently than trypsin, may provide a more complete coverage. However, this would only be necessary if mutation of all putative phosphorylation sites to phospho-null Ala within a given GST-Shank3 protein still resulted in ^{32}P incorporation.

In our validation of previously identified putative phosphorylation sites, slight to moderate reductions were observed with all single phospho-null mutants tested (Figure 4.3A). Ser1511 phosphorylation in GST-Shank3 (1468-1740) accounted for approximately 43% of all phosphorylation events on the WT protein, suggesting that other sites still contribute to overall phosphorylation. The other phosphorylation sites tested did not reach any statistically significant reduction in phosphorylation; however, with only two replicates, these results may be underpowered. As none of these mutants completely disrupted

phosphorylation, it does provide evidence that multiple CaMKII phosphorylation sites are present within these proteins.

A recent kinome-wide siRNA screen identified Shank3 as a substrate for ERK2 (Wang et al., 2019a). Similar to our studies, this report identified putative phosphorylation sites *in vitro* using purified Shank3 fragments separately incubated with the kinases ERK2, PKA, GSK3β, or casein kinase 2 followed by mass spectrometry. ERK2 phosphorylation at Shank3 Ser1134, Ser1163, and Ser1253 were identified as regulators of Shank3 stability, while Shank3 with all three sites mutated to Ala had a longer half-life and reduced ubiquitination. All three of these sites are present in GST-Shank3 #5 (1131-1467), which was not phosphorylated by CaMKII. However, this data identified a number of residues phosphorylated by other kinases that also appear in our CaMKII proteomics data (Table 4.2). ERK2, GSK3β, and casein kinase 2 all shared 1-2 phosphorylation sites identified in our CaMKII phospho-proteomics, with the functional relevance of these sites still unknown. PKA and CaMKII shared multiple phosphorylation sites; one, Ser685, is explored in-depth in the following chapter.

		Identified *In Vitro*				
Residue	**Detected *In Vivo***	**CaMKII**	**ERK2**	**PKA**	**GSK3B**	**CK2**
Ser375	+	++	nd	+	+	+
Thr551/Ser557	+ (557)	++	nd	+	nd	nd
Ser685	+	++	nd	++	nd	nd
Ser781	+	++	nd	+	nd	nd
Ser801	+	+	nd	+	nd	nd
Ser875	-	+	++	nd	+	nd
Ser891	+	++	nd	+	nd	nd
Ser1472	+	+	nd	++	nd	nd

Table 4.2: Comparison of Shank3 phosphorylation sites from *in vitro* kinase assays.

Identification of putative phosphorylation sites between multiple *in* vitro kinase assays using different Ser/Thr kinases. Since results for CaMKII and the other kinases were performed different, positive results are indicated with (+), phosphorylated, (++), strongly phosphorylated, or nd, no detection. Data for *in vivo* mass spectrometry from (Huttlin et al., 2010; Wang et al., 2019b). Data for ERK, PKA, GSK3β, and casein kinase 2 from (Wang et al., 2019a).

CHAPTER V

CAMKII PHOSPHORYLATION OF SHANK3: SER685 PHOSPHORYLATION MODULATES ABI1-SHANK3 INTERACTION

5.1 Introduction

Phosphorylation of scaffolding proteins can regulate their binding interactions, subcellular distribution, and ultimately their physiological function (Iasevoli et al., 2012). Several phospho-proteomics studies have reported that Shank3 is phosphorylated at multiple sites when isolated from brain tissues, and in some instances the kinase and residue have been identified. For example, ribosomal S6 kinase 2 (RSK2) phosphorylates Shank3 at Ser1648 *in vitro* and in primary neurons (Thomas et al., 2005). Recently, Shank3 was shown to be phosphorylated *in vivo* at Ser685, immediately adjacent to the ABI1 binding motif (Wang et al., 2019b). A phospho-null S685A mutation or a missense S685I mutation, identified in a patient with ASD, reduced the ABI1-Shank3 interaction and impaired dendritic spine development and synaptic transmission. *In vitro* studies indicated that PKA, but not ERK2, GSK3β, or casein kinase 2, phosphorylated Ser685 (Wang et al., 2019b). However, a direct effect of Shank3 Ser685 phosphorylation, or of a phospho-mimetic mutation of Ser685 to an acidic residue, on ABI1 binding was not reported.

Synaptic plasticity involves dynamic changes in the actin cytoskeleton and spine morphology that are modulated by both Ca^{2+} and cAMP signaling (Borovac et al., 2018; Dell'Acqua et al., 2006; Lee et al., 2009; Strack et al., 1997; Zhong et al., 2009). Both

CaMKII and PKA are able to phosphorylate the same residue in various proteins. For instance, both CaMKII and PKA can phosphorylate the C-terminus of connexin43 at Serine 364, 365, 369, or 373, which alter gap junction assembly (Huang et al., 2011; Lampe and Lau, 2004). Furthermore, both kinases can phosphorylate Ser120 on the Rpt6 subunit of the 26 S proteasome to enhance proteasome activity in neurons (Djakovic et al., 2009; Zhang et al., 2007). However, CaMKII and PKA can phosphorylate the same protein at different residues, resulting in different physiological outcomes. The GluA1 subunit of the AMPA-type glutamate receptor is such a protein, where CaMKII phosphorylation at Ser831 increases single channel conductance (Barria et al., 1998; Kristensen et al., 2011), while PKA phosphorylation of Ser845 increases surface GluA1 expression (Oh et al., 2005; Roche et al., 1996). Notably, phospho-proteomics analyses revealed that phosphorylation of several sites in Shank3 is increased following CaMKII activation in isolated synaptic fractions (Dosemeci and Jaffe, 2010; Jaffe et al., 2004), Thus, it seems likely that both PKA and CaMKII can target Shank3, but the potential role of CaMKII in Shank3 Ser685 phosphorylation has not been investigated.

In the previous chapter, Shank3 Ser685 was identified as a potential CaMKII phosphorylation site based on our proteomics data. In this chapter, we tested the hypothesis that Shank3 Ser685 is also targeted by CaMKII for phosphorylation. We found that both PKA and CaMKII can phosphorylate a GST-Shank3 fusion protein containing residues 572-691, and that this phosphorylation is prevented by mutation of Ser685 to a phospho-null alanine residue. Consistent with prior studies, any mutation of Ser685

disrupts Shank3 interactions with ABI1. However, we show for the first time that Ser685 phosphorylation by CaMKII significantly enhances ABI1 interaction with Shank3.

5.2 CaMKII and PKA Phosphorylate Shank3 685

As an initial test of our hypothesis that CaMKII can phosphorylate Shank3 at Ser685, a site previously shown to be phosphorylated by PKA, we generated a GST fusion protein containing Shank3 amino acids 572-691, which includes the PDZ domain and the adjacent ABI1-binding motif. GST was used as a negative control and a GST fusion protein containing the AMPA receptor subunit GluA1 C-terminal residues 827-901 was used as a positive control because CaMKII and PKA specifically phosphorylate Ser831 (Barria et al., 1998) and Ser845 (Roche et al., 1996), respectively. These three GST proteins were separately incubated with equimolar catalytic domain concentrations of purified CaMKIIα or PKA for 1-5 minutes and then analyzed by SDS-PAGE followed by autoradiography (Figure 5.1). As expected, GST alone was not phosphorylated, but GST-GluA1 was phosphorylated by both CaMKIIα and PKA. GST-Shank3 was similarly phosphorylated by both CaMKIIα and PKA over a 5-min time course. While PKA reproducibly phosphorylated Shank3 more efficiently than GluA1, CaMKII displayed the reverse substrate preference. Nevertheless, these *in vitro* data show that CaMKII can phosphorylate Shank3 in a region of the protein that is also phosphorylated by PKA.

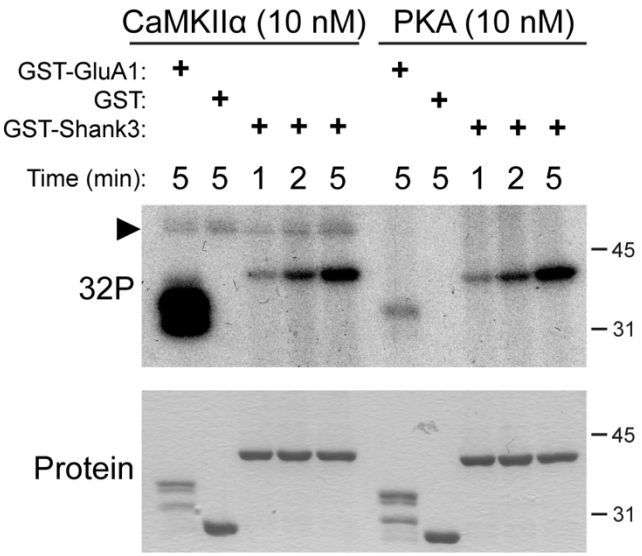

Figure 5.1: CaMKIIα and PKA phosphorylate Shank3 *in vitro*.

The indicated GST fusion proteins were incubated with CaMKIIα (10 nM) or PKA (10 nM) and [γ-^{32}P]ATP (see Methods), and then analyzed by SDS-PAGE followed by Coomassie blue staining (bottom) and autoradiography to detect ^{32}P-incorporation (top). Reactions ran for 1-5 minutes as indicated, before stopping with 4X sample buffer. Black arrowhead indicates CaMKIIα autophosphorylation. Representative of at least 3 biological replicates. From (Perfitt et al., 2020).

Ser685 had been previously identified as the main site of PKA phosphorylation within this region of Shank3 (Wang et al., 2019b). To confirm this finding and also test whether CaMKIIα also phosphorylates Ser685 within GST-Shank3 (572-691), we mutated Ser685 in the GST-Shank3 fusion protein to a phospho-null Ala residue (S685A). GST-Shank3-WT or -S685A were incubated with CaMKIIα or PKA (Figure 5.2), with GST-GluA1 as a positive control, as in Figure 5.1. While GST-Shank3-WT was strongly phosphorylated by both CaMKIIα and PKA, ^{32}P-incorporation into GST-Shank3-S685A was barely detectable following incubation with either kinase. These data demonstrate that Ser685 in Shank3 is the major site within this domain that can be phosphorylated *in vitro* by both CaMKII and PKA.

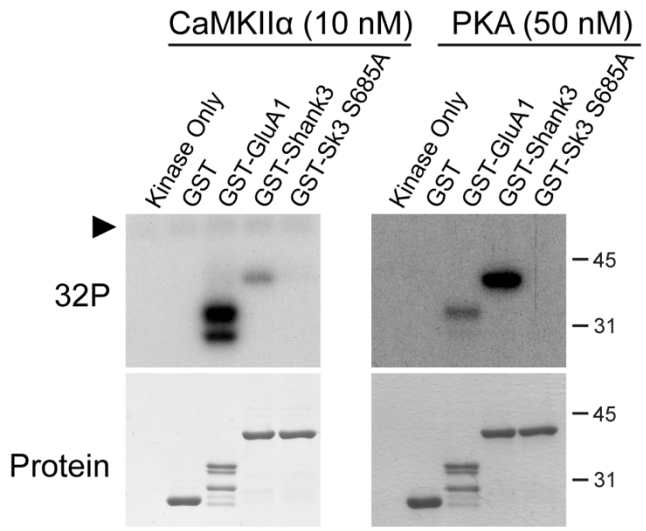

Figure 5.2: CaMKIIα and PKA phosphorylate Shank3 at Ser685.

The indicated GST fusion proteins were phosphorylated by CaMKIIα (10 nM) or PKA (50 nM) for 5 min and then analyzed as in Figure 5.1. Black arrowhead indicates CaMKIIα autophosphorylation. Representative of at least 3 biological replicates. From (Perfitt et al., 2020).

5.3 Mutation of Ser685 Interferes with ABI1 Binding

Ser685 lies immediately C-terminal to the ABI1 binding motif in Shank3 (Proepper et al., 2007). WT Shank3 may be partially phosphorylated at Ser685 when expressed in HEK293 cells because a phospho-null S685A mutation reduces ABI1 co-immunoprecipitation with Shank3 (Wang et al., 2019b). Therefore, we hypothesized that a phospho-mimetic Ser685 to aspartate (S685D) mutation may enhance the interaction with ABI1 relative to the S685A mutant. To test this hypothesis, we co-expressed HA-tagged ABI1 and GFP-tagged full length Shank3 with either the wild type (WT) sequence or with mutations of Ser685 to alanine (S685A), or a phospho-mimetic aspartate (S685D) in HEK293T cells. Cells were lysed and Shank3 was immunoprecipitated using a GFP antibody (Figure 5.3A). We detected a robust and specific co-immunoprecipitation of ABI1

with GFP-Shank3-WT, as previously demonstrated. Moreover, S685A mutation in GFP-Shank3 significantly reduced the levels of co-immunoprecipitated HA-ABI1, consistent with a prior report. However, there was a quantitatively similar reduction in the co-immunoprecipitation of HA-ABI1 with the GFP-Shank3-S685D mutant. As a control, we used a similar approach to test for effects of the Shank3 S685A and S685D mutations on co-immunoprecipitation of the HA-tagged C-terminal domain of the L-type Ca^{2+} channel $Ca_V1.3$ (HA-$Ca_V1.3$-CTD), which binds to the canonical PDZ domain (residues 572-663) in Shank3 (Zhang et al., 2005) in close proximity to the ABI1 binding site and Ser685. However, neither Ser685 mutation had an effect on the levels of co-immunoprecipitated HA-$Ca_V1.3$-CTD. Therefore, the Ser685 mutations specifically interfere with ABI1-Shank3 binding, presumably by disrupting interactions involving amino acids adjacent to the core ABI1 binding motif. However, since introduction of negative charge by S685D mutation has the same effect as the uncharged S685A mutation, it is unclear whether Shank3 Ser685 phosphorylation affects the interaction with ABI1.

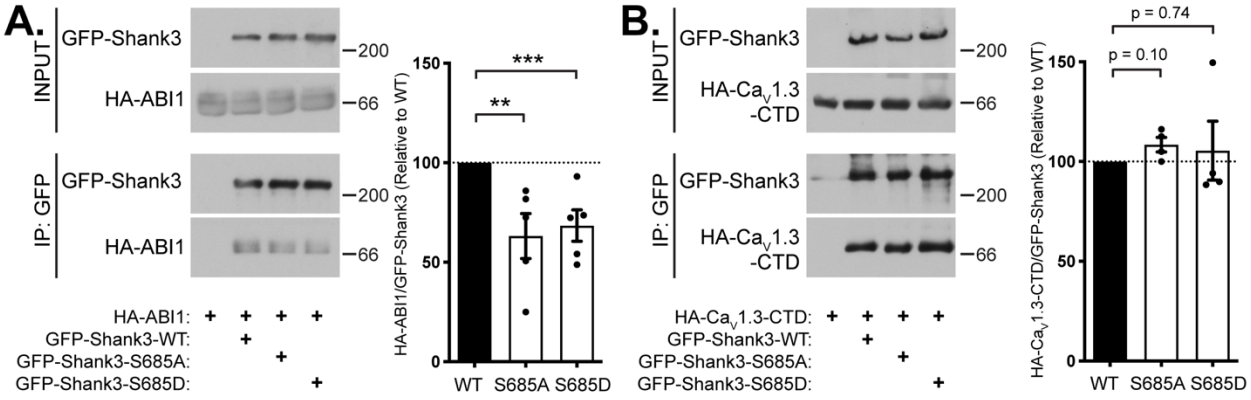

Figure 5.3: Mutation of GFP-Shank3 Ser685 disrupts ABI1 binding.

A, B. Lysates of HEK293T cells expressing HA-ABI1 (**A**) or HA-$Ca_V1.3$-CTD (**B**) and either empty vector, GFP-Shank3-WT, GFP-Shank3-S685A, or GFP-Shank3-S685D were immunoprecipitated

(IP) using a GFP antibody. Input samples and IP complexes were resolved by SDS-PAGE and immunoblotted for GFP-Shank3 and HA-ABI1 (**A**) or HA-Ca_V1.3-CTD (**B**). HA/GFP signals for each IP lane were calculated and normalized to GFP-Shank3-WT. Both GFP-Shank3-685A and GFP-Shank3-685D significantly reduce HA-ABI1 co-immunoprecipitation (GFP-Shank3-S685A: 37±11% reduced compared to WT, ** $p < 0.01$, GFP-Shank3-S685D: 32±8% reduced compared to WT, *** $p < 0.001$, one sample Student's t-test with equal variance compared to theoretical mean of 100). Mutation of S685 had no effect on HA-Ca_V1.3-CTD co-immunoprecipitation (one sample Student's t-test with equal variance compared to theoretical mean of 100). The immunoblots shown are representative of 4-5 biological replicates that were quantified. Error bars, mean ± SEM. From (Perfitt et al., 2020)

5.4 Phosphorylation of Ser685 by CaMKIIα Enhances ABI1-Shank3 Binding

We directly tested for an effect of Shank3 Ser685 phosphorylation on ABI1 binding *in vitro*. The GST-Shank3-WT or GST-Shank3-S685A proteins were phosphorylated for an extended time (20 min) using purified CaMKIIα (see Methods) or incubated under control conditions (lacking CaMKIIα) and then mixed with lysates of HEK293T cells expressing HA-ABI1. Immunoblot analysis of GST protein complexes revealed that specific binding of HA-ABI1 to non-phosphorylated control GST-Shank3-WT and GST-Shank3-S685A was indistinguishable (Figure 5.4). However, pre-phosphorylation of GST-Shank3-WT by CaMKIIα increased ABI1 binding by about 50%, and this effect was abrogated by S685A mutation (Figure 5.4). These data directly demonstrate that Shank3 Ser685 phosphorylation can enhance the association with ABI1.

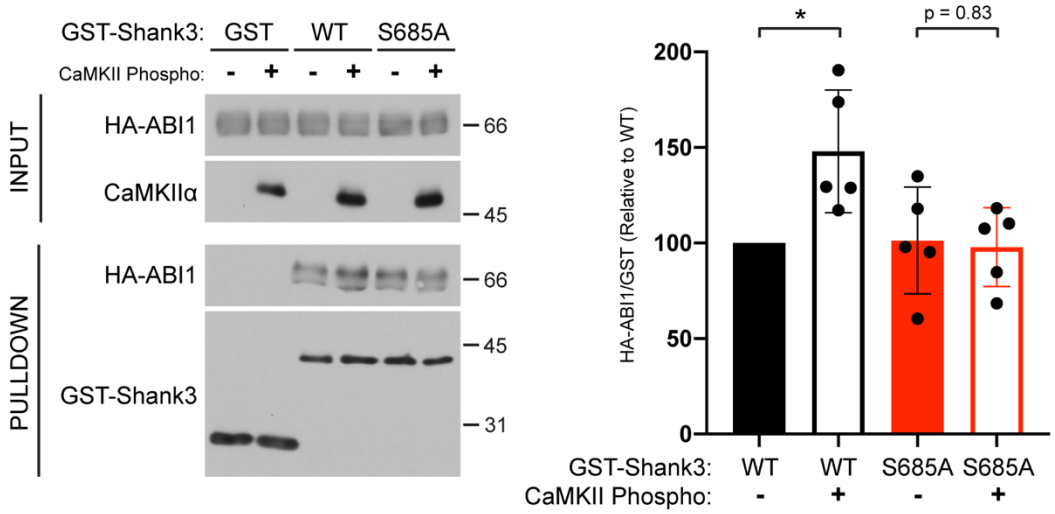

Figure 5.4: CaMKIIα phosphorylation of Shank3 Ser685 enhances ABI1 binding.

Left, GST, GST-Shank3 WT, or GST-Shank3-S685A were pre-phosphorylated with CaMKIIα and incubated with HEK293T cell lysate expressing HA-ABI1. Control protein samples were pre-incubated in the absence of CaMKIIα. Isolated GST complexes were then analyzed by immunoblotting as indicated (see Methods). Immunoblots are representative of 5 independent experiments. *Right,* HA/GST signals from each pulldown lane were normalized to GST-Shank3-WT/no CaMKII condition. Incubation with CaMKIIα significantly increases HA-ABI1 binding to GST-Shank3-WT (148±14% increased relative to no CaMKII condition, * $p < 0.05$, one sample Student's t-test with equal variance compared to theoretical mean of 100), which is not observed with GST-Shank3-S685A (unpaired Student's t-test with equal variance). Error bars, mean ± SEM. From (Perfitt et al., 2020).

5.5 Discussion

Dynamic changes in the size and morphology of dendritic spines and postsynaptic densities during synaptic development and synaptic plasticity are mediated in part by the re-organization of multiprotein complexes that are assembled by numerous scaffolding proteins (Sheng and Hoogenraad, 2007). Phosphorylation of some synaptic proteins has been shown to modulate their interaction with scaffolding proteins (Chung et al., 2004; Zacchi et al., 2014). Here, we provide direct evidence that phosphorylation of a major

synaptic scaffolding protein, Shank3, specifically modulates the binding of ABI1, a key synaptic modulator of F-actin cytoskeleton.

Shank3 is a member of a larger family of proteins that also includes Shank1 and Shank2. All three Shanks have been linked to ASD, as well as intellectual disability and schizophrenia (Eltokhi et al., 2018; Monteiro and Feng, 2017; Sala et al., 2015). They also share a similar overall domain organization, with high amino acid sequence similarity in SH3, PDZ, and SAM domains. Although there is low overall sequence similarity outside of the canonical protein interaction domains, the proline-rich ABI1 binding motif is conserved between Shank2 and Shank3, but not Shank1 (Lim et al., 1999; Proepper et al., 2007). Our data significantly extend prior studies by showing that Ser685 in Shank3, immediately adjacent to the ABI1 binding motif (residues 677-684), can be phosphorylated by CaMKII, and confirm a prior report that PKA phosphorylates this residue. Although several proteomics studies have shown that Shank3 phosphorylation in isolated postsynaptic densities is increased under conditions that favor CaMKII activation (Dosemeci and Jaffe, 2010; Jaffe et al., 2004), this is the first study to show that CaMKII phosphorylates Shank3 using purified proteins. Moreover, we show for the first time that Ser685 phosphorylation directly enhances binding of ABI1 *in vitro*. Interestingly, comparison of the amino acid sequences surrounding the ABI1-binding sites in Shank3 and Shank2 reveals that Shank3 Ser685 is conserved as Shank2 Thr153. Further studies will be required to determine whether phosphorylation of Thr153 in Shank2 by CaMKII, PKA or other kinases can also modulate ABI1 binding.

As noted above, a prior study reported Shank3 Ser685 phosphorylation by PKA, and confirmed that Ser685 is phosphorylated *in vivo* by proteomics analysis and using phospho-site specific antibodies (Wang et al., 2019b). Ser685 mutation to alanine was also shown to decrease ABI1 binding to Shank3, consistent with the hypothesis that Shank3 Ser685 phosphorylation by PKA enhances the interaction with ABI1 *in situ*. Moreover, co-immunoprecipitation of the two proteins from lysates of cortical neurons was decreased following pre-treatment with H89, a PKA inhibitor (Wang et al., 2019b). However, neither the putative effect of H89 to decrease Ser685 phosphorylation in neurons nor a direct effect of Ser685 phosphorylation, or a phospho-mimetic mutation of Ser685 to aspartate or glutamate, to enhance the interaction with ABI1 was reported in this prior study. Nevertheless, given these prior findings, it was surprising that our current studies revealed that phospho-mimetic S685D and phospho-null S685A mutations had quantitatively similar effects to decrease the association of ABI1. However, neither mutation affected binding of the C-terminal domain of $Ca_V1.3$ to the nearby Shank3 PDZ domain.

Since our findings using the GFP-Shank3-S685D protein called into question the role of Ser685 phosphorylation in modulating the interaction with ABI1, it was important to directly investigate the putative effect of phosphorylation. We found that CaMKII phosphorylation of the GST-Shank3-WT protein *in vitro* enhanced the binding of ABI1, while the pre-incubation of GST-Shank3-S685A with CaMKII and ATP had no effect on ABI1 binding. Thus, our findings directly demonstrate for the first time that Shank3 Ser685 phosphorylation indeed enhances the binding of ABI1. Notably, while S685A mutation

had no effect on *in vitro* binding of ABI1 to GST-Shank3, the same mutation significantly reduced co-immunoprecipitation of HA-ABI1 with GFP-Shank3 when the proteins were co-expressed in mammalian (HEK293) cells. This discrepancy may be explained by the partial phosphorylation of GFP-Shank3 at Ser685 by endogenous PKA, CaMKII or another kinase in mammalian cells, enhancing the interaction with HA-ABI1, whereas GST-Shank3 purified from bacteria is not phosphorylated. It is also noteworthy that indistinguishable amounts of HA-ABI1 co-immunoprecipitate with GFP-Shank3-S685A and -S685D; thus, the S685D mutation is not a phospho-mimetic mutation in this context. The failure of phospho-mimetic mutations is not unprecedented and is presumably under-reported in the literature because it is a negative result. This may be explained by the fact that aspartate (or glutamate) residues carry only a single negative charge as compared to the nominal two negative charges on much larger phosphorylated serine or threonine residues at physiological pH.

In summary, the present findings directly demonstrate that phosphorylation of Shank3 at Ser685 can enhance ABI1 binding. The potential importance of this mechanism is reinforced by studies of an ASD-linked *de novo* S685I mutation in Shank3, which has the same effect as the S685A mutation to decrease ABI1 binding by preventing phosphorylation (Wang et al., 2019b). Expression of Shank3-S685I in cultured neurons results in complex synaptic changes and knock-in Shank3-S685I mutant mice display a subset of ASD-related behavioral phenotypes (Wang et al., 2019b). Since Ser685 can be phosphorylated by either PKA or CaMKII, it will be important to investigate the relative importance of cAMP and Ca^{2+} signaling in physiological regulation of Ser685

phosphorylation and ABI1 interaction with Shank3, and the role of these mechanisms in synaptic plasticity. Further studies should determine whether Shank3 Ser685 phosphorylation is altered in mouse models of neuropsychiatric disorders, including mice carrying CaMKII mutations that have been linked to ASD and intellectual disability (Cohen et al., 2018; Doshi-Velez et al., 2013; Stephenson et al., 2017).

CHAPTER VI

CAMKII PHOSPHORYLATION OF SHANK3: THR551 IN THE NON-CANONICAL PDZ DOMAIN REGULATES GKAP-SHANK3 INTERACTION

6.1 Introduction

Chapter IV identified a number of putative CaMKII phosphorylation sites on Shank3. For most of these residues, the physiological relevance and functional impact of phosphorylation is unknown. To begin characterizing these sites, we compared their location to known protein-binding domains in Shank3. Interestingly, we identified Thr551 and Ser557 as two putative phosphorylation sites that lie N-terminal to the Shank3 PDZ domain (residues 543-564). Thr551 and Ser557 are on the same phospho-peptide detected in our mass spectrometry analysis, but we were unable to definitively determine if one or both sites were phosphorylated. This region of Shank3 lies immediately N-terminal to the canonical PDZ domain. A recent study determined the crystal structure of the PDZ domain with this the N-terminal extension in complex with the PDZ-binding motif of GKAP (Zeng et al., 2016). Intriguingly, the GKAP peptide interacts with both the PDZ domain and the N-terminal extension (Figure 6.1A). The CaMKII phosphorylation sites Thr551 and Ser557 are both located on β sheets that interact with GKAP (Figure 6.1A, orange and black residues). Phosphorylation of either residue could potentially misalign these β sheets. Therefore, we hypothesized that CaMKII phosphorylation of the Shank3 N-terminal extension could modulate the GKAP-Shank3 interaction.

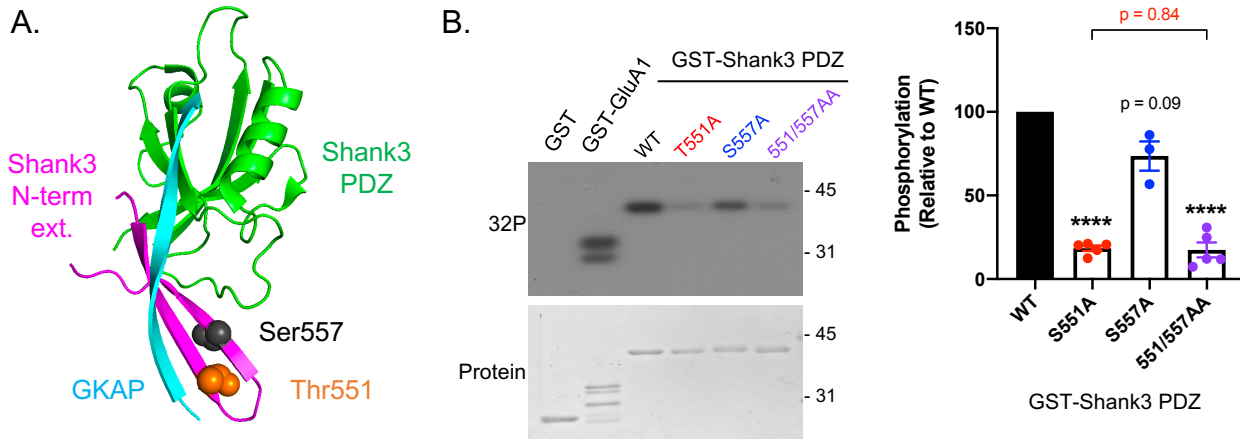

Figure 6.1: Thr551 is the primary CaMKII phosphorylation site in the Shank3 PDZ N-terminal extension.

A. Crystal structure of the GKAP-Shank3 complex (PDB: 5izu). Green: Canonical Shank3 PDZ domain; magenta: Shank3 PDZ N-terminal extension; cyan: GKAP C-tail; orange: Thr551 putative phosphorylation site; black: Ser557 putative phosphorylation site. **B**. *Left*, GST-fusion proteins were incubated with 10 nM CaMKII and radiolabeled ATP for 2 minutes, separated by SDS-PAGE, and exposed to film to measure ^{32}P incorporation. Representative of 3-4 replicates. *Right*, quantification of ^{32}P/protein signals relative to GST-Shank3 PDZ WT (537-663). T551A and 551/557AA are significantly less phosphorylated relative to WT, while S557A is not. Error bars, mean ± SEM.

6.2 CaMKII Phosphorylates Shank3 Thr551

Since Thr551 and/or Ser557 could be phosphorylated, we generated GST-Shank3 fusion proteins expressing residues 537-663, containing the N-terminal extension and the canonical PDZ domain. This fusion protein contains no other CaMKII phosphorylation sites detected in our initial proteomics analysis (see Figure 4.2). We then introduced phospho-null Ala mutations at Thr551 or Ser557 individually or together to generate GST-Shank3 T551A, S557A, and 551/557AA, respectively. GST-Shank3 was incubated with purified CaMKII and [γ-^{32}P] ATP for 2 min. Separate reactions with GST and GST-GluA1 acted as negative and positive controls, respectively (Figure 6.1B). Both GST-GluA1 and

GST-Shank3 WT were robustly phosphorylated. However, GST-Shank3 T551A and 551/557AA had significantly less phosphorylation relative to WT (T551A: 82±2% reduced compared to WT; 551/557AA: 83±4% reduced compared to WT, n=4, **** $p < 0.0001$, one sample Student's t-test with equal variance compared to theoretical value of 100). While GST-Shank3 S557A had slightly less ^{32}P incorporation that WT, the reduction was not statistically significant. In addition, phosphorylation of GST-Shank3 551/557AA was not significantly reduced compared to T551A single mutant (n=4, $p = 0.84$, paired t-test with equal variance). Therefore, Thr551 is the primary CaMKII phosphorylation site within the Shank3 N-terminal extension of the PDZ domain.

6.3 GKAP Binding Requires the Canonical Shank3 PDZ Domain

To confirm that GKAP primarily binds through the Shank3 PDZ domain, we expressed HA-GKAP with mAp-Shank3-WT or mAp-Shank3-ΔPDZ (which has a deletion of the canonical PDZ domain, but retains the N-terminal extension) in HEK293T cells. Shank3 was immunoprecipitated from soluble cell lysates, and complexes were immunoblotted for HA-GKAP (Figure 6.2). As expected, HA-GKAP robustly co-immunoprecipitates with mAp-Shank3-WT, but not mAp-Shank3-PDZ. These data confirm prior observations that the Shank3 PDZ domain is essential for GKAP binding, and that the N-terminal extension of the Shank3 PDZ domain is not sufficient to support GKAP co-immunoprecipitation under these conditions.

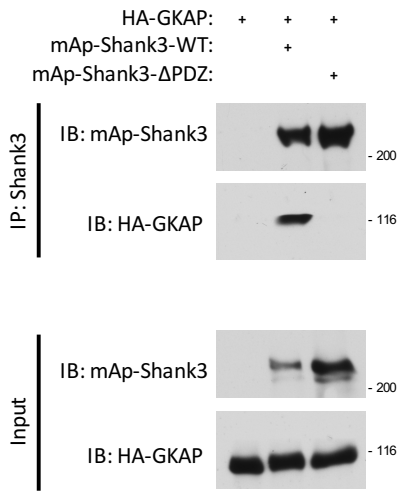

Figure 6.2: GKAP binding to Shank3 requires the canonical Shank3 PDZ domain.
Soluble fractions of HEK293T cell lysates expressing HA-GKAP and mAp-Shank3-WT or mAp-Shank3-PDZ were immunoprecipitated using a Shank3 antibody. HA-GKAP co-immunoprecipitates with mAp-Shank3-WT, but not mAp-Shank3-ΔPDZ. Representative of 3 biological replicates.

6.4 CaMKII and Thr551 Affect GKAP-Shank3 Interaction

As an initial test for an effect of Shank3 Thr551 phosphorylation on the binding of GKAP, we mutated Thr551 in full-length GFP-Shank3 to phospho-null Ala (GFP-Shank3-T551A) or phospho-mimetic Asp (GFP-Shank3-T551D). We hypothesized that if phosphorylation disrupted GKAP-Shank3 binding, then the co-immunoprecipitation of HA-GKAP with GFP-Shank3-T551D should be reduced relative to co-immunoprecipitation with GFP-Shank3-T551A. Indeed, we detected a significant reduction in HA-GKAP co-immunoprecipitation with GFP-Shank3-T551D relative to GFP-Shank3-T551A (45±9% reduced relative to GFP-Shank3-T551A, n=4, * $p < 0.05$, one sample Student's t-test with equal variance compared to theoretical value of 100) (Figure 6.3A). If this reduction in co-immunoprecipitation is due to the T551D mutation mimicking phosphorylation, then endogenous phosphorylation should also disrupt GKAP binding. To test this, we

transfected HEK293T cells with HA-GKAP and GFP-Shank3-WT in the absence or presence of CaMKIIα-T286D/T305A/T306A (CaMKIIα-D/AA), a constitutively active form of the kinase (Marks et al., 2018). Both HA-GKAP and GFP-Shank3 signals from cells co-expressing CaMKIIα-D/AA show decreased electrophoretic mobility, indicating that both proteins are robustly phosphorylated by CaMKII (Figure 6.3B). Co-immunoprecipitation of HA-GKAP with GFP-Shank3 was significantly reduced when constitutively active CaMKII was co-expressed compared to lysates expressing HA-GKAP and Shank3 alone (49±12% reduced compared to no CaMKII condition, n=4, * $p < 0.05$, one sample Student's t-test with equal variance compared to theoretical value of 100).

To test if other Shank3 PDZ binding partners are affected by Thr551 phosphorylation, we compared the interactions of T551A- or T551D-mutated GFP-Shank3 with the C-terminal domain of L-type Ca^{2+} channel $Ca_V1.3$. HEK293T cells expressing an HA-tagged $Ca_V1.3$ C-terminal domain (HA-$Ca_V1.3$-CTD) with GFP-Shank3-WT, GFP-Shank3-T551A, or GFP-Shank3-T551D were lysed and immunoprecipitated using a GFP antibody (Figure 6.3C). We observed no statistically significant difference in how much HA-GKAP was co-immunoprecipitated between the different GFP-Shank3 constructs (n=4, $p > 0.05$, one sample Student's t-test with equal variance compared to theoretical value of 100). These data suggest that CaMKII phosphorylation at Shank3 Thr551 specifically disrupts binding of GKAP to Shank3.

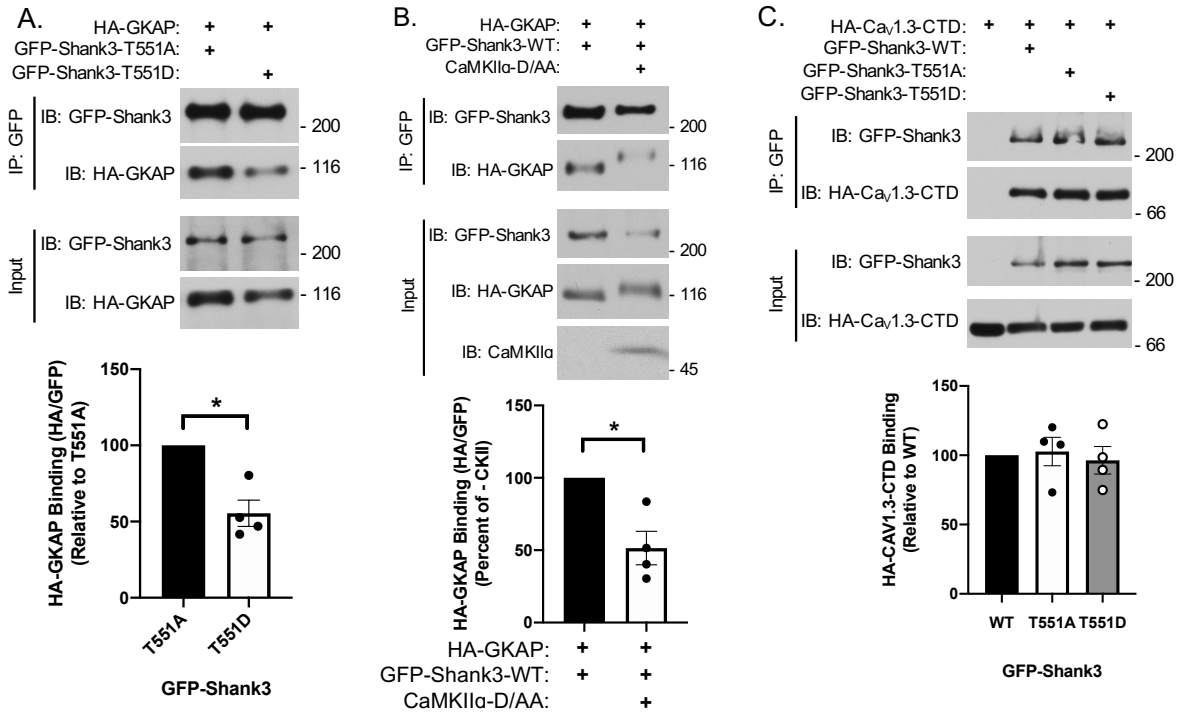

Figure 6.3: GFP-Shank3-T551D and CaMKII activity disrupt GKAP-Shank3 binding.
A. HEK293T cell lysates expressing HA-GKAP and GFP-Shank3-T551A or GFP-Shank3-T551D were immunoprecipitated for GFP and immunoblotted as indicated. HA-GKAP co-immunoprecipitates significantly less with GFP-Shank3-T551D compared to GFP-Shank3-T551A. **B.** HEK293T cell lysates expressing HA-GKAP and GFP-Shank3-WT in the absence or presence of co-transfected CaMKIIα-D/AA were immunoprecipitated for GFP and immunoblotted as indicated. HA-GKAP co-immunoprecipitates significantly less with GFP-Shank3-WT in the presence of CaMKII. Note the reduced mobility of GFP-Shank3 and HA-GKAP in the presence of CaMKII. **C.** HEK293T cell lysates expressing HA-Ca_V1.3-CTD and GFP-Shank3-WT, -T551A, or -T551D were immunoprecipitated for GFP and immunoblotted as indicated. No significant difference in co-immunoprecipitated HA-Ca_V1.3-CTD is detected. Immunoblots representative of 4 biological replicates. Error bars, mean ± SEM.

Our *in vitro* phosphorylation data indicated that Shank3 Ser557 may be weakly phosphorylated by CaMKII. Therefore, we compared the effects of phospho-mimetic (Asp) and phospho-null (Ala) mutations at Thr551 or Ser557 in GST-Shank3 (537-828) in

the binding of GKAP in transfected HEK293T cell lysates. GST complexes were isolated and separated by SDS-PAGE and immunoblotted for GKAP and GST-Shank3 (Figure 6.4). Neither phospho-null mutation had an effect on GKAP binding, but both the T551D and S557D mutations significantly reduced GKAP binding (T551D: 62±5% reduced compared to WT, n=4, $p < 0.001$; S557D: 38±9% reduced compared to WT, n=4, $p < 0.05$, one sample Student's t-test with equal variance compared to theoretical value of 100). Therefore, phosphorylation at Ser557 may also play a role in modulating GKAP binding.

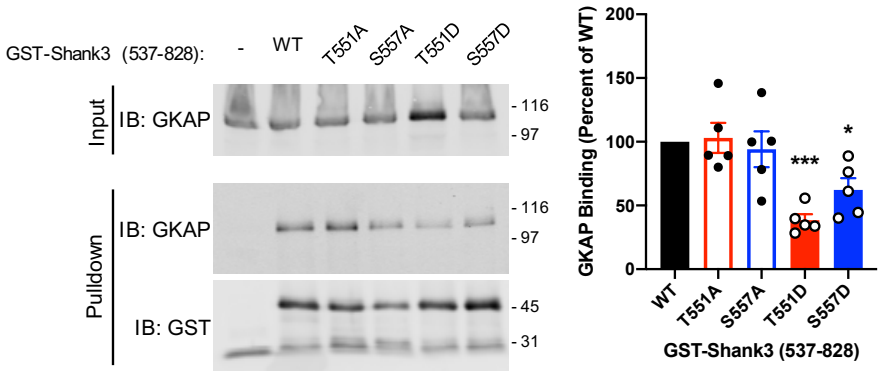

Figure 6.4: GKAP binding is reduced by Shank3 T551D or S557D mutations.

GST-Shank3 fusion proteins were incubated with HEK293T cell lysates expressing untagged GKAP, isolated using glutathione agarose, separated by SDS-PAGE and immunoblotted as indicated. Both T551D and S557D significantly pulled down less GKAP compared to WT GST-Shank3 (537-828). Representative of 4 biological replicates. Error bars, mean ± SEM.

6.5 CaMKII Phosphorylation at Thr551 Reduces GKAP Binding

We directly tested for an effect of Shank3 Thr551 phosphorylation on GKAP binding *in vitro*. The GST-Shank3-WT or GST-Shank3-T551A proteins were phosphorylated for an extended time (20 min) using purified CaMKIIα or incubated under control conditions (lacking CaMKIIα) and then mixed with lysates of HEK293T cells expressing HA-GKAP.

Immunoblot analysis of GST protein complexes revealed that specific binding of HA-GKAP to non-phosphorylated control GST-Shank3-WT and GST-Shank3-T551A was indistinguishable (Figure 6.5A). However, pre-phosphorylation of GST-Shank3-WT by CaMKIIα decreased GKAP binding by about 50%, and this effect was abrogated by T551A mutation (Figure 6.5A). As an additional control, we performed a similar experiment with HEK293T lysates expressing HA-Ca_V1.3-CTD, another Shank3 PDZ domain binding protein. Neither CaMKII phosphorylation or the T551A mutation had any effect on HA-Ca_V1.3-CTD binding (Figure 6.5B). These data directly demonstrate that Shank3 Thr551 phosphorylation specifically disrupts binding of GKAP to Shank3.

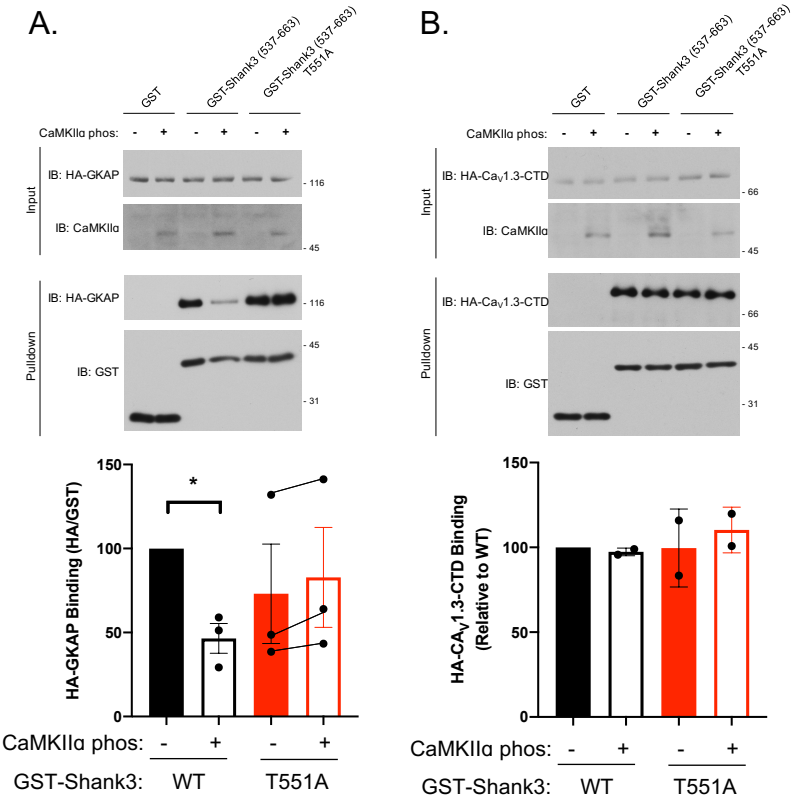

Figure 6.5: CaMKII Phosphorylation at Thr551 directly reduces GKAP binding.

A. GST, GST-Shank3 WT, or GST-Shank3-S685A were pre-phosphorylated with CaMKIIα and incubated with HEK293T cell lysate expressing HA-GKAP. Control protein samples were pre-

incubated in the absence of CaMKIIα. Isolated GST complexes were then analyzed by immunoblotting as indicated. T551A -/+ conditions are not statistically different from WT or from each other. **B.** Parallel experiments were performed with HEK293T cell lysates expressing HA-Ca_V1.3-CTD. No significant difference in pulled down HA-Ca_V1.3-CTD is observed. Representative of 2-3 replicates. Error bars, mean ± SEM.

6.6 Discussion

In this chapter, we show that Shank3 Thr551 is the preferred site of CaMKII phosphorylation in the Shank3 N-terminal extension of the canonical PDZ domain. The Shank3 N-terminal extension is critical for high affinity binding of GKAP to Shank3, and several of our observations support the conclusion that CaMKII phosphorylation at Thr551 reduces the binding of GKAP. We demonstrate that mutations of Thr551 to phospho-mimetic Asp reduce GKAP co-immunoprecipitation and overexpression of a constitutively active CaMKII in HEK293T cells results in phosphorylation of Shank3 and reduces GKAP binding as well. We also show that direct phosphorylation of a GST-Shank3 fusion protein containing Thr551 disrupts GKAP binding and this is prevented in a phospho-null T551A mutant.

We show that GKAP co-immunoprecipitation with mAp-Shank3 from HEK293T cells requires the canonical PDZ domain of Shank3 (Figure 6.2). This observation supports previous characterization of GKAP binding to Shank3. In those studies, deletion of the BC loop in the canonical Shank3 PDZ domain completely prevented GKAP binding. In contrast, deletion of the N-terminal extension only reduced GKAP binding by 50% (Zeng et al., 2016). Our observation that phosphorylation of Thr551 does not completely disrupt the interaction between Shank3 and GKAP (Figure 6.5) is consistent with these findings,

leading us to hypothesize that the reduction of GKAP binding to Shank3 following Thr551 phosphorylation will allow for an increase in the relative binding of other PDZ interacting proteins that are not sensitive to modification at Thr551, such as $Ca_V1.3$ (Figure 6.3C). Future studies will determine which Shank3 PDZ-binding proteins are affected and the functional relevance of this mechanism.

Although Thr551 is the primary phosphorylation site identified in the N-terminal extension, Ser557 may also be phosphorylated. There is no difference in phosphorylation between T551A and 551/557AA mutants, suggesting that Ser557 is not phosphorylated *in vitro* under the conditions used here. Future studies will need to determine if CaMKII can significantly phosphorylate Ser557 using longer incubation times and/or *in vivo*. Alternatively, Ser557 may be targeted by other kinases. These studies are very significant because Ser557 mutation to Asp can decrease GKAP binding to GST-Shank3(537-828) to a similar extent as a Thr551 mutation to Asp. Thus, dual phosphorylation of both sites may have a synergistic effect to decrease the binding of GKAP. Functional studies should include Shank3-551/557AA or Shank3-551/557DD mutants to properly block or mimic the dual phosphorylation in the N-terminal extension.

Our studies also show that the electrophoretic mobility of both GFP-Shank3 and HA-GKAP is markedly reduced by the co-expression of constitutively active CaMKII (CaMKIIα-D/AA). This reduction likely indicates that CaMKII can phosphorylate several sites in both Shank3 (see Figure 4.2) and GKAP. CaMKII phosphorylation of GKAP has been previously described at N-terminal residues that affect other GKAP protein

interactions, such as binding with PSD-95 (Shin et al., 2012). This does not exclude the possibility that CaMKII phosphorylation of GKAP may also affect GKAP-Shank3 binding. CaMKII phosphorylation of GKAP could be tested by mutating known phosphorylation sites to phospho-null Ala, or looking for CaMKII phosphorylation of a GST-GKAP fusion protein containing the C-terminus that binds to Shank3. Alternatively, HEK293T cell cultures could be separately transfected with either HA-GKAP or GFP-Shank3 and CaMKIIα-D/AA, so that CaMKII can only phosphorylate either GKAP or GFP-Shank3, respectively prior to cell lysis for protein interaction assays. The potential biological implications of the reduced binding of GKAP to Shank3 following Thr551 phosphorylation will be discussed in Chapter VIII.

CHAPTER VII

ROLE OF SHANK3 IN LTCC-DEPENDENT SIGNALING TO THE NUCLEUS AND ACTIVITY-DEPENDENT GENE EXPRESSION

7.1 Introduction

Neuronal depolarization stimulates Ca^{2+} influx and multiple intracellular signaling pathways that are essential for normal brain functions. One example is excitation-transcription (E-T) coupling: Ca^{2+}-dependent phosphorylation of the nuclear transcription factor CREB at Ser^{133} stimulates the transcription of immediate early genes encoding multiple proteins (e.g., c-Fos, BDNF, homer1a) that play key roles in learning and memory (Bading, 2013; Benito et al., 2011; Dolmetsch, 2003; Flavell and Greenberg, 2008). Disruptions in activity-dependent gene expression are associated with multiple neuropsychiatric disorders (Ebert and Greenberg, 2013; Gallo et al., 2018) that have been linked to mutations in Ca^{2+} signaling proteins, including L-type calcium channels (LTCCs) and calcium/calmodulin-dependent protein kinase II (CaMKII) (Akita et al., 2018; Chia et al., 2018; Cohen et al., 2018; Dick et al., 2016; Kury et al., 2017; Limpitikul et al., 2016; Moon et al., 2018; Nyegaard et al., 2010; Pinggera et al., 2015; Pinggera et al., 2017; Pinggera and Striessnig, 2016; Proietti Onori et al., 2018; Stephenson et al., 2017). For example, Timothy Syndrome is caused by mutations in the $Ca_V1.2$ LTCC $\alpha1$ subunit that can disrupt neuronal E-T coupling (Li et al., 2016), contributing to neurobehavioral symptoms of this complex disorder, including autism spectrum disorder (ASD). Recent

studies have shown that the initiation of this LTCC-dependent E-T coupling requires recruitment of multiple CaMKII holoenzymes to a nanodomain close to LTCCs (Ma et al., 2014; Wang et al., 2017b; Wheeler et al., 2008), and that E-T coupling is disrupted by a CaMKII mutation linked to intellectual disability (Cohen et al., 2018). Disruptions of CaMKII binding to the NTD of $Ca_V1.3$ disrupt E-T coupling (Wang et al., 2017b). In addition, binding of the Shank3 PDZ domain to a C-terminal PDZ-binding motif in $Ca_V1.3$ LTCCs is important for LTCC clustering in neuronal dendrites and signaling to increase CREB phosphorylation (Zhang et al., 2005). Although these protein-protein interactions may support the organization and function of this LTCC nanodomain, the exact role of Shank3, as well as the Shank3-CaMKII interaction, remain incompletely understood. Therefore, we hypothesized that the direct interaction of CaMKII with Shank3 characterized in chapter 3 is important for CaMKII function within the LTCC nanodomain that is required for neuronal E-T coupling.

7.2 Effects of Shank3 Overexpression on LTCC Signaling to the Nucleus

Previous studies indicate that Shank3 is critical for optimal LTCC signaling that increases Ser^{133} phosphorylation of the CREB transcription factor in the nucleus (Zhang et al., 2005). This pathway can be initiated by local Ca^{2+} influx, without requiring global increases in Ca^{2+}, and requires CaMKII recruitment to this LTCC nanodomain (Ma et al., 2014; Wang et al., 2017b; Wheeler et al., 2008). Since Shank3 interacts with several other proteins, in addition to the C-terminal domain of $Ca_V1.3$ LTCCs (via its PDZ domain (Zhang et al., 2005)) and CaMKII (current observation), any effects of manipulating Shank3 expression on signaling to the nucleus may involve multiple mechanisms. The

role of CaMKII-binding to Shanks may be revealed by comparing the effects of expressing Shank3-WT and Shank3-AAA (which cannot bind CaMKII). As a complementary tool, we also generated a Shank3 mutant lacking the entire PDZ domain (Shank3-ΔPDZ) that is unable to interact with the C-terminal domain of $Ca_V1.3$ (Figure 7.1A). Comparing the effects of expressing Shank3-WT and Shank3-ΔPDZ in neurons reveals the role of the Shank3 PDZ domain binding to $Ca_V1.3$, and potentially other proteins.

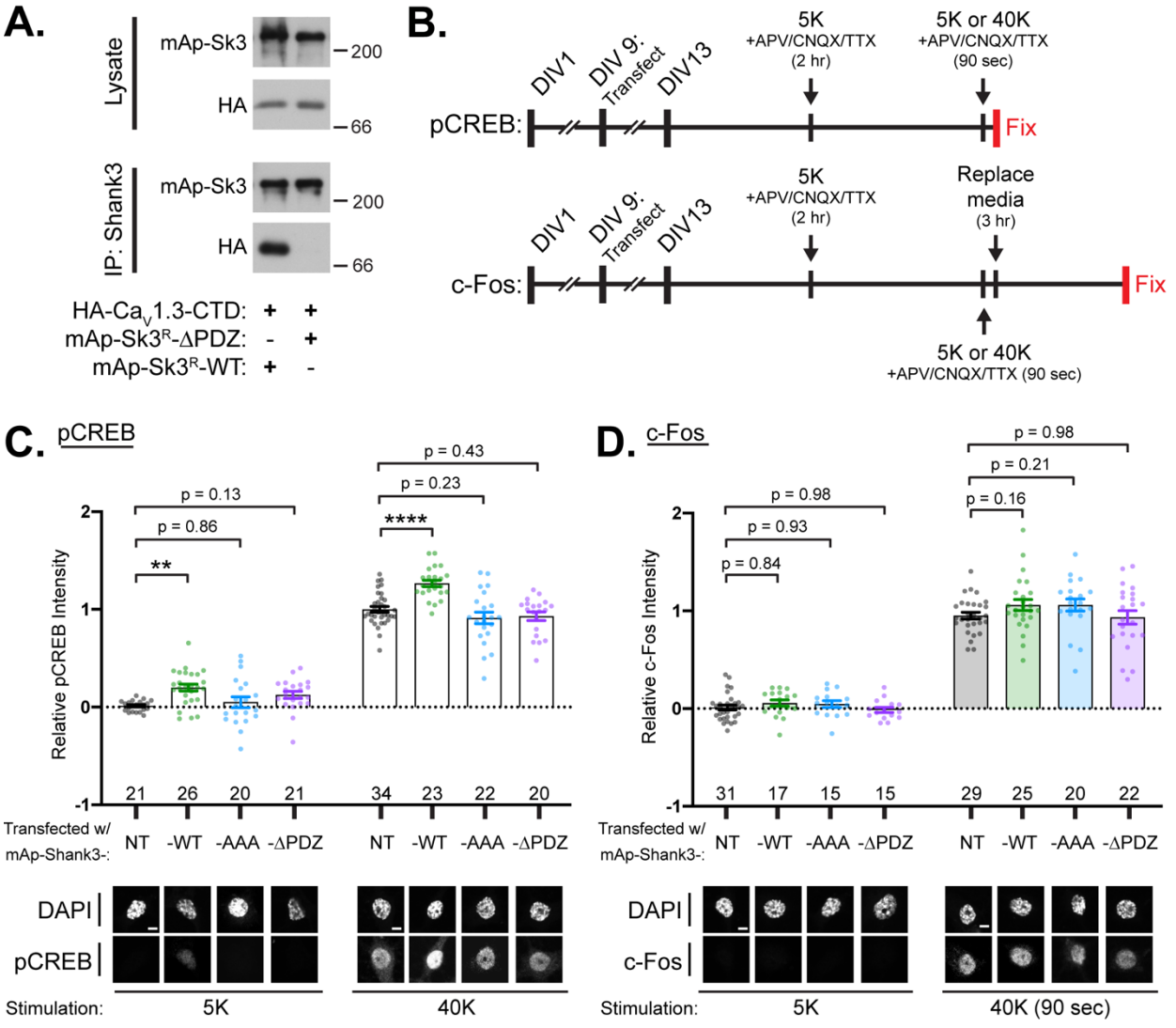

Figure 7.1: Effects on Shank3 overexpression on LTCC signaling to the nucleus.

A. Shank3 was immunoprecipitated from soluble fractions of HEK293T cells expressing HA-$Ca_V1.3$-CTD with mAp-Shank3^R-WT or mAp-Shank3^R-ΔPDZ. Immunoblots (representative of 3 biological replicates) demonstrate that HA-$Ca_V1.3$-CTD co-immunoprecipitates with mAp-Shank3^R-WT, but not with mAp-Shank3^R-ΔPDZ. **B.** Schematic of experimental protocols. Primary hippocampal neurons were transfected (see below) and then incubated to stimulate LTCC signaling to the nucleus (see Methods). Neurons were either fixed and stained using DAPI and pSer133-CREB antibodies after a 90 s depolarization (top: for panel C), or incubated for an additional 3 hours in conditioned media before fixation and staining with DAPI and c-Fos antibodies (bottom: for panel D). **C**. Overexpression of mAp-Shank3-WT, but not mAp-Shank3-AAA or mAp-Shank3--ΔPDZ, increases the levels of pCREB staining relative to non-transfected neurons under basal and depolarized conditions (2-way ANOVA with 2 factors (Mutant, Stimulation) Mutant $F_{(3,179)} = 17.86$ $p < 0.0001$, Stimulation $F_{(1,179)} = 1108$ $p < 0.0001$, Interaction $F_{(3,179)} = 4.442$ $p < 0.01$, Dunnett's multiple comparisons test, ** $p < 0.01$, **** $p < 0.0001$). **D**. The expression of c-Fos is not affected by overexpression of mAp-Shank3-WT, mAp-Shank3-AAA or mAp-Shank3--ΔPDZ. (2-way ANOVA with 2 factors (Mutation, Stimulation) Mutation $F_{(3,166)} = 2.152$, Stimulation $F_{(1,166)} = 830.1$ $p < 0.0001$, Interaction $F_{(3,166)} = 0.3284$, Dunnett's multiple comparisons test). The bar graphs reports the mean ± SEM, with the superimposed data points representing values from single cells accumulated from 3-5 independent neuronal cultures/transfections. Images below the bar graphs are of representative nuclei for each condition. *Scale bars*, 5 μm.

We initially compared the effects of overexpressing the wildtype or mutated Shank3 proteins on LTCC/CaMKII-dependent signaling to the nucleus in cultured hippocampal neurons using a well-established stimulation paradigm (Figure 7.1B, *top*) (Li et al., 2016; Ma et al., 2014; Wang et al., 2017b; Wheeler et al., 2008). Intrinsic neuronal activity was blocked by pre-incubation in 5 mM K^+ Tyrode's solution (5K) containing APV and CNQX (to block activation of NMDA- and AMPA-type glutamate receptors) and tetrodotoxin (TTX: to inhibit voltage-dependent sodium channels). Neurons were then depolarized by replacing the solution with 40 mM K^+ Tyrode's solution (40K) in the presence of APV, CNQX, and TTX for 90 seconds. It is well established that this treatment robustly

increases nuclear staining detected using a phospho-Ser^{133}-specific CREB antibody (pCREB intensity) that can be completely disrupted by the selective LTCC blocker nimodipine (10 μM) (Wheeler et al., 2012) (Wang et al, 2017). To determine whether this depolarization also induces gene expression, the depolarization buffer was replaced with conditioned media after 90 s, and neurons were fixed 3 hours later to immuno-stain them for expression of the c-Fos immediate early gene (Figure 7.1B, *bottom*). The brief neuronal depolarization is sufficient to induce a robust increase in c-Fos protein staining 3 hour later (Figure 7.1D), that can be completely blocked by preincubation with 10 μM nimodipine (Perfitt and Colbran, unpublished observation).

In order to identify transfected neurons, Shank3-WT, -AAA, and -ΔPDZ were overexpressed as mApple-tagged proteins. Approximately 3 days after transfection, cultures were fixed under basal (5K) conditions or after the 90 s 40K depolarization (see above) and examined by confocal microscopy to quantify pCREB signals in mApple- and CaMKIIα-expressing DAPI stained nuclei relative to CaMKIIα-expressing DAPI stained nuclei in non-transfected cultures. The overexpression of mAp-Shank3-WT resulted in a small but significant increase in pCREB intensity in both unstimulated and depolarized neurons relative to non-transfected neurons (Figure 7.1C, compare green and black bars). Notably, this increase of pCREB intensity was not detected in neurons overexpressing similar levels of mAp-Shank3-AAA or mAp-Shank3-ΔPDZ (Figure 7.1C, blue and purple bars). However, the modest increases in pCREB intensity following overexpression of mAp-Shank3-WT were not sufficient to enhance c-Fos expression in unstimulated or depolarized neurons (Figure 7.1D). Taken together, these data indicate

that under these conditions the overexpression of Shank3 has relatively limited effects on LTCC signaling to the nucleus, perhaps because these cells contain significant levels of endogenous Shank3.

7.3 Shank3 is Required for LTCC-CREB Phosphorylation and Gene Expression

In order to further investigate the role of Shank3 in LTCC signaling to the nucleus, we adopted an shRNA knockdown approach to suppress the expression of endogenous Shank3. First, we confirmed that a previously used shRNA targeting Shank3 (Verpelli et al., 2011) essentially completely suppressed the expression of mAp-Shank3-WT or mAp-Shank3-AAA in HEK293 cells, whereas a control shRNA (Boudkkazi et al., 2014) has no effect (Figure 7.2A, lanes 2 and 3). Moreover, the Shank3 shRNA has no effect on expression of an shRNA-resistant form of Shank3 (mAp-Shank3^{R}) (Figure 7.2A, lanes 6-8). Subsequent studies showed that staining for Shank3 protein in CaMKII-positive primary hippocampal neurons was reliably decreased in neurons expressing the Shank3 shRNA relative to nearby non-transfected neurons (Figure 7.2B), further demonstrating its efficacy.

Prior studies indicated that deletion of five C-terminal amino acids from $Ca_V1.3$, which prevents binding to Shank3, has little impact on LTCC gating, or on the whole cell LTCC current amplitude or current-voltage relationship in heterologous cells and in cultured neurons, or on total $Ca_V1.3$-LTCC-mediated neuronal Ca^{2+} influx (Zhang et al., 2005). However, the impact of neuronal Shank3 knockdown on LTCC-mediated Ca^{2+} influx has not been determined. Therefore, we used Fura-2 to assess somatic Ca^{2+} responses during a 40K depolarization, implemented as for our studies of pCREB levels and c-Fos

expression (see Methods). Comparison of average Ca^{2+} responses (ΔF/F0) over time in neurons expressing control or Shank3 shRNA from four independent experiments revealed no statistically significant difference (Figure 7.2C, *left*). Similarly, Shank3 knockdown had no statistically significant impact on total Ca^{2+} influx, as estimated from the areas under the curve from each experiment (Figure 7.2C, *right*), However, there was a trend for a small reduction of Ca^{2+} influx in Shank3 shRNA neurons. Taken together, these data indicate that knockdown of Shank3 expression results in little reduction of global Ca^{2+} influx via LTCCs under these conditions.

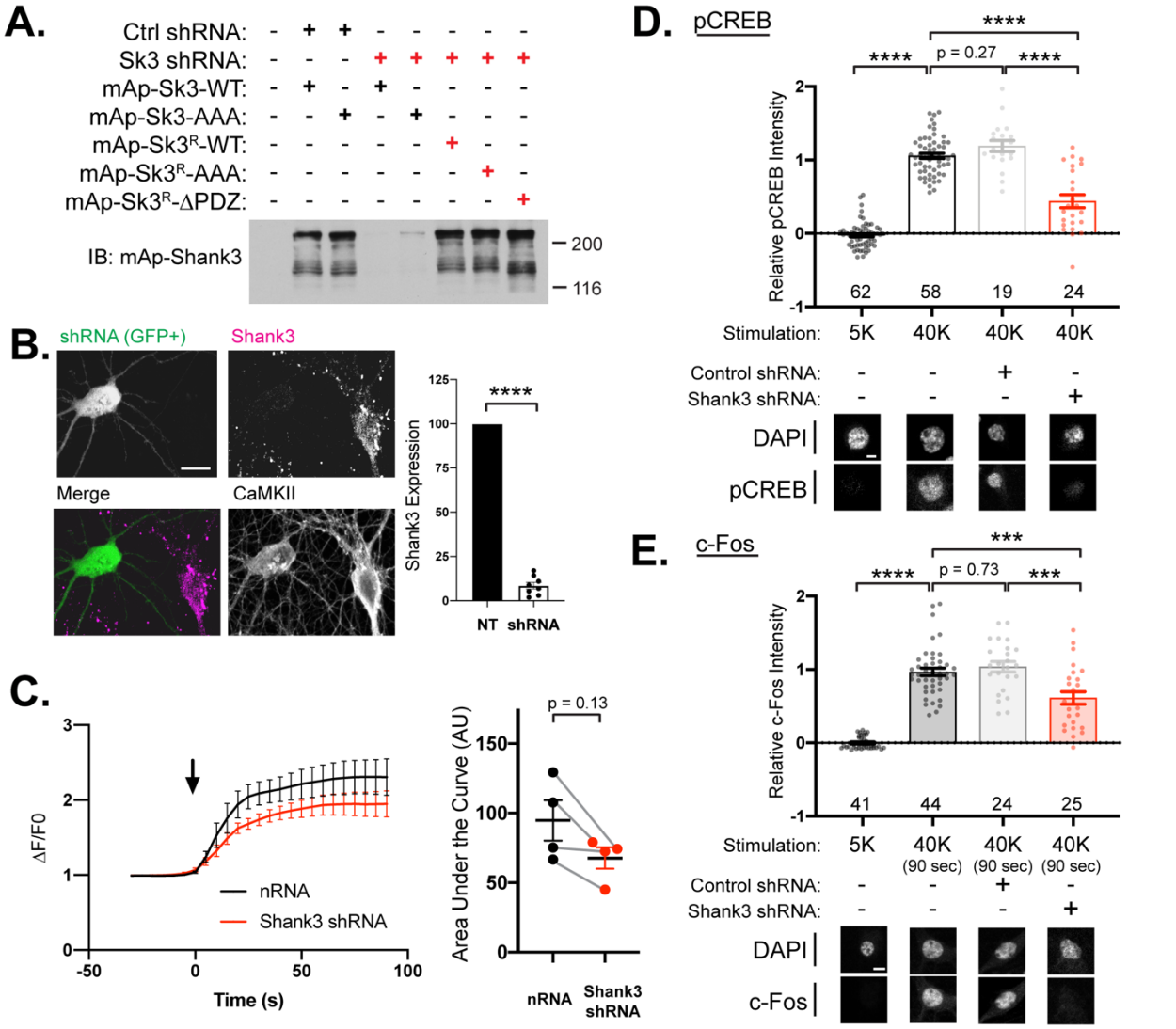

Figure 7.2. Shank3 knockdown disrupts pCREB signaling and c-Fos expression.

A. Validation of Shank3 shRNA and mApple-Shank3 shRNA-resistant (mAp-Shank3^R) expression vectors. Expression of shRNA, mAp-Shank3 and mAp-Shank3^R in HEK293T cells. Lysates of cells expressing (as indicated above) a control shRNA or Shank3 shRNA, along with mAp-Shank3 constructs with the wild type shRNA target sequences (mAp-Shank3-WT and mAp-Shank3-AAA) or contain 'silent' mutations that confer shRNA resistance (mAp-Shank3^R constructs) were immunoblotted for Shank3 (NeuroMab antibody). **B**. DIV13 primary hippocampal neurons transfected at DIV10 with Shank3 shRNA (GFP+) and stained for Shank3 (magenta: CST antibody) and CaMKIIα (a marker of excitatory neurons, white). Neurons expressing the Shank3 shRNA contain substantially reduced levels of Shank3 (reduced by 91±2% relative to nearby non-transfected excitatory neurons: **** $p < 0.0001$, one-sample unpaired Student's t-test with equal variance compared to a theoretical value of 100). The bar graph reports the mean ± SEM, with each data point representing a single cell accumulated from 3 independent neuronal cultures/transfections. *Scale bars*, 20 µm. **C.** Shank3 knockdown has little effect on global Ca^{2+} influx. *Left*, Fura-2-loaded hippocampal neurons transfected with control shRNA (nRNA) or Shank3 shRNA were equilibrated with Tyrode's solution containing 5 mM KCl for 3-5 min and switched (black arrow) to Tyrode's solution containing 40 mM KCl for 90 s. The graph plots mean ± SEM ΔF/F0 values for the last 30 s of the equilibration period and during the 90 s depolarization from four independent experiments (12-90 cells per replicate). The data were analyzed using a 2-way repeated measures ANOVA: Factor 1 (time), $F_{(1.342,8.049)}=32.63$, $p=0.0003$. Factor 2 (control/shRNA), $F_{(1,6)}=1.703$ $p=0.2398$. Interaction, $F_{(35,210)}=0.8281$, $p=0.7423$. *Right*, Comparison of average areas under the curve (AUC) from each independent experiment revealed no statistically significant difference (n=4, p=0.13. Paired Student's t test with equal variance). **D**. The robust increase in pCREB levels following a brief depolarization (as in Figure 6A) is significantly reduced in cells expressing the Shank3 shRNA (red bar), but not control shRNA (grey bar) (5K versus 40K: unpaired Student's t-test with equal variance, **** $p < 0.0001$; 40K stimulations: 1-way ANOVA, $F_{(2,98)} = 38.17$, $p < 0.0001$. Tukey's post-hoc test, **** $p < 0.0001$). **E**. Similarly, the robust increase in c-Fos expression 3 hours after the brief depolarization is significantly reduced in cells expressing Shank3 shRNA (red bar), but not control shRNA (grey bar) (5K versus 40K: unpaired Student's t-test with equal variance, **** $p < 0.0001$; 40K stimulations: 1-way ANOVA, $F_{(2,90)} = 9.990$ $p < 0.001$, Tukey's post-hoc test, *** $p < 0.001$). The bar graph report the mean ± SEM with each data point representing a single cell accumulated from 3 independent neuronal cultures/transfections. Images below the bar graphs are of representative nuclei for each condition. *Scale bars*, 5 µm.

Neuronal cultures were then transfected to express either control or Shank3 shRNA and depolarized for 90 s. While control shRNA had no effect on pCREB intensity (Figure 7.2D, grey bar), neurons expressing Shank3 shRNA had a significant, if partial, reduction in pCREB intensity relative to non-transfected neurons and control shRNA expressing neurons (Figure 7.2D, red bar). This decrease in pCREB intensity in neurons expressing the Shank3 shRNA was mirrored by a parallel decrease of c-Fos expression when assessed 3 hours after the brief depolarization (Figure 7.2E, red bar), whereas c-Fos was robustly expressed in non-transfected neurons and neurons expressing control shRNA 3 hours after stimulation. Thus, Shank3 expression appears to be necessary for the full extent of both CREB phosphorylation as well as c-Fos expression following a brief neuronal depolarization.

7.4 Rescue of shRNA Effects by Shank3-WT, but not Shank3-AAA or -ΔPDZ.

We then investigated whether the Shank3 shRNA-induced suppression of CREB phosphorylation and c-Fos expression following neuronal depolarization could be rescued by Shank3 re-expression from shRNA-resistant constructs (mAp-Shank3^{R}). Neurons were transfected to express Shank3 shRNA alone or Shank3 shRNA plus either mAp-Shank3^{R}-WT, mAp-Shank3^{R}-AAA, or mAp-Shank3^{R}-ΔPDZ. Following a brief 90 s depolarization, pCREB staining was quantified in neurons expressing the shRNA, and in nearby non-transfected neurons within the same dish, to provide an internal control for each experiment with a similar robust increase of the pCREB intensity under all conditions (Figure 7.3A, black bars). As seen in Figure 6.2D, expression of the Shank3 shRNA

significantly, if partially, reduced the pCREB signal (Figure 6.3A, red bar), but expression of mAp-Shank3^{R}-WT rescued pCREB intensity to a level slightly but significantly higher than that in non-transfected neurons (Figure 7.3A, green bar). However, the level of pCREB intensity was not rescued by expression of either mAp-Shank3^{R}-AAA or mAp-Shank3^{R}-ΔPDZ (Figure 7.3A, blue and purple bars). Moreover, analysis of parallel neuronal cultures 3 hours following the end of the brief depolarization revealed that the partial suppression of c-Fos expression by the Shank3 shRNA was also rescued by mAp-Shank3^{R}-WT, but not by mAp-Shank3^{R}-AAA or mAp-Shank3^{R}-ΔPDZ (Figure 7.3B). However, c-Fos expression in neurons expressing both the Shank3 shRNA and mAp-Shank3^{R}-WT was not significantly different from c-Fos levels in nearby non-transfected neurons, in contrast to pCREB intensity levels with this transfection condition. Taken together, these findings significantly extend previous studies by showing that the Shank3 PDZ domain is important for LTCC signaling to the nucleus, presumably by binding to $Ca_V1.3$ (Zhang et al., 2005), and that CaMKII binding to Shank3 also plays a key role in this pathway. Importantly, these interactions with Shank3 play a key role not only in the depolarization-induced increases of CREB phosphorylation, but also for the downstream increase in the expression of c-Fos, an important immediate early gene.

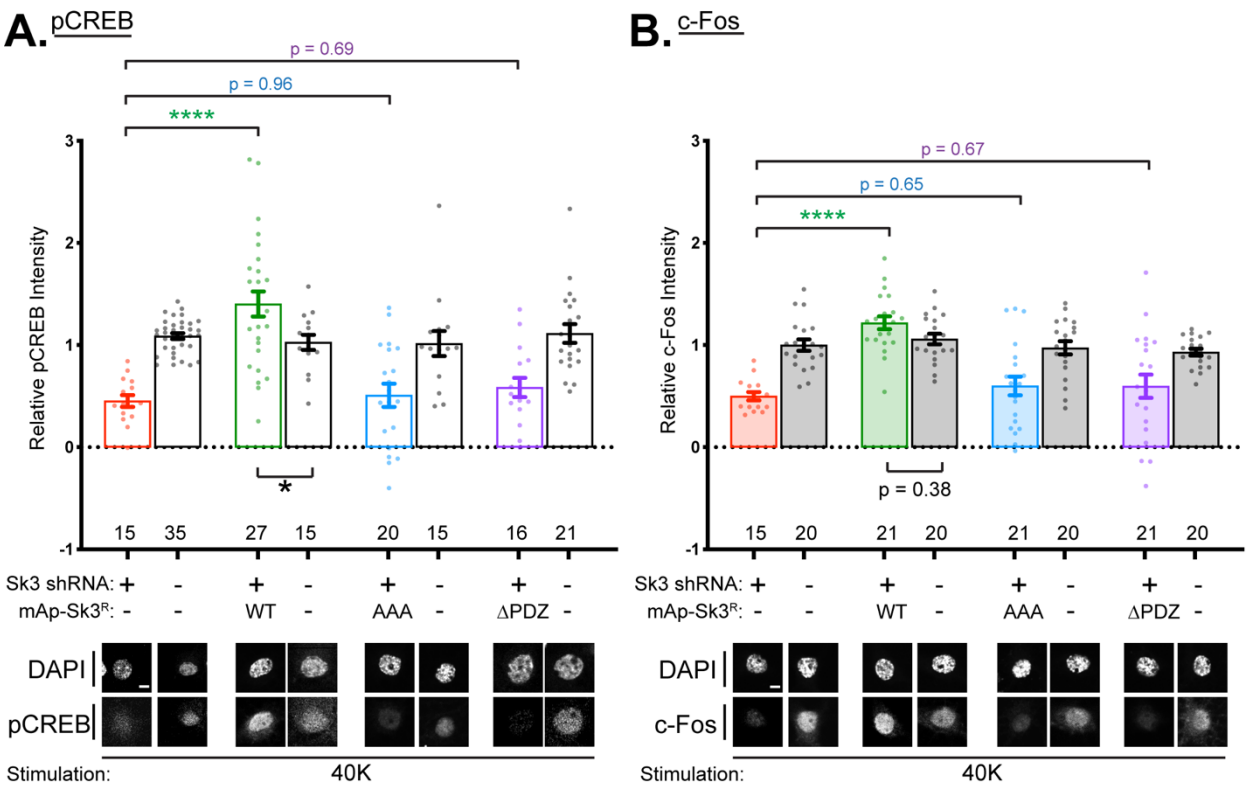

Figure 7.3. Rescue of pCREB signaling and c-Fos gene expression after Shank3 shRNA knockdown.

The Shank3 shRNA construct was transfected alone or with shRNA-resistant mAp-Shank3^{R}-WT (green bar), mAp-Shank3^{R}-AAA (blue bar), or mAp-Shank3^{R}-ΔPDZ (purple bar). Neurons were depolarized for 90 s and the levels of pCREB (A) and c-Fos (B) were determined (see Methods) in transfected (colored bars) and nearby non-transfected (black bars) neurons. **A.** The expression of mAp-Shank3^{R}-WT, but not mAp-Shank3^{R}-AAA, or mAp-Shank3^{R}-ΔPDZ rescued signaling to pCREB relative to shRNA alone. In addition, neurons expressing Shank3-WT had significantly higher pCREB signal relative to nearby, non-transfected neurons. (2-way ANOVA with 2 factors (Mutant, Transfection) Mutant $F_{(3,156)} = 10.14$ $p < 0.0001$, Transfection $F_{(1,156)} = 22.70$ $p < 0.0001$, Interaction $F_{(3,156)} = 12.29$ $p < 0.0001$, comparison between mutants: Dunnett's multiple comparisons test, **** $p < 0.0001$; comparison between transfected/non-transfected cells: Sidak's multiple comparisons test, * $p < 0.05$). **B**. The expression of mAp-Shank3^{R}-WT, but not mAp-Shank3^{R}-AAA, or mAp-Shank3^{R}-ΔPDZ rescued signaling to increase c-Fos expression relative to shRNA alone. (2-way ANOVA with 2 factors (Mutant, Transfection) Mutant $F_{(3,150)} = 13.80$ $p < 0.0001$, Transfection $F_{(1,150)} = 26.52$ $p < 0.0001$, Interaction $F_{(3,150)} = 8.149$ $p < 0.0001$, comparison between mutants: Dunnett's multiple comparisons test, **** $p < 0.0001$; comparison between transfected/non-transfected cells: Sidak's multiple comparisons test). The bar graph reports the

mean ± SEM, with each data point representing a single cell, accumulated from 4-5 independent neuronal cultures/transfections. Images below the bar graphs are of representative nuclei for each condition. *Scale bars*, 5 μm.

7.5 Discussion

Our studies show that Shank3 has important roles in E-T coupling initiated by LTCC-dependent Ca^{2+} influx, which activates CaMKII to stimulate CREB phosphorylation and c-Fos expression. Precise regulation of gene transcription is important for long-term, activity-dependent changes in synaptic properties and behavior. Diverse stimulation paradigms increase Ser^{133} phosphorylation of the nuclear CREB transcription factor to stimulate immediate early gene transcription, and CREB is important for learning and long-term memory (reviewed in (Alberini, 2009; Kandel, 2012; Kida and Serita, 2014; Shaywitz and Greenberg, 2000). Plasma membrane LTCCs are major regulators of nuclear CREB phosphorylation and immediate early gene expression following depolarization (Bading, 2013; Dolmetsch, 2003; Flavell and Greenberg, 2008; Wheeler et al., 2008). Both of the major neuronal LTCC α1 subunits, $Ca_V1.2$ and $Ca_V1.3$, can initiate LTCC-CREB signaling, depending on the brain region (Hetzenauer et al., 2006) and the strength of depolarization (Zhang et al., 2006). The C-terminal domains (CTDs) of both $Ca_V1.2$ and $Ca_V1.3$ contain canonical binding motifs for class 1 PDZ domains, and deletion of these motifs disrupts channel trafficking and clustering, as well as downstream signaling to increase CREB phosphorylation, although these mutations do not appear to affect global increases in Ca^{2+} following neuronal depolarization (Weick et al., 2003; Zhang et al., 2005). These CTD mutations might disrupt CREB signaling by interfering with the local LTCC nanodomain and/or with conformational changes in LTCCs that are

required for E-T coupling (Li et al., 2016). However, CTDs of $Ca_V1.2$ and $Ca_V1.3$ interact with distinct proteins. The CTD of $Ca_V1.3$, but not $Ca_V1.2$, can interact with PDZ domains of Shank1 or Shank3 (Zhang et al., 2005), but the roles of Shanks in LTCC-CREB signaling have not been previously investigated. Our shRNA experiments showed that the expression of Shank3 is essential for maximal LTCC-CREB-c-Fos signaling, with a little impact on global increases in Ca^{2+} concentrations. Moreover, shRNA rescue experiments revealed that the PDZ domain in Shank3 is required for this signaling, consistent with the idea that interaction of the Shank3 PDZ domain with the $Ca_V1.3$ CTD is important for the initiation of E-T coupling, and significantly extending prior findings. Residual E-T coupling following Shank3 knockdown may be mediated by Shank3-independent $Ca_v1.2$ LTCC signaling, although our data cannot preclude contributions from low levels of residual Shank3 expression or from Shank1. Nevertheless, our observations strongly support a model in which Shank3 actions within the LTCC/Ca^{2+} nanodomain are required for efficient E-T coupling to increase both CREB phosphorylation and c-Fos expression.

The form of LTCC-dependent E-T coupling studied herein also requires direct interaction of CaMKII with the N-terminal domain of $Ca_V1.3$ $\alpha1$ subunits in LTCC nanodomains (Wang et al., 2017b; Wheeler et al., 2008). How can this observation be reconciled with the current finding that LTCC-CREB signaling is also disrupted by mutation of the tri-basic residue motif in Shank3 to prevent CaMKII-binding? Since CaMKII holoenzymes can bind simultaneously to multiple CaMKAPs (Robison et al., 2005b), different subunits within a single dodecameric CaMKII holoenzyme may interact with $Ca_V1.3$ and Shank3,

potentially providing a conformational constraint on LTCC cytoplasmic domains that could affect Ca^{2+} influx. Alternatively, $Ca_V1.3$ and Shank3 may recruit two different CaMKII holoenzymes to the LTCC nanodomain to facilitate a trans-holoenzyme autophosphorylation that appears to be required for shuttling Ca^{2+}/CaM to the nucleus to stimulate CREB phosphorylation (Cohen et al., 2018; Ma et al., 2014). Both hypotheses predict that loss of any one of these three proteins or disruption of any one of their mutual interactions would interfere with this form of E-T coupling.

Although mutual interactions of CaMKII, Shank3 and $Ca_V1.3$ LTCCs are required to initiate this form of E-T coupling, the precise role of these interactions remains unresolved. Knockdown of CaMKII or Shank3 expression has at most a rather modest effect on depolarization-induced global Ca^{2+} signals under our conditions (Wang et al., 2017b) (Figure #). However, it remains possible that CaMKII and/or Shank3 modulate Ca^{2+} concentrations within the LTCC nanodomain. CaMKII can potentiate net Ca^{2+} influx via $Ca_V1.3$ LTCCs by decreasing Ca^{2+}-dependent inactivation in heterologous cells (Jenkins et al., 2010); critically, this modulation requires co-expression of densin, another synaptic CaMKAP containing a PDZ domain that binds to the $Ca_V1.3$ CTD. Like Shank3, densin has no direct effect on the biophysical properties of LTCCs (Jenkins et al., 2010; Zhang et al., 2005), but Shank3 presumably competes with densin for binding to the CTD of $Ca_V1.3$, perhaps disrupting CaMKII- and densin-dependent facilitation of Ca^{2+} influx via $Ca_V1.3$. However, since this would reduce overall Ca^{2+} influx, it seems unlikely that such a competition plays a role in initiating E-T coupling, although it is possible that Shank3 can support CaMKII modulation of $Ca_V1.3$ inactivation in a similar (or perhaps distinct)

manner. CaMKII also was reported to mediate the effects of IGF1 to facilitate $Ca_V1.3$ currents at weaker depolarizing membrane potentials, as well as CREB phosphorylation (Gao et al., 2006). Specific mechanisms underlying both of these effects of CaMKII on $Ca_V1.3$ remain poorly understood, but it is possible that CaMKII phosphorylation of $Ca_V1.3$ $\alpha1$ or β subunits or Shank3 is involved. A significant challenge in elucidating these mechanisms will be to assess their impact within the context of the LTCC/Ca^{2+} nanodomain that initiates E-T coupling. Clearly, further studies will be needed to more precisely define these biochemical mechanisms within the LTCC nanodomain.

Shank3 is a commonly mutated gene in individuals diagnosed with ASD or other neuropsychiatric disorders (Gauthier et al., 2010; Herbert, 2011), and c-Fos expression is dysregulated in rodent models of autism (Dubiel and Kulesza, 2015; Orlandini et al., 1996; Williams and Umemori, 2014). Interestingly, increases or decreases in Shank3 expression appear to be associated with distinct neuropsychiatric phenotypes (Bozdagi et al., 2010; Han et al., 2013; Uchino and Waga, 2013). Moreover, three unique point mutations in $Ca_V1.3$ identified in patients with ASD result in gain-of-function phenotypes (Pinggera et al., 2015; Pinggera et al., 2017) and a point mutant in $Ca_V1.2$ associated with Timothy Syndrome increases CREB phosphorylation (Li et al., 2016), indicating that CREB may be hyper-phosphorylated in some neuropsychiatric disorders. Diverse changes in E-T coupling may result from disruption of the LTCC nanodomain due to altered interactions between ASD-linked postsynaptic proteins (Bourgeron, 2009). Our recent work showed that an ASD-linked *de novo* CaMKIIα-E183V mutation disrupts interactions with Shank3 and several other CaMKAPs (Stephenson et al., 2017), including

the $Ca_V1.3$-NTD (Perfitt, Stephenson, and Colbran, unpublished observations). Thus, even though initial studies failed to detect gross changes in CaMKII expression following genetic disruptions of Shank3 (e.g., (Peca et al., 2011)), the present findings suggest that more detailed investigations of the role of CaMKII in animal models of neuropsychiatric disorders are warranted.

CHAPTER VIII

DISCUSSION AND FUTURE DIRECTIONS

8.1 Summary of Results

The work presented in this dissertation provides novel insights into the complex roles of CaMKII and interacting proteins, such as Shank3 and LTCC $Ca_V1.3$, in initiation of E-T coupling to the nucleus. We have biochemically characterized a novel protein-protein interaction between CaMKII and Shank3. The CaMKII-binding domain of Shank3 has no previously known function, but has similarities to the CaMKII-binding domains of $Ca_V1.3$ and mGlu5. Together, these proteins form a novel subclass of CaMKAPs containing a tribasic residue motif that is essential for CaMKII-binding. Shank3 is also phosphorylated by CaMKII at multiple sites, well separated from the CaMKII-binding domain in the primary amino acid sequence. These phosphorylation sites have distinct functional roles, such as enhancing the ABI1-Shank3 interaction (Ser685) and disrupting the GKAP-Shank3 interaction (Thr551). On a cellular level, the CaMKII-Shank3 interaction is a critical component of LTCC signaling from the synapse to the nucleus in excitatory hippocampal neurons. Collectively, these findings present a thorough investigation of the hypotheses presented in Chapter I and throughout the dissertation.

Future research into the biochemical and biophysical properties of the CaMKII-$Ca_V1.3$-Shank3 complex are still warranted, along with further identification of the functional role of the many CaMKII phosphorylation sites identified in our mass spectrometry data. Our

investigation into LTCC signaling was conducted in cultured hippocampal neurons, a well-established model system. Translation of our findings into *in vivo* mouse models would allow future researchers to test animal behavior and electrophysiological changes to complement and extend the findings presented here. Below are some considerations for such future experimental studies.

8.2 Molecular Determinants of the CaMKII-Ca_V1.3-Shank3 Complex

The work presented in Chapter III demonstrates that CaMKII directly interacts with Shank3 in a Thr286 autophosphorylation-dependent manner. Previous studies had characterized the CaMKII-Ca_V1.3 and Ca_V1.3-Shank3 interactions (Wang et al., 2017b; Zhang et al., 2005). Of note, CaMKII seems to bind similarly to Ca_V1.3-NTD in the presence of Ca^{2+}/CaM or after Thr286 phosphorylation, while my studies find Ca^{2+}/CaM only partially supports the Shank3-CaMKII interaction (Figure 3.2C). Our hypothesis for functional studies with these three proteins assumed all three existed in a complex simultaneously. Indeed, CaMKII holoenzymes normally contain 12 subunits which can support multiple interactions with different postsynaptic proteins (Robison et al., 2005b). Heterologous cell experiments in this dissertation use a construct that only expressed the CTD of Ca_V1.3 and not the full-length protein. Co-immunoprecipitation studies with our various WT and binding mutant proteins, would provide a simple experiment setup to further explore the exact stoichiometry of proteins in these complexes.

Recent studies of LTCCs in neurons demonstrate that they exist in clusters on the plasma membrane (Moreno et al., 2016; Zhang et al., 2016). Preliminary data from our lab has

tested if CaMKII plays a role in this clustering. HEK293 cells, co-expressing HA-tagged $Ca_V1.3$, FLAG-tagged $Ca_V1.3$, and CaMKIIα. Immunoprecipitation of HA-$Ca_V1.3$ using a HA antibody weakly co-immunoprecipitated CaMKII under basal conditions. However, when cell lysates were treated to activate CaMKIIα, HA-$Ca_V1.3$ not only robustly co-immunoprecipitated CaMKIIα, but FLAG-$Ca_V1.3$ as well, presumably through protein-protein interactions (X. Wang, unpublished observations). The co-immunoprecipitation of FLAG-$Ca_V1.3$ is reduced by deletion of the CaMKII association domain, suggesting that holoenzyme formation is one mechanism for channel clustering. Similarly, Shank3 can oligomerize with itself through its C-terminal SAM domain (Naisbitt et al., 1999). As a scaffolding protein, Shank3 may be regulating $Ca_V1.3$ channel clustering specifically, since it does not bind to $Ca_V1.2$ (Figure 9.4) (Zhang et al., 2005). Initial experiments would parallel the HEK293 co-immunoprecipitation experiment described above, substituting CaMKII for Shank3. If Shank3 is able to co-immunoprecipitate HA-$Ca_V1.3$ and FLAG-$Ca_V1.3$, then deletion of the Shank3 binding domain required for oligomerization (Shank3-ΔSAM) could be tested. Further experiments could include co-expression of CaMKII as well as the CaMKII-binding mutant Shank3-AAA. Future studies to directly test for channel clustering could compare CaV1.3 clusters using super-resolution microscopy or STORM in the absence or presence of Shank3 in intact neurons.

The Ca^{2+} nanodomain model presented in Section 1.6.1 suggests that a CaMKIIγ holoenzyme is *trans*-phosphorylated by a CaMKII subunit located within a different holoenzyme (Ma et al., 2014). This phosphorylation traps Ca^{2+}/CaM with CaMKIIγ as it shuttles to the nucleus. This phosphorylation does not require autophosphorylation within

the same holoenzyme, as kinase-dead CaMKIIγ-K43R was shown to be phosphorylated by CaMKIIβ. However, *trans*-phosphorylation between holoenzymes is inefficient or requires high concentrations of CaMKII (Hanson et al., 1994). One explanation for *trans*-phosphorylation to occur *in vivo* is that the CaMKII binding sites on both $Ca_V1.3$ and Shank3 position two separate CaMKII holoenzymes in a way that favors *trans*-phosphorylation. Combination of HEK293 cell lysates separately transfected to express kinase-dead CaMKIIγ-K43R or WT CaMKIIα/β alone would unlikely result in substantial phosphorylation of Thr287 on CaMKIIγ as the catalytically-active CaMKII would be located a separate holoenzyme. Preliminary data from our lab shows that when these separate holoenzymes are tethered in close proximity, using the FKBP-rapamycin-FRB system in vitro, that CaMKIIγ-K43R can be phosphorylated at Thr287 (X. Wang, unpublished observations). Co-expression of CaMKII with $Ca_V1.3$ and Shank3 may increase phosphorylation on CaMKIIγ, while co-expression of $Ca_V1.3$ or Shank3 binding mutants would reduce phosphorylation.

Recent studies in multiple brain regions and cell types point to CaMKIIγ as the specific CaMKII isoform that localizes to the nucleus for E-T coupling (Cohen et al., 2018; Ma et al., 2014). Our biochemical studies primarily used CaMKIIα, as it is the major isoform found in the mammalian forebrain (Bennett et al., 1983). Our current data suggests Shank3 binds CaMKII in the catalytic domain, which is highly conserved between isoforms (Zalcman et al., 2018). However, CaMKII isoforms could display different binding affinities to Shank3 or $Ca_V1.3$. If a difference was discovered, it may point to Shank3 or

$Ca_V1.3$ as the preferred binding site for CaMKIIγ holoenzymes during CaMKII *trans*-phosphorylation described above.

8.3 Functional Roles of CaMKII Phosphorylation Sites on Shank3

Our *in vitro* phospho-proteomics data identified 22 putative CaMKII phosphorylation sites on Shank3 over the full length of the protein. Two of these sites, Ser685 and Thr551, have functional relevance for modulating Shank3 binding to ABI1 and GKAP, respectively. However, the potential function for the other phosphorylation sites is unknown.

One potential function for CaMKII phosphorylation may be the regulation of Shank oligomerization. Shank proteins homo- and hetero-oligomerize via the C-terminal SAM domain. Shank oligomerization is a dynamic process; for example, previous studies have shown that the interaction between Shank SAM domains can be regulated based on Zn^{2+} binding (Arons et al., 2016). CaMKII has putative phosphorylation sites at Shank3 Ser1593 and Ser1623, which lie approximately 40 residues N-terminal of the SAM domain and Zn^{2+} binding site. We have shown that CaMKII phosphorylation can affect ABI1 and GKAP binding even though the relevant sites lie outside their canonical binding domains, so phosphorylation near the C-terminal SAM domain may also affect how Shank3 binds to other Shank molecules. Unlike Shank1, which is targeted to the PSD via its PDZ domain, the C-terminal region of Shank2 and Shank3 targets these proteins to the PSD (Boeckers et al., 2005; Sala et al., 2001). Therefore, phosphorylation of residues within

the minimum targeting region of Shank2 and Shank3 may also affect their subcellular localization in neurons.

Our studies of CaMKII phosphorylation utilized *in vitro* phosphorylation of purified proteins. However, an *in vitro* phosphorylation site cannot be physiologically relevant if it is not phosphorylated *in vivo*. Multiple mass spectrometry datasets show that Shank3 Ser685 is phosphorylated *in vivo* (Huttlin et al., 2010; Wang et al., 2019b). However, Thr551 phosphorylation *in vivo* has not been detected. This could be due to the single long tryptic peptide fragment containing Thr551 being poorly detected in these mass spectrometry studies, or it could be hard to identify in samples containing the multitude of proteins in the PSD. Therefore, any further functional studies into this phosphorylation site should confirm that it is phosphorylated in brain tissue. Our in vitro mass spectrometry used purified CaMKII and GST-Shank3 fusion proteins; potential *in vivo* studies could immunoprecipitate Shank3 from mouse forebrain, excise the Shank3 band after running on a gel, and send that enriched Shank3 sample for mass spectrometry analysis using alternative proteases predicted to generate smaller, more easily detected fragments that can clearly distinguish Thr551 and Ser557 phosphorylation. For example, Asp N digest would generate a peptide containing Thr551, N-DRTKRLFRHY**T**VGSY-C, and another containing Ser557, N-D**S**LTSHS-C. Both peptides are smaller than the peptide generated by trypsin in the present studies, N-HY**T**VGSYD**S**LTSHSDYVIDD-C. These smaller peptides should allow for better resolution and quantification of these phosphorylation sites by mass spectrometry. Ideally, this method would identify Thr551 and any other phosphorylation sites that have not yet been detected *in vivo*.

Shank3 isolation and analysis by mass spectrometry may also provide functional data on protein interactions. For instance, GST-fusion proteins containing the C-terminal regions of GKAP or $Ca_V1.3$, which both bind to Shank3 at the PDZ domain, could be used to perform pulldowns from brain lysates. Thr551-phosphorylated Shank3 would not bind as strongly to GST-GKAP compared to GST-$Ca_V1.3$. Brain lysate from CaMKIIα-KO mice, which may have reduced Thr551 phosphorylation, could also be tested. Reduced Thr551-phosphorylated Shank3 would result in a more similar pulldown of Shank3 between the two GST-fusion proteins. These experiments may not only identify phosphorylated Shank3 Thr551 *in vivo*, but also provide evidence for its functional importance in the regulation of binding interactions.

An alternative approach to identify Thr551 *in vivo* is to develop a phospho-antibody against this site. As this residue and the 12 amino acids flanking it are conserved in Shank1 (Thr635) and Shank2 (Thr229), generation of a Shank3-specific pThr551 antibody may be difficult. However, a phospho-antibody could be used to detect phosphorylation at those residues following specific immunoprecipitation of all three Shank family members. Since phosphorylation of Thr551 may be differentially regulated amongst the three Shank family members, an antibody that could detect phosphorylation of the 3 proteins would be a useful biochemical tool to study these mechanisms.

The Shank3 Thr551 phosphorylation site, which disrupts GKAP binding, may have broader physiological functions in intact neurons. For instance, phosphorylation at this site has no effect on $Ca_V1.3$-CTD binding to Shank3 (Figure 6.5). Thr551 phosphorylation may be a mechanism to uncouple GKAP-Shank3 and allow for $Ca_V1.3$ to bind to Shank3. Increased $Ca_V1.3$-Shank3 binding may enhance excitation-transcription coupling to increase pCREB. Therefore, we hypothesized that expression of GFP-Shank3-T551A, which cannot be phosphorylated by CaMKII to disrupt binding, would have weaker pCREB signal compared to GFP-Shank3-WT. In a preliminary test for the role of this phosphorylation site in LTCC-dependent CREB signaling, we overexpressed GFP-Shank3-WT or GFP-Shank3-T551A in primary hippocampal neurons. Cultures were stimulated to activate LTCC-dependent signaling to the nucleus, fixed, and stained for pCREB. Our preliminary data shows that GFP-Shank3-WT overexpression causes the same slight increase in pCREB relative to non-transfected neurons that we observed previously (Figure 7.1C). However, neurons transfected with GFP-Shank3-T551A show a reduced signal compared to WT-overexpressing and non-transfected neurons (Figure 8.1). While the T551A mutation may alter binding of other PDZ binding proteins besides $Ca_V1.3$, our preliminary evidence suggests that LTCC binding and therefore signaling to the nucleus may be modified by phosphorylation at Thr551. Further studies are needed to expand upon this preliminary data, including testing of phospho-mimetic Shank3-T551D.

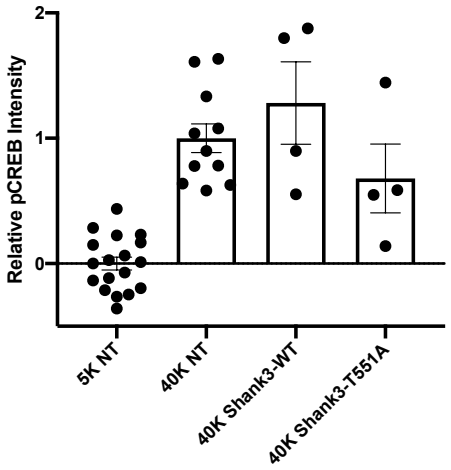

Figure 8.1: Shank3 Thr551 mutation may affect LTCC signaling to the nucleus.

Overexpression of GFP-Shank3-WT causes a slight increase in pCREB intensity in stimulated primary hippocampal neurons, but overexpression of GFP-Shank3-T551A may prevent this increase, and even reduce pCREB intensity relative to non-transfected control neurons (5K versus 40K: unpaired Student's t-test with equal variance, **** $p < 0.0001$; 40K stimulations: 1-way ANOVA, $F_{(2,16)} = 1.596$, $p = 0.23$. Tukey's post-hoc test, WT vs T551A, $p = 0.21$). Preliminary data from one biological replicate.

8.4 Relevance of the Shank3-CaMKII Interaction *In Vivo*

Our studies overexpressing mAp-Shank3 in primary hippocampal cultures reveal that WT Shank3 overexpression results in increased CREB phosphorylation, but our binding mutants do not (Figure 7.1C). My initial hypothesis was that the binding mutants Shank3-AAA and Shank3-ΔPDZ would result in a significant decrease in CREB phosphorylation relative to non-transfected neurons and neurons transfected with Shank3-WT. These data would suggest that our binding mutants do not act as dominant negatives, as pCREB intensity is similar to non-transfected cells. However, their overexpression in neurons may have some other effect on synaptic physiology or animal behavior that cannot be observed in primary cultures. Therefore, future directions for this study would express mAp-Shank3-WT, mAp-Shank3-AAA, or mAp-Shank3-ΔPDZ using Herpes Simplex Virus

(HSV) viral vectors to be injected into the dorsal hippocampus of *Shank3B* KO mice, to complement our studies performed in primary hippocampal neurons. HSV allows for the insertion of large DNA coding sequences and stable expression of the protein of interest in neurons for weeks at a time (Lachmann, 2004). This method would allow for testing of many hippocampal-dependent learning tasks, such as Morris Water Maze and novel object recognition, followed by brain slice physiology to test for basic synaptic properties. In these animals, we may observe more drastic dominant-negative effects that we did not observe in our pCREB and c-Fos assays. (Figure 7.3B). In addition to studying the electrophysiological and behavioral phenotypes of these mice, overexpression of these different mutants may disrupt normal activity-dependent gene transcription. Expression of c-Fos after exploration of a novel area or object may be reduced in mice expressing mutant Shank3. These studies may be broadened outside the hippocampus to test the role of LTCC-dependent signaling in other brain regions.

To fully address the physiological function of the AAA mutation, a transgenic mouse model would provide more flexibility. CRISPR/cas9 could be used to generate a global knock-in of the AAA mutation. As Shank3 mutation may cause developmental abnormalities between genotypes, an inducible model of the AAA mutation could be considered another approach. The sequence encoding ^{949}RRK^{951} lies within mouse exon 22, and mice already exist with this exon floxed at its 3' end (Wang et al., 2016). A Shank3-ΔPDZ mouse may prove more difficult to generate, as floxing the exons containing the PDZ domain instead results in reduced expression of Shank3 (Monteiro and Feng, 2017). An alternative method would be to use a BAC transgene expressing

Shank3-ΔPDZ in *Shank3* knockout mice. This could provide a start for generating an inducible mouse model to test both normal learning, followed by expression of mutant Shank3 to test for memory recall. Of course, any experimental manipulation of the Shank3 gene should be coupled with an analysis of Shank1 and Shank2, to see if there is any upregulation or compensatory mechanism (Jin et al., 2019). This will be especially important for any studies in the hippocampus, where Shank1 and Shank2 are also expressed.

In contrast to experiments in the hippocampus, Shank3 is the primary Shank isoform expressed in medium spiny neurons in the striatum (Peca et al., 2011). Unlike the hippocampus, the striatum received both glutamatergic and dopaminergic inputs, which may affect signaling. While the striatum-associated restrictive and repetitive behaviors are heavily studied in the ASD field, the striatum is also important for normal motor activity and habit learning (Lerner and Kreitzer, 2011). *Shank3B* KO mice injected with our Shank3 viral vectors listed above, this time in the dorsal striatum. It will be interesting to determine whether these virally infected mice display any autism-associated phenotypes, even though the mutations are not designed to mimic a human ASD-linked mutation. However, disruption of the Shank3-CaMKII interaction could result in other striatal phenotypes, such as changes in locomotor activity, Evidence suggests Shank3 plays a more prominent role in indirect pathway/D2 dopamine receptor-expressing striatal medium spiny neurons (MSNs) (Wang et al., 2017a). Indeed, a translational profiling of D1- and D2-expressing MSNs only identified Shank3 in D2-expressing neurons (Doyle et

al., 2008). This suggests that disruptions in Shank3 may result in D2-expressing MSN hypoactivity and striatopallidal dysfunction.

8.5 Non-Neuronal Roles of CaMKII-Shank3 Signaling

Since its initial characterization, Shank3 has been detected in the heart (Lim et al., 1999). However, research into the role of cardiac Shank3 has been limited. Shank3 protein has been reported to co-immunoprecipitate with a cardiac-specific Phospholipase C (PLC) isoform, PLCβ1b, which contains an alternatively-spliced C-tail that interacts with the Shank3 SH3 domain (Grubb et al., 2011a; Grubb et al., 2015). In this role, Shank3 targets PLCβ1b and Shank3 knockdown reduces PLCβ1b activity (Grubb et al., 2011a). Shank3 may be scaffolding PLCβ1b in close proximity to Homer/mGlu5 complexes in cardiomyocytes, as mGlu5 is a G_q coupled GPCR that stimulates PLC activation (Grubb et al., 2011b; Iglesias et al., 2007; Neves et al., 2002). Shank3 may therefore be acting as a scaffold in cardiomyocytes to bring signaling molecules in close proximity to each other, similar to its function in the PSD. This scaffolding may be distinct from the PSD, however, due to different signaling molecules expressed in cardiac cells versus neurons.

CaMKIIδ is the major CaMKII isoform expressed in cardiomyocytes, where it plays a role in adverse cardiac remodeling, hypertrophy, and other disease states (Grueter et al., 2007; Hoch et al., 1999; Kreusser and Backs, 2014; Wu and Anderson, 2014). Shank3 scaffolding could play a role in this response; neonatal rat myocytes expressing Shank3-AAA or a mouse model of the Shank3-AAA mutant discussed in Section 8.4 would provide a useful system to study the importance of cardiac Shank3 scaffolding in a

pathophysiological state. Although most patients with Phelan-McDermid Syndrome or other Shank3 gene mutations do not have major heart malfunction, multiple cases of congenital heart disease and unusual arterial dilation have been reported in PMS patients (Deibert et al., 2019). Similarly, cardiac phenotypes have not been reported in the multitude of available *Shank3* mutant mice, but the cardiac phenotype may be relatively mild with little impact on neurological studies. In-depth evaluation of cardiomyocyte function in *Shank3* mouse models may reveal novel phenotypes that may help to elucidate the role of Shank3 in the heart.

There is some evidence that Shank3 may be expressed in pancreatic β cells (mentioned in (Redecker et al., 2007), but data not shown). However, there is more evidence for Shank2 protein expression in the pancreas, which contains the CaMKII binding motif and PDZ domain (Redecker et al., 2001). Ca^{2+} influx through LTCCs occurs after glucose stimulation and depolarization in pancreatic β cells (Braun et al., 2008) and CaMKII can facilitate LTCCs in β cells to properly secrete insulin (Dadi et al., 2014). If Shank2/3 is scaffolding CaMKII and $Ca_V1.3$ within β cells (Sandoval et al., 2017), then loss of this close proximity may affect insulin secretion. If Shank2 is the primary scaffold in pancreatic endocrine cells, then human patients with *SHANK3* mutations would not demonstrate any pancreatic abnormalities. However, there are *Shank2* mutant mouse lines that have been generated and could be used to study pancreatic Shank2 function *in vivo*. LTCC Ca^{2+} influx may also trigger E-T coupling to CREB. CREB has been shown to promote expression of β cell-specific genes after application of PKA agonist forskolin (Van de Velde et al., 2019). However, it is unknown if depolarization or glucose-stimulated LTCC

activation stimulates CREB through CaMKII-dependent mechanisms. Further studies would need to test for expression of CaMKIIγ with the NLS in pancreatic β cells, but if so, LTCC-dependent E-T coupling may offer another pathway to stimulate β cell-specific gene expression.

8.6 Final Summary Statement

In conclusion, this dissertation demonstrates the importance of protein-protein interactions for efficient and specific signaling in excitatory neurons. Disruptions of these protein interactions through our experimental manipulations significantly affects signaling from the synapse to the nucleus and activity-dependent gene expression. The biochemical tools generated from this project will provide the foundation for further studies of Shank3 binding and Shank3 phosphorylation in activity-dependent regulation of gene transcription, synaptic plasticity, learning, and memory.

REFERENCES

Abraham, W.C., Logan, B., Greenwood, J.M., and Dragunow, M. (2002) Induction and experience-dependent consolidation of stable long-term potentiation lasting months in the hippocampus. *J Neurosci* **22**, 9626-9634.

Akita, T., Aoto, K., Kato, M., Shiina, M., Mutoh, H., Nakashima, M., Kuki, I., Okazaki, S., Magara, S., Shiihara, T., Yokochi, K., Aiba, K., Tohyama, J., Ohba, C., Miyatake, S., Miyake, N., Ogata, K., Fukuda, A., Matsumoto, N., and Saitsu, H. (2018) De novo variants in CAMK2A and CAMK2B cause neurodevelopmental disorders. *Annals of clinical and translational neurology* **5**, 280-296.

Alberini, C.M. (2009) Transcription Factors in Long-Term Memory and Synaptic Plasticity. *Physiol Rev* **89**.

Arons, M.H., Lee, K., Thynne, C.J., Kim, S.A., Schob, C., Kindler, S., Montgomery, J.M., and Garner, C.C. (2016) Shank3 Is Part of a Zinc-Sensitive Signaling System That Regulates Excitatory Synaptic Strength. *J Neurosci* **36**, 9124-9134.

Arons, M.H., Thynne, C.J., Grabrucker, A.M., Li, D., Schoen, M., Cheyne, J.E., Boeckers, T.M., Montgomery, J.M., and Garner, C.C. (2012) Autism-associated mutations in ProSAP2/Shank3 impair synaptic transmission and neurexin-neuroligin-mediated transsynaptic signaling. *J Neurosci* **32**, 14966-14978.

Bading, H. (2013) Nuclear calcium signalling in the regulation of brain function. *Nat Rev Neurosci* **14**, 593-608.

Baltaci, S.B., Mogulkoc, R., and Baltaci, A.K. (2018) Molecular Mechanisms of Early and Late LTP. *Neurochemical research* **44**, 281-296.

Barria, A., Derkach, V., and Soderling, T. (1998) Identification of the Ca2+/calmodulin-dependent protein kinase II regulatory phosphorylation site in the alpha-amino-3-hydroxyl-5-methyl-4-isoxazole-propionate-type glutamate receptor. *J Biol Chem* **272**, 32727-32730.

Barria, A., Muller, D., Derkach, V., Griffith, L.C., and Soderling, T.R. (1997) Regulatory phosphorylation of AMPA-type glutamate receptors by CaM-KII during long-term potentiation. *Science (New York, NY)* **276**, 2042-2045.

Baucum, A.J., 2nd, Jalan-Sakrikar, N., Jiao, Y., Gustin, R.M., Carmody, L.C., Tabb, D.L., Ham, A.J., and Colbran, R.J. (2010) Identification and validation of novel spinophilin-associated proteins in rodent striatum using an enhanced ex vivo shotgun proteomics approach. *Mol Cell Proteomics* **9**, 1243-1259.

Baucum, A.J., 2nd, Shonesy, B.C., Rose, K.L., and Colbran, R.J. (2015) Quantitative Proteomics Analysis of CaMKII Phosphorylation and the CaMKII Interactome in the Mouse Forebrain. *ACS Chem Neurosci* **6**, 615-631.

Bayer, K.U., De Koninck, P., Leonard, A.S., Hell, J.W., and Schulman, H. (2001) Interaction with the NMDA receptor locks CaMKII in an active conformation. *Nature* **411**, 801-805.

Bayer, K.U., LeBel, E., McDonald, G.L., O'Leary, H., Schulman, H., and De Koninck, P. (2006) Transition from reversible to persistent binding of CaMKII to postsynaptic sites and NR2B. *J Neurosci* **26**, 1164-1174.

Benito, E., Valor, L.M., Jimenez-Minchan, M., Huber, W., and Barco, A. (2011) cAMP response element-binding protein is a primary hub of activity-driven neuronal gene expression. *J Neurosci* **31**, 18237-18250.

Benke, T.A., Luthi, A., Isaac, J.T., and Collingridge, G.L. (1998) Modulation of AMPA receptor unitary conductance by synaptic activity. *Nature* **393**, 793-797.

Bennett, M.K., Erondu, N.E., and Kennedy, M.B. (1983) Purification and characterization of a calmodulin-dependent protein kinase that is highly concentrated in brain. *J Biol Chem* **258**, 12735-12744.

Beri, S., Tonna, N., Menozzi, G., Bonaglia, M.C., Sala, C., and Giorda, R. (2007) DNA methylation regulates tissue-specific expression of Shank3. *J Neurochem* **101**, 1380-1391.

Bers, D.M. (2002) Cardiac excitation-contraction coupling. *Nature* **415**, 198-205.

Bidinosti, M., Botta, P., Kruttner, S., Proenca, C.C., Stoehr, N., Bernhard, M., Fruh, I., Mueller, M., Bonenfant, D., Voshol, H., Carbone, W., Neal, S.J., McTighe, S.M., Roma, G., Dolmetsch, R.E., Porter, J.A., Caroni, P., Bouwmeester, T., Luthi, A., and Galimberti, I. (2016) CLK2 inhibition ameliorates autistic features associated with SHANK3 deficiency. *Science (New York, NY)* **351**, 1199-1203.

Bliss, T.V., and Gardner-Medwin, A.R. (1973) Long-lasting potentiation of synaptic transmission in the dentate area of the unanaestetized rabbit following stimulation of the perforant path. *J Physiol* **232**, 357-374.

Bliss, T.V., and Lomo, T. (1973) Long-lasting potentiation of synaptic transmission in the dentate area of the anaesthetized rabbit following stimulation of the perforant path. *J Physiol* **232**, 331-356.

Boeckers, T.M., Bockmann, J., Kreutz, M.R., and Gundelfinger, E.D. (2002) ProSAP/Shank proteins - a family of higher order organizing molecules of the

postsynaptic density with an emerging role in human neurological disease. *J Neurochem* **81**, 903-910.

Boeckers, T.M., Liedtke, T., Spilker, C., Dresbach, T., Bockmann, J., Kreutz, M.R., and Gundelfinger, E.D. (2005) C-terminal synaptic targeting elements for postsynaptic density proteins ProSAP1/Shank2 and ProSAP2/Shank3. *J Neurochem* **92**, 519-524.

Boeckers, T.M., Winter, C., Smalla, K.H., Kreutz, M.R., Bockmann, J., Seidenbecher, C., Garner, C.C., and Gundelfinger, E.D. (1999) Proline-rich synapse-associated proteins ProSAP1 and ProSAP2 interact with synaptic proteins of the SAPAP/GKAP family. *Biochem Biophys Res Commun* **264**, 247-252.

Borovac, J., Bosch, M., and Okamoto, K. (2018) Regulation of actin dynamics during structural plasticity of dendritic spines: Signaling messengers and actin-binding proteins. *Mol Cell Neurosci* **91**, 122-130.

Boudkkazi, S., Brechet, A., Schwenk, J., and Fakler, B. (2014) Cornichon2 dictates the time course of excitatory transmission at individual hippocampal synapses. *Neuron* **82**, 848-858.

Bourgeron, T. (2009) A synaptic trek to autism. *Current opinion in neurobiology* **19**, 231-234.

Bozdagi, O., Sakurai, T., Papapetrou, D., Wang, X., Dickstein, D.L., Takahashi, N., Kajiwara, Y., Yang, M., Katz, A.M., Scattoni, M.L., Harris, M.J., Saxena, R., Silverman, J.L., Crawley, J.N., Zhou, Q., Hof, P.R., and Buxbaum, J.D. (2010) Haploinsufficiency of the autism-associated Shank3 gene leads to deficits in synaptic function, social interaction, and social communication. *Molecular autism* **1**, 15.

Brakeman, P.R., Lanahan, A.A., O'Brien, R., Roche, K., Barnes, C.A., Huganir, R.L., and Worley, P.F. (1997) Homer: a protein that selectively binds metabotropic glutamate receptors. *Nature* **386**, 284-288.

Braun, M., Ramracheya, R., Bengtsson, M., Zhang, Q., Karanauskaite, J., Partridge, C., Johnson, P.R., and Rorsman, P. (2008) Voltage-gated ion channels in human pancreatic beta-cells: electrophysiological characterization and role in insulin secretion. *Diabetes* **57**, 1618-1628.

Carbonetto, S. (2014) A blueprint for research on Shankopathies: a view from research on autism spectrum disorder. *Dev Neurobiol* **74**, 85-112.

Carlezon, W.A., Jr., Duman, R.S., and Nestler, E.J. (2005) The many faces of CREB. *Trends Neurosci* **28**, 436-445.

Carr, D.W., Stofko-Hahn, R.E., Fraser, I.D., Cone, R.D., and Scott, J.D. (1992) Localization of the cAMP-dependent protein kinase to the postsynaptic densities by A-kinase anchoring proteins. Characterization of AKAP 79. *J Biol Chem* **267**, 16816-16823.

Carroll, R.C., Lissin, D.V., von Zastrow, M., Nicoll, R.A., and Malenka, R.C. (1999) Rapid redistribution of glutamate receptors contributes to long-term depression in hippocampal cultures. *Nature neuroscience* **2**, 454-460.

Carvalho, A.L., Duarte, C.B., and Carvalho, A.P. (2000) Regulation of AMPA receptors by phosphorylation. *Neurochemical research* **25**, 1245-1255.

Catterall, W.A. (2000a) From ionic currents to molecular mechanisms: the structure and function of voltage-gated sodium channels. *Neuron* **26**, 13-25.

Catterall, W.A. (2000b) Structure and regulation of voltage-gated Ca2+ channels. *Annu Rev Cell Dev Biol* **16**, 521-555.

Catterall, W.A. (2011) Voltage-gated calcium channels. *Cold Spring Harb Perspect Biol* **3**, a003947.

Chao, L.H., Stratton, M.M., Lee, I.H., Rosenberg, O.S., Levitz, J., Mandell, D.J., Kortemme, T., Groves, J.T., Schulman, H., and Kuriyan, J. (2011) A mechanism for tunable autoinhibition in the structure of a human Ca2+/calmodulin- dependent kinase II holoenzyme. *Cell* **146**, 732-745.

Chen, Z., Borek, D., Padrick, S.B., Gomez, T.S., Metlagel, Z., Ismail, A., Umetani, J., Billadeau, D.D., Otwinowski, Z., and Rosen, M.K. (2010) Structure and Control of the Actin Regulatory WAVE Complex. *Nature* **468**, 533-538.

Chia, P.H., Zhong, F.L., Niwa, S., Bonnard, C., Utami, K.H., Zeng, R., Lee, H., Eskin, A., Nelson, S.F., Xie, W.H., Al-Tawalbeh, S., El-Khateeb, M., Shboul, M., Pouladi, M.A., Al-Raqad, M., and Reversade, B. (2018) A homozygous loss-of-function CAMK2A mutation causes growth delay, frequent seizures and severe intellectual disability. *Elife* **7**.

Cho, K.O., Hunt, C.A., and Kennedy, M.B. (1992) The rat brain postsynaptic density fraction contains a homolog of the Drosophila discs-large tumor suppressor protein. *Neuron* **9**, 929-942.

Chowanadisai, W., Graham, D.M., Keen, C.L., Rucker, R.B., and Messerli, M.A. (2014) A zinc transporter gene required for development of the nervous system. *Commun Integr Biol* **6**, e26207.

Chung, H.J., Huang, Y.H., Lau, L.F., and Huganir, R.L. (2004) Regulation of the NMDA receptor complex and trafficking by activity-dependent phosphorylation of the NR2B subunit PDZ ligand. *J Neurosci* **24**, 10248-10259.

Citri, A., and Malenka, R.C. (2007) Synaptic plasticity: multiple forms, functions, and mechanisms. *Neuropsychopharmacology : official publication of the American College of Neuropsychopharmacology* **33**, 18-41.

Clifton, N.E., Trent, S., Thomas, K.L., and Hall, J. (2019) Regulation and Function of Activity-Dependent Homer in Synaptic Plasticity. *Mol Neuropsychiatry* **5**, 147-161.

Cohen, S.M., Suutari, B., He, X., Wang, Y., Sanchez, S., Tirko, N.N., Mandelberg, N.J., Mullins, C., Zhou, G., Wang, S., Kats, I., Salah, A., Tsien, R.W., and Ma, H. (2018) Calmodulin shuttling mediates cytonuclear signaling to trigger experience-dependent transcription and memory. *Nature communications* **9**, 2451.

Colbran, R.J. (1993) Inactivation of Ca2+/calmodulin-dependent protein kinase II by basal autophosphorylation. *J Biol Chem* **268**, 7163-7170.

Colbran, R.J., and Soderling, T.R. (1990) Calcium/calmodulin-independent autophosphorylation sites of calcium/calmodulin-dependent protein kinase II. Studies on the effect of phosphorylation of threonine 305/306 and serine 314 on calmodulin binding using synthetic peptides. *J Biol Chem* **265**, 11213-11219.

Cook, S.G., Bourke, A.M., O'Leary, H., Zaegel, V., Lasda, E., Mize-Berge, J., Quillinan, N., Tucker, C.L., Coultrap, S.J., Herson, P.S., and Bayer, K.U. (2018) Analysis of the CaMKIIalpha and beta splice-variant distribution among brain regions reveals isoform-specific differences in holoenzyme formation. *Sci Rep* **8**, 5448.

Costales, J.L., and Kolevzon, A. (2015) Phelan-McDermid Syndrome and SHANK3: Implications for Treatment. *Neurotherapeutics : the journal of the American Society for Experimental NeuroTherapeutics* **12**, 620-630.

Coultrap, S.J., Freund, R.K., O'Leary, H., Sanderson, J.L., Roche, K.W., Dell'Acqua, M.L., and Bayer, K.U. (2014) Autonomous CaMKII mediates both LTP and LTD using a mechanism for differential substrate site selection. *Cell reports* **6**, 431-437.

Dadi, P.K., Vierra, N.C., Ustione, A., Piston, D.W., Colbran, R.J., and Jacobson, D.A. (2014) Inhibition of pancreatic beta-cell Ca2+/calmodulin-dependent protein kinase II reduces glucose-stimulated calcium influx and insulin secretion, impairing glucose tolerance. *J Biol Chem* **289**, 12435-12445.

Davies, A., Hendrich, J., Van Minh, A.T., Wratten, J., Douglas, L., and Dolphin, A.C. (2007) Functional biology of the alpha(2)delta subunits of voltage-gated calcium channels. *Trends Pharmacol Sci* **28**, 220-228.

De Jongh, K.S., Warner, C., and Catterall, W.A. (1990) Subunits of purified calcium channels. Alpha 2 and delta are encoded by the same gene. *J Biol Chem* **265**, 14738-14741.

De Koninck, P., and Schulman, H. (1998) Sensitivity of CaM kinase II to the frequency of Ca2+ oscillations. *Science (New York, NY)* **279**, 227-230.

De Rubeis, S., He, X., Goldberg, A.P., Poultney, C.S., Samocha, K., Cicek, A.E., Kou, Y., Liu, L., Fromer, M., Walker, S., Singh, T., Klei, L., Kosmicki, J., Shih-Chen, F., Aleksic, B., Biscaldi, M., Bolton, P.F., Brownfeld, J.M., Cai, J., Campbell, N.G., Carracedo, A., Chahrour, M.H., Chiocchetti, A.G., Coon, H., Crawford, E.L., Curran, S.R., Dawson, G., Duketis, E., Fernandez, B.A., Gallagher, L., Geller, E., Guter, S.J.,

Hill, R.S., Ionita-Laza, J., Jimenz Gonzalez, P., Kilpinen, H., Klauck, S.M., Kolevzon, A., Lee, I., Lei, I., Lei, J., Lehtimaki, T., Lin, C.F., Ma'ayan, A., Marshall, C.R., McInnes, A.L., Neale, B., Owen, M.J., Ozaki, N., Parellada, M., Parr, J.R., Purcell, S., Puura, K., Rajagopalan, D., Rehnstrom, K., Reichenberg, A., Sabo, A., Sachse, M., Sanders, S.J., Schafer, C., Schulte-Ruther, M., Skuse, D., Stevens, C., Szatmari, P., Tammimies, K., Valladares, O., Voran, A., Li-San, W., Weiss, L.A., Willsey, A.J., Yu, T.W., Yuen, R.K., Cook, E.H., Freitag, C.M., Gill, M., Hultman, C.M., Lehner, T., Palotie, A., Schellenberg, G.D., Sklar, P., State, M.W., Sutcliffe, J.S., Walsh, C.A., Scherer, S.W., Zwick, M.E., Barett, J.C., Cutler, D.J., Roeder, K., Devlin, B., Daly, M.J., and Buxbaum, J.D. (2014) Synaptic, transcriptional and chromatin genes disrupted in autism. *Nature* **515**, 209-215.

Deibert, E., Crenshaw, M., and Miller, M.S. (2019). A patient with Phelan-McDermid syndrome and dilation of the great vessels. In Clin Case Rep (England), pp. 607-611.

Dell'Acqua, M.L., Smith, K.E., Gorski, J.A., Horne, E.A., Gibson, E.S., and Gomez, L.L. (2006) Regulation of neuronal PKA signaling through AKAP targeting dynamics. *Eur J Cell Biol* **85**, 627-633.

Dick, I.E., Joshi-Mukherjee, R., Yang, W., and Yue, D.T. (2016) Arrhythmogenesis in Timothy Syndrome is associated with defects in Ca(2+)-dependent inactivation. *Nature communications* **7**, 10370.

Dittgen, T., Nimmerjahn, A., Komai, S., Licznerski, P., Waters, J., Margrie, T.W., Helmchen, F., Denk, W., Brecht, M., and Osten, P. (2004) Lentivirus-based genetic manipulations of cortical neurons and their optical and electrophysiological monitoring in vivo. *Proc Natl Acad Sci U S A* **101**, 18206-18211.

Djakovic, S.N., Schwarz, L.A., Barylko, B., DeMartino, G.N., and Patrick, G.N. (2009) Regulation of the proteasome by neuronal activity and calcium/calmodulin-dependent protein kinase II. *J Biol Chem* **284**, 26655-26665.

Dolmetsch, R. (2003) Excitation-transcription coupling: signaling by ion channels to the nucleus. *Science's STKE : signal transduction knowledge environment* **2003**, Pe4.

Dosemeci, A., and Jaffe, H. (2010) Regulation of phosphorylation at the postsynaptic density during different activity states of Ca2+/calmodulin-dependent protein kinase II. *Biochem Biophys Res Commun* **391**, 78-84.

Dosemeci, A., Weinberg, R.J., Reese, T.S., and Tao-Cheng, J.H. (2016) The Postsynaptic Density: There Is More than Meets the Eye. *Frontiers in synaptic neuroscience* **8**, 23.

Doshi-Velez, F., Ge, Y., and Kohane, I. (2013) Comorbidity clusters in autism spectrum disorders: an electronic health record time-series analysis. *Pediatrics* **133**, e54-63.

Doyle, J.P., Dougherty, J.D., Heiman, M., Schmidt, E.F., Stevens, T.R., Ma, G., Bupp, S., Shrestha, P., Shah, R.D., Doughty, M.L., Gong, S., Greengard, P., and Heintz, N. (2008) Application of a translational profiling approach for the comparative analysis of CNS cell types. *Cell* **135**, 749-762.

Du, Y., Weed, S.A., Xiong, W.C., Marshall, T.D., and Parsons, J.T. (1998) Identification of a novel cortactin SH3 domain-binding protein and its localization to growth cones of cultured neurons. *Mol Cell Biol* **18**, 5838-5851.

Dubiel, A., and Kulesza, R.J. (2015) Prenatal valproic acid exposure disrupts tonotopic c-Fos expression in the rat brainstem. *Neuroscience* **311**, 349-361.

Dudek, S.M., and Bear, M.F. (1992) Homosynaptic long-term depression in area CA1 of hippocampus and effects of N-methyl-D-aspartate receptor blockade. *Proc Natl Acad Sci U S A* **89**, 4363-4367.

Duffney, L.J., Wei, J., Cheng, J., Liu, W., Smith, K.R., Kittler, J.T., and Yan, Z. (2013) Shank3 deficiency induces NMDA receptor hypofunction via an actin-dependent mechanism. *J Neurosci* **33**, 15767-15778.

Duffney, L.J., Zhong, P., Wei, J., Matas, E., Cheng, J., Qin, L., Ma, K., Dietz, D.M., Kajiwara, Y., Buxbaum, J.D., and Yan, Z. (2015) Autism-like Deficits in Shank3-Deficient Mice Are Rescued by Targeting Actin Regulators. *Cell reports* **11**, 1400-1413.

Durand, C.M., Betancur, C., Boeckers, T.M., Bockmann, J., Chaste, P., Fauchereau, F., Nygren, G., Rastam, M., Gillberg, I.C., Anckarsater, H., Sponheim, E., Goubran-Botros, H., Delorme, R., Chabane, N., Mouren-Simeoni, M.C., de Mas, P., Bieth, E., Roge, B., Heron, D., Burglen, L., Gillberg, C., Leboyer, M., and Bourgeron, T. (2006) Mutations in the gene encoding the synaptic scaffolding protein SHANK3 are associated with autism spectrum disorders. *Nat Genet* **39**, 25-27.

Durand, C.M., Perroy, J., Loll, F., Perrais, D., Fagni, L., Bourgeron, T., Montcouquiol, M., and Sans, N. (2012) SHANK3 mutations identified in autism lead to modification of dendritic spine morphology via an actin-dependent mechanism. *Mol Psychiatry* **17**, 71-84.

Ebert, D.H., and Greenberg, M.E. (2013) Activity-dependent neuronal signalling and autism spectrum disorder. *Nature* **493**, 327-337.

Elgersma, Y., Sweatt, J.D., and Giese, K.P. (2004) Mouse genetic approaches to investigating calcium/calmodulin-dependent protein kinase II function in plasticity and cognition. *J Neurosci* **24**, 8410-8415.

Eltokhi, A., Rappold, G., and Sprengel, R. (2018) Distinct Phenotypes of Shank2 Mouse Models Reflect Neuropsychiatric Spectrum Disorders of Human Patients With SHANK2 Variants. *Frontiers in molecular neuroscience* **11**, 240.

Erondu, N.E., and Kennedy, M.B. (1985) Regional distribution of type II Ca2+/calmodulin-dependent protein kinase in rat brain. *J Neurosci* **5**, 3270-3277.

Ertel, E.A., Campbell, K.P., Harpold, M.M., Hofmann, F., Mori, Y., Perez-Reyes, E., Schwartz, A., Snutch, T.P., Tanabe, T., Birnbaumer, L., Tsien, R.W., and Catterall, W.A. (2000). Nomenclature of voltage-gated calcium channels. In Neuron (United States), pp. 533-535.

Failla, P., Romano, C., Alberti, A., Vasta, A., Buono, S., Castiglia, L., Luciano, D., Di Benedetto, D., Fichera, M., and Galesi, O. (2007). Schizophrenia in a patient with subtelomeric duplication of chromosome 22q. In Clin Genet (Denmark), pp. 599-601.

Feng, B., Raghavachari, S., and Lisman, J. (2011) Quantitative estimates of the cytoplasmic, PSD, and NMDAR-bound pools of CaMKII in dendritic spines. *Brain Res* **1419**, 46-52.

Fitzjohn, S.M., Palmer, M.J., May, J.E., Neeson, A., Morris, S.A., and Collingridge, G.L. (2001) A characterisation of long-term depression induced by metabotropic glutamate receptor activation in the rat hippocampus in vitro. *J Physiol* **537**, 421-430.

Flavell, S.W., Cowan, C.W., Kim, T.K., Greer, P.L., Lin, Y., Paradis, S., Griffith, E.C., Hu, L.S., Chen, C., and Greenberg, M.E. (2006) Activity-dependent regulation of MEF2

transcription factors suppresses excitatory synapse number. *Science (New York, NY)* **311**, 1008-1012.

Flavell, S.W., and Greenberg, M.E. (2008) Signaling mechanisms linking neuronal activity to gene expression and plasticity of the nervous system. *Annual review of neuroscience* **31**, 563-590.

Gaertner, T.R., Kolodziej, S.J., Wang, D., Kobayashi, R., Koomen, J.M., Stoops, J.K., and Waxham, M.N. (2004) Comparative analyses of the three-dimensional structures and enzymatic properties of alpha, beta, gamma and delta isoforms of Ca2+-calmodulin-dependent protein kinase II. *J Biol Chem* **279**, 12484-12494.

Gall, C.M., Hess, U.S., and Lynch, G. (1998) Mapping brain networks engaged by, and changed by, learning. *Neurobiol Learn Mem* **70**, 14-36.

Gallo, F.T., Katche, C., Morici, J.F., Medina, J.H., and Weisstaub, N.V. (2018) Immediate Early Genes, Memory and Psychiatric Disorders: Focus on c-Fos, Egr1 and Arc. *Frontiers in behavioral neuroscience* **12**, 79.

Gao, L., Blair, L.A., Salinas, G.D., Needleman, L.A., and Marshall, J. (2006) Insulin-like growth factor-1 modulation of CaV1.3 calcium channels depends on Ca2+ release from IP3-sensitive stores and calcium/calmodulin kinase II phosphorylation of the alpha1 subunit EF hand. *J Neurosci* **26**, 6259-6268.

Gauthier, J., Champagne, N., Lafreniere, R.G., Xiong, L., Spiegelman, D., Brustein, E., Lapointe, M., Peng, H., Cote, M., Noreau, A., Hamdan, F.F., Addington, A.M., Rapoport, J.L., Delisi, L.E., Krebs, M.O., Joober, R., Fathalli, F., Mouaffak, F., Haghighi, A.P., Neri, C., Dube, M.P., Samuels, M.E., Marineau, C., Stone, E.A., Awadalla, P., Barker, P.A., Carbonetto, S., Drapeau, P., and Rouleau, G.A. (2010) De novo mutations in the gene

encoding the synaptic scaffolding protein SHANK3 in patients ascertained for schizophrenia. *Proc Natl Acad Sci U S A* **107**, 7863-7868.

Giese, K.P., Fedorov, N.B., Filipkowski, R.K., and Silva, A.J. (1998) Autophosphorylation at Thr286 of the alpha calcium-calmodulin kinase II in LTP and learning. *Science (New York, NY)* **279**, 870-873.

Gitlin, M. (2006) Treatment-resistant bipolar disorder. *Mol Psychiatry* **11**, 227-240.

Goyal, D.K., and Miyan, J.A. (2014) Neuro-immune abnormalities in autism and their relationship with the environment: a variable insult model for autism. *Front Endocrinol (Lausanne)* **5**, 29.

Granger, A.J., Shi, Y., Lu, W., Cerpas, M., and Nicoll, R.A. (2012) LTP requires a reserve pool of glutamate receptors independent of subunit type. *Nature* **493**, 495-500.

Grooms, S.Y., Noh, K.M., Regis, R., Bassell, G.J., Bryan, M.K., Carroll, R.C., and Zukin, R.S. (2006) Activity bidirectionally regulates AMPA receptor mRNA abundance in dendrites of hippocampal neurons. *J Neurosci* **26**, 8339-8351.

Grubb, D.R., Iliades, P., Cooley, N., Yu, Y.L., Luo, J., Filtz, T.M., and Woodcock, E.A. (2011a) Phospholipase Cbeta1b associates with a Shank3 complex at the cardiac sarcolemma. *FASEB journal : official publication of the Federation of American Societies for Experimental Biology* **25**, 1040-1047.

Grubb, D.R., Luo, J., and Woodcock, E.A. (2015) Phospholipase Cbeta1b directly binds the SH3 domain of Shank3 for targeting and activation in cardiomyocytes. *Biochem Biophys Res Commun* **461**, 519-524.

Grubb, D.R., Luo, J., Yu, Y.L., and Woodcock, E.A. (2011b) Scaffolding protein Homer 1c mediates hypertrophic responses downstream of Gq in cardiomyocytes. *FASEB*

journal : official publication of the Federation of American Societies for Experimental Biology **26**, 596-603.

Grueter, C.E., Abiria, S.A., Wu, Y., Anderson, M.E., and Colbran, R.J. (2008) Differential regulated interactions of calcium/calmodulin-dependent protein kinase II with isoforms of voltage-gated calcium channel beta subunits. *Biochemistry* **47**, 1760-1767.

Grueter, C.E., Colbran, R.J., and Anderson, M.E. (2007) CaMKII, an emerging molecular driver for calcium homeostasis, arrhythmias, and cardiac dysfunction. *J Mol Med (Berl)* **85**, 5-14.

Gustin, R.M., Shonesy, B.C., Robinson, S.L., Rentz, T.J., Baucum, A.J., 2nd, Jalan-Sakrikar, N., Winder, D.G., Stanwood, G.D., and Colbran, R.J. (2011) Loss of Thr286 phosphorylation disrupts synaptic CaMKIIalpha targeting, NMDAR activity and behavior in pre-adolescent mice. *Mol Cell Neurosci* **47**, 286-292.

Halt, A.R., Dallapiazza, R.F., Zhou, Y., Stein, I.S., Qian, H., Juntti, S., Wojcik, S., Brose, N., Silva, A.J., and Hell, J.W. (2012a) CaMKII binding to GluN2B is critical during memory consolidation. *The EMBO journal* **31**, 1203-1216.

Halt, A.R., Dallapiazza, R.F., Zhou, Y., Stein, I.S., Qian, H., Juntti, S., Wojcik, S., Brose, N., Silva, A.J., and Hell, J.W. (2012b). CaMKII binding to GluN2B is critical during memory consolidation. In The EMBO journal, pp. 1203-1216.

Han, K., Holder, J.L., Jr., Schaaf, C.P., Lu, H., Chen, H., Kang, H., Tang, J., Wu, Z., Hao, S., Cheung, S.W., Yu, P., Sun, H., Breman, A.M., Patel, A., Lu, H.C., and Zoghbi, H.Y. (2013) SHANK3 overexpression causes manic-like behaviour with unique pharmacogenetic properties. *Nature* **503**, 72-77.

Han, Q., Kim, Y.H., Wang, X., Liu, D., Zhang, Z.J., Bey, A.L., Lay, M., Chang, W., Berta, T., Zhang, Y., Jiang, Y.H., and Ji, R.R. (2016) SHANK3 Deficiency Impairs Heat Hyperalgesia and TRPV1 Signaling in Primary Sensory Neurons. *Neuron*.

Hanson, P.I., Meyer, T., Stryer, L., and Schulman, H. (1994) Dual role of calmodulin in autophosphorylation of multifunctional CaM kinase may underlie decoding of calcium signals. *Neuron* **12**, 943-956.

Hardingham, G.E., Pruunsild, P., Greenberg, M.E., and Bading, H. (2017) Lineage divergence of activity-driven transcription and evolution of cognitive ability. *Nat Rev Neurosci* **19**, 9-15.

Harony-Nicolas, H., De Rubeis, S., Kolevzon, A., and Buxbaum, J.D. (2015) Phelan McDermid Syndrome: From Genetic Discoveries to Animal Models and Treatment. *Journal of child neurology* **30**, 1861-1870.

Hashimoto, Y., Schworer, C.M., Colbran, R.J., and Soderling, T.R. (1987) Autophosphorylation of Ca2+/calmodulin-dependent protein kinase II. Effects on total and Ca2+-independent activities and kinetic parameters. *J Biol Chem* **262**, 8051-8055.

Hell, J.W. (2014) CaMKII: claiming center stage in postsynaptic function and organization. *Neuron* **81**, 249-265.

Herbert, M.R. (2011) SHANK3, the synapse, and autism. *The New England journal of medicine* **365**, 173-175.

Herring, B.E., and Nicoll, R.A. (2016) Long-Term Potentiation: From CaMKII to AMPA Receptor Trafficking. *Annu Rev Physiol* **78**, 351-365.

Hetzenauer, A., Sinnegger-Brauns, M.J., Striessnig, J., and Singewald, N. (2006) Brain activation pattern induced by stimulation of L-type Ca2+-channels: contribution of Ca(V)1.3 and Ca(V)1.2 isoforms. *Neuroscience* **139**, 1005-1015.

Hoch, B., Meyer, R., Hetzer, R., Krause, E.G., and Karczewski, P. (1999) Identification and expression of delta-isoforms of the multifunctional Ca2+/calmodulin-dependent protein kinase in failing and nonfailing human myocardium. *Circ Res* **84**, 713-721.

Hoeflich, K.P., and Ikura, M. (2002) Calmodulin in action: diversity in target recognition and activation mechanisms. *Cell* **108**, 739-742.

Hofer, N.T., Tuluc, P., Ortner, N.J., Nikonishyna, Y.V., Fernandes-Quintero, M.L., Liedl, K.R., Flucher, B.E., Cox, H., and Striessnig, J. (2020) Biophysical classification of a CACNA1D de novo mutation as a high-risk mutation for a severe neurodevelopmental disorder. *Molecular autism* **11**, 4.

Holbro, N., Grunditz, A., and Oertner, T.G. (2009) Differential distribution of endoplasmic reticulum controls metabotropic signaling and plasticity at hippocampal synapses. *Proc Natl Acad Sci U S A* **106**, 15055-15060.

Hosokawa, T., Mitsushima, D., Kaneko, R., and Hayashi, Y. (2014) Stoichiometry and phosphoisotypes of hippocampal AMPA-type glutamate receptor phosphorylation. *Neuron* **85**, 60-67.

Hu, J.H., Park, J.M., Park, S., Xiao, B., Dehoff, M.H., Kim, S., Hayashi, T., Schwarz, M.K., Huganir, R.L., Seeburg, P.H., Linden, D.J., and Worley, P.F. (2010) Homeostatic scaling requires group I mGluR activation mediated by Homer1a. *Neuron* **68**, 1128-1142.

Huang, R.Y.C., Laing, J.G., Kanter, E.M., Berthoud, V.M., Bao, M., Rohrs, H.W., Townsend, R.R., and Yamada, K.A. (2011) Identification of CaMKII Phosphorylation Sites in Connexin43 by High-Resolution Mass Spectrometry. *Journal of proteome research* **10**, 1098-1109.

Hudmon, A., and Schulman, H. (2002) Neuronal CA2+/calmodulin-dependent protein kinase II: the role of structure and autoregulation in cellular function. *Annual review of biochemistry* **71**, 473-510.

Huganir, R.L., and Nicoll, R.A. (2013) AMPARs and synaptic plasticity: the last 25 years. *Neuron* **80**, 704-717.

Huttlin, E.L., Jedrychowski, M.P., Elias, J.E., Goswami, T., Rad, R., Beausoleil, S.A., Villen, J., Haas, W., Sowa, M.E., and Gygi, S.P. (2010) A tissue-specific atlas of mouse protein phosphorylation and expression. *Cell* **143**, 1174-1189.

Iasevoli, F., Tomasetti, C., and de Bartolomeis, A. (2012) Scaffolding proteins of the post-synaptic density contribute to synaptic plasticity by regulating receptor localization and distribution: relevance for neuropsychiatric diseases. *Neurochemical research* **38**, 1-22.

Iglesias, I., Castillo, C.A., Leon, D., Ruiz, M.A., Albasanz, J.L., and Martin, M. (2007) Metabotropic glutamate receptor/phospholipase C system in female rat heart. *Brain Res* **1153**, 1-11.

Irvine, E.E., Danhiez, A., Radwanska, K., Nassim, C., Lucchesi, W., Godaux, E., Ris, L., and Giese, K.P. (2011) Properties of contextual memory formed in the absence of αCaMKII autophosphorylation. *Mol Brain* **4**, 8.

Ishida, H., Skorobogatov, A., Yamniuk, A.P., and Vogel, H.J. (2018) Solution structures of the SH3 domains from Shank scaffold proteins and their interactions with Cav1.3 calcium channels. *FEBS letters*.

Ito, M. (1989) Long-term depression. *Annual review of neuroscience* **12**, 85-102.

Jaffe, H., Vinade, L., and Dosemeci, A. (2004) Identification of novel phosphorylation sites on postsynaptic density proteins. *Biochem Biophys Res Commun* **321**, 210-218.

Jalan-Sakrikar, N., Bartlett, R.K., Baucum, A.J., 2nd, and Colbran, R.J. (2012) Substrate-selective and calcium-independent activation of CaMKII by alpha-actinin. *J Biol Chem* **287**, 15275-15283.

Jenkins, M.A., Christel, C.J., Jiao, Y., Abiria, S., Kim, K.Y., Usachev, Y.M., Obermair, G.J., Colbran, R.J., and Lee, A. (2010) Ca2+-dependent facilitation of Cav1.3 Ca2+ channels by densin and Ca2+/calmodulin-dependent protein kinase II. *J Neurosci* **30**, 5125-5135.

Jiang, Y.H., and Ehlers, M.D. (2013) Modeling autism by SHANK gene mutations in mice. *Neuron* **78**, 8-27.

Jiao, Y., Jalan-Sakrikar, N., Robison, A.J., Baucum, A.J., Bass, M.A., and Colbran, R.J. (2011) Characterization of a central Ca2+/calmodulin-dependent protein kinase IIalpha/beta binding domain in densin that selectively modulates glutamate receptor subunit phosphorylation. *J Biol Chem* **286**, 24806-24818.

Jin, C., Kang, H.R., Kang, H., Zhang, Y., Lee, Y., Kim, Y., and Han, K. (2019) Unexpected Compensatory Increase in Shank3 Transcripts in Shank3 Knock-Out Mice Having Partial Deletions of Exons. *Frontiers in molecular neuroscience* **12**, 228.

Kammermeier, P.J., and Worley, P.F. (2007) Homer 1a uncouples metabotropic glutamate receptor 5 from postsynaptic effectors. *Proc Natl Acad Sci U S A* **104**, 6055-6060.

Kandel, E.R. (2012) The molecular biology of memory: cAMP, PKA, CRE, CREB-1, CREB-2, and CPEB. *Mol Brain* **5**, 14.

Kandel, E.R., Schwartz, J.H., Jessell, T.M., Siegelbaum, S.A., and Hudspeth, A.J. (2013). Principles of Neural Science, 5th edn (New York, NY.: McGraw-Hill).

Kennedy, M.B., and Greengard, P. (1981) Two calcium/calmodulin-dependent protein kinases, which are highly concentrated in brain, phosphorylate protein I at distinct sites. *Proc Natl Acad Sci U S A* **78**, 1293-1297.

Kida, S., and Serita, T. (2014) Functional roles of CREB as a positive regulator in the formation and enhancement of memory. *Brain Res Bull* **105**, 17-24.

Kobrinsky, E., Schwartz, E., Abernethy, D.R., and Soldatov, N.M. (2002) Voltage-gated mobility of the Ca2+ channel cytoplasmic tails and its regulatory role. *J Biol Chem* **278**, 5021-5028.

Kornau, H.C., Schenker, L.T., Kennedy, M.B., and Seeburg, P.H. (1995) Domain interaction between NMDA receptor subunits and the postsynaptic density protein PSD-95. *Science (New York, NY)* **269**, 1737-1740.

Kreusser, M.M., and Backs, J. (2014) Integrated mechanisms of CaMKII-dependent ventricular remodeling. *Front Pharmacol* **5**, 36.

Kristensen, A.S., Jenkins, M.A., Banke, T.G., Schousboe, A., Makino, Y., Johnson, R.C., Huganir, R., and Traynelis, S.F. (2011) Mechanism of Ca2+/calmodulin-

dependent kinase II regulation of AMPA receptor gating. *Nature neuroscience* **14**, 727-735.

Kury, S., van Woerden, G.M., Besnard, T., Proietti Onori, M., Latypova, X., Towne, M.C., Cho, M.T., Prescott, T.E., Ploeg, M.A., Sanders, S., Stessman, H.A.F., Pujol, A., Distel, B., Robak, L.A., Bernstein, J.A., Denomme-Pichon, A.S., Lesca, G., Sellars, E.A., Berg, J., Carre, W., Busk, O.L., van Bon, B.W.M., Waugh, J.L., Deardorff, M., Hoganson, G.E., Bosanko, K.B., Johnson, D.S., Dabir, T., Holla, O.L., Sarkar, A., Tveten, K., de Bellescize, J., Braathen, G.J., Terhal, P.A., Grange, D.K., van Haeringen, A., Lam, C., Mirzaa, G., Burton, J., Bhoj, E.J., Douglas, J., Santani, A.B., Nesbitt, A.I., Helbig, K.L., Andrews, M.V., Begtrup, A., Tang, S., van Gassen, K.L.I., Juusola, J., Foss, K., Enns, G.M., Moog, U., Hinderhofer, K., Paramasivam, N., Lincoln, S., Kusako, B.H., Lindenbaum, P., Charpentier, E., Nowak, C.B., Cherot, E., Simonet, T., Ruivenkamp, C.A.L., Hahn, S., Brownstein, C.A., Xia, F., Schmitt, S., Deb, W., Bonneau, D., Nizon, M., Quinquis, D., Chelly, J., Rudolf, G., Sanlaville, D., Parent, P., Gilbert-Dussardier, B., Toutain, A., Sutton, V.R., Thies, J., Peart-Vissers, L., Boisseau, P., Vincent, M., Grabrucker, A.M., Dubourg, C., Tan, W.H., Verbeek, N.E., Granzow, M., Santen, G.W.E., Shendure, J., Isidor, B., Pasquier, L., Redon, R., Yang, Y., State, M.W., Kleefstra, T., Cogne, B., Petrovski, S., Retterer, K., Eichler, E.E., Rosenfeld, J.A., Agrawal, P.B., Bezieau, S., Odent, S., Elgersma, Y., and Mercier, S. (2017) De Novo Mutations in Protein Kinase Genes CAMK2A and CAMK2B Cause Intellectual Disability. *American journal of human genetics* **101**, 768-788.

Lachmann, R.H. (2004) Herpes simplex virus-based vectors. *Int J Exp Pathol* **85**, 177-190.

Lai, Y., Nairn, A.C., and Greengard, P. (1986) Autophosphorylation reversibly regulates the Ca2+/calmodulin-dependence of Ca2+/calmodulin-dependent protein kinase II. *Proc Natl Acad Sci U S A* **83**, 4253-4257.

Lampe, P.D., and Lau, A.F. (2004) The effects of connexin phosphorylation on gap junctional communication. *Int J Biochem Cell Biol* **36**, 1171-1186.

Leblond, C.S., Nava, C., Polge, A., Gauthier, J., Huguet, G., Lumbroso, S., Giuliano, F., Stordeur, C., Depienne, C., Mouzat, K., Pinto, D., Howe, J., Lemière, N., Durand, C.M., Guibert, J., Ey, E., Toro, R., Peyre, H., Mathieu, A., Amsellem, F., Rastam, M., Gillberg, I.C., Rappold, G.A., Holt, R., Monaco, A.P., Maestrini, E., Galan, P., Heron, D., Jacquette, A., Afenjar, A., Rastetter, A., Brice, A., Devillard, F., Assouline, B., Laffargue, F., Lespinasse, J., Chiesa, J., Rivier, F., Bonneau, D., Regnault, B., Zelenika, D., Delepine, M., Lathrop, M., Sanlaville, D., Schluth-Bolard, C., Edery, P., Perrin, L., Tabet, A.C., Schmeisser, M.J., Boeckers, T.M., Coleman, M., Sato, D., Szatmari, P., Scherer, S.W., Rouleau, G.A., Betancur, C., Leboyer, M., Gillberg, C., Delorme, R., and Bourgeron, T. (2014) Meta-analysis of SHANK Mutations in Autism Spectrum Disorders: a gradient of severity in cognitive impairments. *PLoS Genet* **10**, e1004580.

Lee, S.E., Kim, J.A., and Chang, S. (2018) nArgBP2-SAPAP-SHANK, the core postsynaptic triad associated with psychiatric disorders. *Experimental & molecular medicine* **50**, 2.

Lee, S.J., Escobedo-Lozoya, Y., Szatmari, E.M., and Yasuda, R. (2009) Activation of CaMKII in single dendritic spines during long-term potentiation. *Nature* **458**, 299-304.

Lerner, T.N., and Kreitzer, A.C. (2011) Neuromodulatory control of striatal plasticity and behavior. *Current opinion in neurobiology* **21**, 322-327.

Li, B., Tadross, M.R., and Tsien, R.W. (2016) Sequential ionic and conformational signaling by calcium channels drives neuronal gene expression. *Science (New York, NY)* **351**, 863-867.

Li, Q., Lau, A., Morris, T.J., Guo, L., Fordyce, C.B., and Stanley, E.F. (2004) A syntaxin 1, Galpha(o), and N-type calcium channel complex at a presynaptic nerve terminal: analysis by quantitative immunocolocalization. *J Neurosci* **24**, 4070-4081.

Lim, S., Naisbitt, S., Yoon, J., Hwang, J.I., Suh, P.G., Sheng, M., and Kim, E. (1999) Characterization of the Shank family of synaptic proteins. Multiple genes, alternative splicing, and differential expression in brain and development. *J Biol Chem* **274**, 29510-29518.

Limpitikul, W.B., Dick, I.E., Ben-Johny, M., and Yue, D.T. (2016) An autism-associated mutation in CaV1.3 channels has opposing effects on voltage- and Ca(2+)-dependent regulation. *Sci Rep* **6**, 27235.

Lisman, J., Schulman, H., and Cline, H. (2002) The molecular basis of CaMKII function in synaptic and behavioural memory. *Nat Rev Neurosci* **3**, 175-190.

Lisman, J., Yasuda, R., and Raghavachari, S. (2012) Mechanisms of CaMKII action in long-term potentiation. *Nat Rev Neurosci* **13**, 169-182.

Lisman, J.E. (1985) A mechanism for memory storage insensitive to molecular turnover: a bistable autophosphorylating kinase. *Proc Natl Acad Sci U S A* **82**, 3055-3057.

Lledo, P.M., Hjelmstad, G.O., Mukherji, S., Soderling, T.R., Malenka, R.C., and Nicoll, R.A. (1995) Calcium/calmodulin-dependent kinase II and long-term potentiation enhance synaptic transmission by the same mechanism. *Proc Natl Acad Sci U S A* **92**, 11175-11179.

Lu, W., Isozaki, K., Roche, K.W., and Nicoll, R.A. (2010) Synaptic targeting of AMPA receptors is regulated by a CaMKII site in the first intracellular loop of GluA1. *Proc Natl Acad Sci U S A* **107**, 22266-22271.

Lu, Y.M., Jia, Z., Janus, C., Henderson, J.T., Gerlai, R., Wojtowicz, J.M., and Roder, J.C. (1997) Mice lacking metabotropic glutamate receptor 5 show impaired learning and reduced CA1 long-term potentiation (LTP) but normal CA3 LTP. *J Neurosci* **17**, 5196-5205.

Lukmanji, S., Manji, S.A., Kadhim, S., Sauro, K.M., Wirrell, E.C., Kwon, C.S., and Jette, N. (2019) The co-occurrence of epilepsy and autism: A systematic review. *Epilepsy Behav* **98**, 238-248.

Lüscher, C., and Malenka, R.C. (2012) NMDA receptor-dependent long-term potentiation and long-term depression (LTP/LTD). *Cold Spring Harb Perspect Biol* **4**.

Lynch, M.A. (1989) Mechanisms underlying induction and maintenance of long-term potentiation in the hippocampus. *Bioessays* **10**, 85-90.

Ma, H., Groth, R.D., Cohen, S.M., Emery, J.F., Li, B., Hoedt, E., Zhang, G., Neubert, T.A., and Tsien, R.W. (2014) gammaCaMKII shuttles Ca(2)(+)/CaM to the nucleus to trigger CREB phosphorylation and gene expression. *Cell* **159**, 281-294.

MacGillavry, H.D., Kerr, J.M., Kassner, J., Frost, N.A., and Blanpied, T.A. (2015) Shank-cortactin interactions control actin dynamics to maintain flexibility of neuronal spines and synapses. *The European journal of neuroscience* **43**, 179-193.

Malenka, R.C., and Bear, M.F. (2004) LTP and LTD: an embarrassment of riches. *Neuron* **44**, 5-21.

Malik, Z.A., Stein, I.S., Navedo, M.F., and Hell, J.W. (2014) Mission CaMKIIgamma: shuttle calmodulin from membrane to nucleus. *Cell* **159**, 235-237.

Mao, L., and Wang, J.Q. (2003) Group I metabotropic glutamate receptor-mediated calcium signalling and immediate early gene expression in cultured rat striatal neurons. *The European journal of neuroscience* **17**, 741-750.

Marks, C.R., Shonesy, B.C., Wang, X., Stephenson, J.R., Niswender, C.M., and Colbran, R.J. (2018) Activated CaMKIIalpha Binds to the mGlu5 Metabotropic Glutamate Receptor and Modulates Calcium Mobilization. *Mol Pharmacol* **94**, 1352-1362.

Marsden, K.C., Shemesh, A., Bayer, K.U., and Carroll, R.C. (2010) Selective translocation of Ca2+/calmodulin protein kinase IIalpha (CaMKIIalpha) to inhibitory synapses. *Proc Natl Acad Sci U S A* **107**, 20559-20564.

Matsuzaki, M., Honkura, N., Ellis-Davies, G.C., and Kasai, H. (2004) Structural basis of long-term potentiation in single dendritic spines. *Nature* **429**, 761-766.

Matus, A. (2000) Actin-based plasticity in dendritic spines. *Science (New York, NY)* **290**, 754-758.

Mayford, M., Baranes, D., Podsypanina, K., and Kandel, E.R. (1996) The 3'-untranslated region of CaMKII alpha is a cis-acting signal for the localization and translation of mRNA in dendrites. *Proc Natl Acad Sci U S A* **93**, 13250-13255.

Mayford, M., Wang, J., Kandel, E.R., and O'Dell, T.J. (1995) CaMKII regulates the frequency-response function of hippocampal synapses for the production of both LTD and LTP. *Cell* **81**, 891-904.

Mcneill, R.B., and Colbran, R.J. (1995) Interaction of Autophosphorylated Ca2+ Calmodulin-Dependent Protein-Kinase-Ii with Neuronal Cytoskeletal Proteins - Characterization of Binding to a 190-Kda Postsynaptic Density Protein. *Journal of Biological Chemistry* **270**, 10043-10049.

Meyer, T., Hanson, P.I., Stryer, L., and Schulman, H. (1992) Calmodulin trapping by calcium-calmodulin-dependent protein kinase. *Science (New York, NY)* **256**, 1199-1202.

Miller, S.G., and Kennedy, M.B. (1986) Regulation of brain type II Ca2+/calmodulin-dependent protein kinase by autophosphorylation: a Ca2+-triggered molecular switch. *Cell* **44**, 861-870.

Miller, S.G., Patton, B.L., and Kennedy, M.B. (1988) Sequences of autophosphorylation sites in neuronal type II CaM kinase that control Ca2(+)-independent activity. *Neuron* **1**, 593-604.

Mockett, B.G., Guevremont, D., Wutte, M., Hulme, S.R., Williams, J.M., and Abraham, W.C. (2011) Calcium/calmodulin-dependent protein kinase II mediates group I metabotropic glutamate receptor-dependent protein synthesis and long-term depression in rat hippocampus. *J Neurosci* **31**, 7380-7391.

Moessner, R., Marshall, C., Sutcliffe, J., Skaug, J., Pinto, D., Vincent, J., Zwaigenbaum, L., Fernandez, B., Roberts, W., Szatmari, P., and Scherer, S. (2007). Contribution of SHANK3 Mutations to Autism Spectrum Disorder. In American journal of human genetics, pp. 1289-1297.

Monteiro, P., and Feng, G. (2017) SHANK proteins: roles at the synapse and in autism spectrum disorder. *Nat Rev Neurosci*.

Moon, A.L., Haan, N., Wilkinson, L.S., Thomas, K.L., and Hall, J. (2018) CACNA1C: Association With Psychiatric Disorders, Behavior, and Neurogenesis. *Schizophrenia bulletin* **44**, 958-965.

Moosmang, S., Haider, N., Klugbauer, N., Adelsberger, H., Langwieser, N., Muller, J., Stiess, M., Marais, E., Schulla, V., Lacinova, L., Goebbels, S., Nave, K.A., Storm, D.R., Hofmann, F., and Kleppisch, T. (2005) Role of hippocampal Cav1.2 Ca2+ channels in NMDA receptor-independent synaptic plasticity and spatial memory. *J Neurosci* **25**, 9883-9892.

Moreno, C.M., Dixon, R.E., Tajada, S., Yuan, C., Opitz-Araya, X., Binder, M.D., and Santana, L.F. (2016) Ca(2+) entry into neurons is facilitated by cooperative gating of clustered CaV1.3 channels. *Elife* **5**.

Morgan, S.L., and Teyler, T.J. (1999) VDCCs and NMDARs underlie two forms of LTP in CA1 hippocampus in vivo. *Journal of neurophysiology* **82**, 736-740.

Murakoshi, H., Shin, M.E., Parra-Bueno, P., Szatmari, E.M., Shibata, A.C., and Yasuda, R. (2017) Kinetics of Endogenous CaMKII Required for Synaptic Plasticity Revealed by Optogenetic Kinase Inhibitor. *Neuron* **94**, 37-47.e35.

Naisbitt, S., Kim, E., Tu, J.C., Xiao, B., Sala, C., Valtschanoff, J., Weinberg, R.J., Worley, P.F., and Sheng, M. (1999) Shank, a novel family of postsynaptic density proteins that binds to the NMDA receptor/PSD-95/GKAP complex and cortactin. *Neuron* **23**, 569-582.

Nakanishi, S., Nakajima, Y., Masu, M., Ueda, Y., Nakahara, K., Watanabe, D., Yamaguchi, S., Kawabata, S., and Okada, M. (1998) Glutamate receptors: brain function and signal transduction. *Brain Res Brain Res Rev* **26**, 230-235.

Neves, S.R., Ram, P.T., and Iyengar, R. (2002) G protein pathways. *Science (New York, NY)* **296**, 1636-1639.

Nguyen, P.V., Abel, T., and Kandel, E.R. (1994) Requirement of a critical period of transcription for induction of a late phase of LTP. *Science (New York, NY)* **265**, 1104-1107.

Nikandrova, Y.A., Jiao, Y., Baucum, A.J., Tavalin, S.J., and Colbran, R.J. (2010) Ca2+/calmodulin-dependent protein kinase II binds to and phosphorylates a specific SAP97 splice variant to disrupt association with AKAP79/150 and modulate alpha-amino-3-hydroxy-5-methyl-4-isoxazolepropionic acid-type glutamate receptor (AMPAR) activity. *J Biol Chem* **285**, 923-934.

Niswender, C.M., and Conn, P.J. (2010) Metabotropic glutamate receptors: physiology, pharmacology, and disease. *Annu Rev Pharmacol Toxicol* **50**, 295-322.

Norling, L.L., Colca, J.R., Kelly, P.T., McDaniel, M.L., and Landt, M. (1994) Activation of calcium and calmodulin dependent protein kinase II during stimulation of insulin secretion. *Cell Calcium* **16**, 137-150.

Nowycky, M.C., Fox, A.P., and Tsien, R.W. (1985) Three types of neuronal calcium channel with different calcium agonist sensitivity. *Nature* **316**, 440-443.

Nyegaard, M., Demontis, D., Foldager, L., Hedemand, A., Flint, T.J., Sorensen, K.M., Andersen, P.S., Nordentoft, M., Werge, T., Pedersen, C.B., Hougaard, D.M., Mortensen, P.B., Mors, O., and Borglum, A.D. (2010). CACNA1C (rs1006737) is associated with schizophrenia. In Mol Psychiatry (England), pp. 119-121.

Obermair, G.J., Schlick, B., Di Biase, V., Subramanyam, P., Gebhart, M., Baumgartner, S., and Flucher, B.E. (2009) Reciprocal interactions regulate targeting of calcium

channel beta subunits and membrane expression of alpha1 subunits in cultured hippocampal neurons. *J Biol Chem* **285**, 5776-5791.

Oh, M.C., Derkach, V.A., Guire, E.S., and Soderling, T.R. (2005) Extrasynaptic membrane trafficking regulated by GluR1 serine 845 phosphorylation primes AMPA receptors for long-term potentiation. *J Biol Chem* **281**, 752-758.

Oliet, S.H., Malenka, R.C., and Nicoll, R.A. (1997) Two distinct forms of long-term depression coexist in CA1 hippocampal pyramidal cells. *Neuron* **18**, 969-982.

Omkumar, R.V., Kiely, M.J., Rosenstein, A.J., Min, K.T., and Kennedy, M.B. (1996) Identification of a phosphorylation site for calcium/calmodulindependent protein kinase II in the NR2B subunit of the N-methyl-D-aspartate receptor. *J Biol Chem* **271**, 31670-31678.

Orlandini, M., Marconcini, L., Ferruzzi, R., and Oliviero, S. (1996) Identification of a c-fos-induced gene that is related to the platelet-derived growth factor/vascular endothelial growth factor family. *Proc Natl Acad Sci U S A* **93**, 11675-11680.

Peca, J., Feliciano, C., Ting, J.T., Wang, W., Wells, M.F., Venkatraman, T.N., Lascola, C.D., Fu, Z., and Feng, G. (2011) Shank3 mutant mice display autistic-like behaviours and striatal dysfunction. *Nature* **472**, 437-442.

Perfitt, T.L., Stauffer, P.E., Spiess, K.L., and Colbran, R.J. (2020) CaMKIIalpha phosphorylation of Shank3 modulates ABI1-Shank3 interaction. *Biochem Biophys Res Commun*.

Perfitt, T.L., Wang, X., Stephenson, J.R., Nakagawa, T., and Colbran, R.J. (2019) Neuronal L-Type Calcium Channel Signaling to the Nucleus Requires a Novel CaMKIIα-Shank3 Interaction. *bioRxiv*, 551648.

Pettit, D.L., Perlman, S., and Malinow, R. (1994) Potentiated transmission and prevention of further LTP by increased CaMKII activity in postsynaptic hippocampal slice neurons. *Science (New York, NY)* **266**, 1881-1885.

Phelan, M.C., Rogers, R.C., Saul, R.A., Stapleton, G.A., Sweet, K., McDermid, H., Shaw, S.R., Claytor, J., Willis, J., and Kelly, D.P. (2001) 22q13 deletion syndrome. *Am J Med Genet* **101**, 91-99.

Pinggera, A., Lieb, A., Benedetti, B., Lampert, M., Monteleone, S., Liedl, K.R., Tuluc, P., and Striessnig, J. (2015) CACNA1D De Novo Mutations in Autism Spectrum Disorders Activate Cav1.3 L-Type Calcium Channels. *Biol Psychiatry* **77**, 816-822.

Pinggera, A., Mackenroth, L., Rump, A., Schallner, J., Beleggia, F., Wollnik, B., and Striessnig, J. (2017) New gain-of-function mutation shows CACNA1D as recurrently mutated gene in autism spectrum disorders and epilepsy. *Hum Mol Genet*.

Pinggera, A., and Striessnig, J. (2016) Cav 1.3 (CACNA1D) L-type Ca(2+) channel dysfunction in CNS disorders. *J Physiol* **594**, 5839-5849.

Pittenger, C., and Kandel, E.R. (2003) In search of general mechanisms for long-lasting plasticity: Aplysia and the hippocampus. *Philos Trans R Soc Lond B Biol Sci* **358**, 757-763.

Pollard, T.D. (2007) Regulation of actin filament assembly by Arp2/3 complex and formins. *Annu Rev Biophys Biomol Struct* **36**, 451-477.

Ponna, S.K., Myllykoski, M., Boeckers, T.M., and Kursula, P. (2017) Structure of an unconventional SH3 domain from the postsynaptic density protein Shank3 at ultrahigh resolution. *Biochem Biophys Res Commun* **490**, 806-812.

Proepper, C., Johannsen, S., Liebau, S., Dahl, J., Vaida, B., Bockmann, J., Kreutz, M.R., Gundelfinger, E.D., and Boeckers, T.M. (2007) Abelson interacting protein 1 (Abi-1) is essential for dendrite morphogenesis and synapse formation. *The EMBO journal* **26**, 1397-1409.

Proietti Onori, M., Koopal, B., Everman, D.B., Worthington, J.D., Jones, J.R., Ploeg, M.A., Mientjes, E., van Bon, B.W., Kleefstra, T., Schulman, H., Kushner, S.A., Kury, S., Elgersma, Y., and van Woerden, G.M. (2018) The intellectual disability-associated CAMK2G p.Arg292Pro mutation acts as a pathogenic gain-of-function. *Human mutation* **39**, 2008-2024.

Puri, B.K. (2019) Calcium Signaling and Gene Expression. *Adv Exp Med Biol* **1131**, 537-545.

Quitsch, A., Berhorster, K., Liew, C.W., Richter, D., and Kreienkamp, H.J. (2005) Postsynaptic shank antagonizes dendrite branching induced by the leucine-rich repeat protein Densin-180. *J Neurosci* **25**, 479-487.

Raveendran, R., Devi Suma Priya, S., Mayadevi, M., Steephan, M., Santhoshkumar, T.R., Cheriyan, J., Sanalkumar, R., Pradeep, K.K., James, J., and Omkumar, R.V. (2009) Phosphorylation status of the NR2B subunit of NMDA receptor regulates its interaction with calcium/calmodulin-dependent protein kinase II. *J Neurochem* **110**, 92-105.

Redecker, P., Bockmann, J., and Bockers, T.M. (2007) Secretory granules of hypophyseal and pancreatic endocrine cells contain proteins of the neuronal postsynaptic density. *Cell Tissue Res* **328**, 49-55.

Redecker, P., Gundelfinger, E.D., and Boeckers, T.M. (2001) The cortactin-binding postsynaptic density protein proSAP1 in non-neuronal cells. *J Histochem Cytochem* **49**, 639-648.

Robison, A.J., Bartlett, R.K., Bass, M.A., and Colbran, R.J. (2005a) Differential modulation of Ca2+/calmodulin-dependent protein kinase II activity by regulated interactions with N-methyl-D-aspartate receptor NR2B subunits and alpha-actinin. *J Biol Chem* **280**, 39316-39323.

Robison, A.J., Bass, M.A., Jiao, Y., MacMillan, L.B., Carmody, L.C., Bartlett, R.K., and Colbran, R.J. (2005b) Multivalent interactions of calcium/calmodulin-dependent protein kinase II with the postsynaptic density proteins NR2B, densin-180, and alpha-actinin-2. *J Biol Chem* **280**, 35329-35336.

Roche, K.W., O'Brien, R.J., Mammen, A.L., Bernhardt, J., and Huganir, R.L. (1996) Characterization of multiple phosphorylation sites on the AMPA receptor GluR1 subunit. *Neuron* **16**, 1179-1188.

Rorsman, P., Braun, M., and Zhang, Q. (2012) Regulation of calcium in pancreatic α- and β-cells in health and disease. *Cell Calcium* **51**, 300-308.

Rosenbrock, H., Kramer, G., Hobson, S., Koros, E., Grundl, M., Grauert, M., Reymann, K.G., and Schroder, U.H. (2010) Functional interaction of metabotropic glutamate receptor 5 and NMDA-receptor by a metabotropic glutamate receptor 5 positive allosteric modulator. *Eur J Pharmacol* **639**, 40-46.

Sala, C., Futai, K., Yamamoto, K., Worley, P.F., Hayashi, Y., and Sheng, M. (2003) Inhibition of dendritic spine morphogenesis and synaptic transmission by activity-inducible protein Homer1a. *J Neurosci* **23**, 6327-6337.

Sala, C., Piech, V., Wilson, N.R., Passafaro, M., Liu, G., and Sheng, M. (2001) Regulation of dendritic spine morphology and synaptic function by Shank and Homer. *Neuron* **31**, 115-130.

Sala, C., Vicidomini, C., Bigi, I., Mossa, A., and Verpelli, C. (2015) Shank synaptic scaffold proteins: keys to understanding the pathogenesis of autism and other synaptic disorders. *J Neurochem* **135**, 849-858.

Sandoval, A., Duran, P., Gandini, M.A., Andrade, A., Almanza, A., Kaja, S., and Felix, R. (2017) Regulation of L-type CaV1.3 channel activity and insulin secretion by the cGMP-PKG signaling pathway. *Cell Calcium* **66**, 1-9.

Schlick, B., Flucher, B.E., and Obermair, G.J. (2010) Voltage-activated calcium channel expression profiles in mouse brain and cultured hippocampal neurons. *Neuroscience* **167**, 786-798.

Shanks, N.F., Maruo, T., Farina, A.N., Ellisman, M.H., and Nakagawa, T. (2010) Contribution of the global subunit structure and stargazin on the maturation of AMPA receptors. *J Neurosci* **30**, 2728-2740.

Shaywitz, A.J., and Greenberg, M.E. (2000) CREB: a stimulus-induced transcription factor activated by a diverse array of extracellular signals. *Annual review of biochemistry* **68**, 821-861.

Shen, K., and Meyer, T. (1999) Dynamic control of CaMKII translocation and localization in hippocampal neurons by NMDA receptor stimulation. *Science (New York, NY)* **284**, 162-166.

Shen, X., Valencia, C.A., Szostak, J.W., Dong, B., and Liu, R. (2005) Scanning the human proteome for calmodulin-binding proteins. *Proc Natl Acad Sci U S A* **102**, 5969-5974.

Sheng, M., and Hoogenraad, C.C. (2007) The postsynaptic architecture of excitatory synapses: a more quantitative view. *Annual review of biochemistry* **76**, 823-847.

Sheng, M., and Kim, E. (2000) The Shank family of scaffold proteins. *J Cell Sci* **113 (Pt 11)**, 1851-1856.

Shin, S.M., Zhang, N., Hansen, J., Gerges, N.Z., Pak, D.T., Sheng, M., and Lee, S.H. (2012) GKAP/SAPAP orchestrates activity-dependent postsynaptic protein remodeling and homeostatic scaling. *Nature neuroscience* **15**, 1655-1666.

Shiraishi-Yamaguchi, Y., and Furuichi, T. (2007) The Homer family proteins. *Genome Biol* **8**, 206.

Shirao, T., and Gonzalez-Billault, C. (2013) Actin filaments and microtubules in dendritic spines. *J Neurochem* **126**, 155-164.

Shonesy, B.C., Jalan-Sakrikar, N., Cavener, V.S., and Colbran, R.J. (2014) CaMKII: a molecular substrate for synaptic plasticity and memory. *Prog Mol Biol Transl Sci* **122**, 61-87.

Silva, A.J., Paylor, R., Wehner, J.M., and Tonegawa, S. (1992) Impaired spatial learning in alpha-calcium-calmodulin kinase II mutant mice. *Science (New York, NY)* **257**, 206-211.

Snyder, E.M., Philpot, B.D., Huber, K.M., Dong, X., Fallon, J.R., and Bear, M.F. (2001) Internalization of ionotropic glutamate receptors in response to mGluR activation. *Nature neuroscience* **4**, 1079-1085.

Soderling, S.H., and Scott, J.D. (2006) WAVE signalling: from biochemistry to biology. *Biochemical Society transactions* **34**, 73-76.

Soderling, T.R. (1999) The Ca-calmodulin-dependent protein kinase cascade. *Trends Biochem Sci* **24**, 232-236.

Soler, J., Fananas, L., Parellada, M., Krebs, M.O., Rouleau, G.A., and Fatjo-Vilas, M. (2018) Genetic variability in scaffolding proteins and risk for schizophrenia and autism-spectrum disorders: a systematic review. *Journal of psychiatry & neuroscience : JPN* **43**, 170066.

Soorya, L., Kolevzon, A., Zweifach, J., Lim, T., Dobry, Y., Schwartz, L., Frank, Y., Wang, A.T., Cai, G., Parkhomenko, E., Halpern, D., Grodberg, D., Angarita, B., Willner, J.P., Yang, A., Canitano, R., Chaplin, W., Betancur, C., and Buxbaum, J.D. (2013) Prospective investigation of autism and genotype-phenotype correlations in 22q13 deletion syndrome and SHANK3 deficiency. *Molecular autism* **4**, 18.

Stanika, R., Campiglio, M., Pinggera, A., Lee, A., Striessnig, J., Flucher, B.E., and Obermair, G.J. (2016) Splice variants of the CaV1.3 L-type calcium channel regulate dendritic spine morphology. *Sci Rep* **6**, 34528.

Stanley, E.F. (1997) The calcium channel and the organization of the presynaptic transmitter release face. *Trends Neurosci* **20**, 404-409.

Stephenson, J.R., Wang, X., Perfitt, T.L., Parrish, W.P., Shonesy, B.C., Marks, C.R., Mortlock, D.P., Nakagawa, T., Sutcliffe, J.S., and Colbran, R.J. (2017) A Novel Human CAMK2A Mutation Disrupts Dendritic Morphology and Synaptic Transmission, and Causes ASD-Related Behaviors. *J Neurosci* **37**, 2216-2233.

Strack, S., Choi, S., Lovinger, D.M., and Colbran, R.J. (1997) Translocation of autophosphorylated calcium/calmodulin-dependent protein kinase II to the postsynaptic density. *J Biol Chem* **272**, 13467-13470.

Strack, S., and Colbran, R.J. (1998) Autophosphorylation-dependent targeting of calcium/ calmodulin-dependent protein kinase II by the NR2B subunit of the N-methyl-D-aspartate receptor. *J Biol Chem* **273**, 20689-20692.

Strack, S., McNeill, R.B., and Colbran, R.J. (2000a) Mechanism and regulation of calcium/calmodulin-dependent protein kinase II targeting to the NR2B subunit of the N-methyl-D-aspartate receptor. *J Biol Chem* **275**, 23798-23806.

Strack, S., Robison, A.J., Bass, M.A., and Colbran, R.J. (2000b) Association of calcium/calmodulin-dependent kinase II with developmentally regulated splice variants of the postsynaptic density protein densin-180. *J Biol Chem* **275**, 25061-25064.

Sudhof, T.C. (2017) Synaptic Neurexin Complexes: A Molecular Code for the Logic of Neural Circuits. *Cell* **171**, 745-769.

Sudhof, T.C. (2018) Towards an Understanding of Synapse Formation. *Neuron* **100**, 276-293.

Suzuki, T., Okumura-Noji, K., and Nishida, E. (1995) ERK2-type mitogen-activated protein kinase (MAPK) and its substrates in postsynaptic density fractions from the rat brain. *Neurosci Res* **22**, 277-285.

Suzuki, T., Okumura-Noji, K., Tanaka, R., Ogura, A., Nakamura, K., Kudo, Y., and Tada, T. (1993) Characterization of protein kinase C activities in postsynaptic density fractions prepared from cerebral cortex, hippocampus, and cerebellum. *Brain Res* **619**, 69-75.

Swulius, M.T., and Waxham, M.N. (2008) Ca(2+)/calmodulin-dependent protein kinases. *Cell Mol Life Sci* **65**, 2637-2657.

Takeuchi, M., Hata, Y., Hirao, K., Toyoda, A., Irie, M., and Takai, Y. (1997) SAPAPs. A family of PSD-95/SAP90-associated proteins localized at postsynaptic density. *J Biol Chem* **272**, 11943-11951.

Tavalin, S.J., and Colbran, R.J. (2016) CaMKII-mediated phosphorylation of GluN2B regulates recombinant NMDA receptor currents in a chloride-dependent manner. *Mol Cell Neurosci* **79**, 45-52.

Terenzio, M., Schiavo, G., and Fainzilber, M. (2017) Compartmentalized Signaling in Neurons: From Cell Biology to Neuroscience. *Neuron* **96**, 667-679.

Thomas, G.M., Rumbaugh, G.R., Harrar, D.B., and Huganir, R.L. (2005) Ribosomal S6 kinase 2 interacts with and phosphorylates PDZ domain-containing proteins and regulates AMPA receptor transmission. *Proc Natl Acad Sci U S A* **102**, 15006-15011.

Toro, R., Konyukh, M., Delorme, R., Leblond, C., Chaste, P., Fauchereau, F., Coleman, M., Leboyer, M., Gillberg, C., and Bourgeron, T. (2010) Key role for gene dosage and synaptic homeostasis in autism spectrum disorders. *Trends Genet* **26**, 363-372.

Traynelis, S.F., Wollmuth, L.P., McBain, C.J., Menniti, F.S., Vance, K.M., Ogden, K.K., Hansen, K.B., Yuan, H., Myers, S.J., and Dingledine, R. (2010) Glutamate receptor ion channels: structure, regulation, and function. *Pharmacol Rev* **62**, 405-496.

Trettel, F., Rigamonti, D., Hilditch-Maguire, P., Wheeler, V.C., Sharp, A.H., Persichetti, F., Cattaneo, E., and MacDonald, M.E. (2000) Dominant phenotypes produced by the HD mutation in STHdh(Q111) striatal cells. *Hum Mol Genet* **9**, 2799-2809.

Tu, J.C., Xiao, B., Naisbitt, S., Yuan, J.P., Petralia, R.S., Brakeman, P., Doan, A., Aakalu, V.K., Lanahan, A.A., Sheng, M., and Worley, P.F. (1999) Coupling of mGluR/Homer and PSD-95 complexes by the Shank family of postsynaptic density proteins. *Neuron* **23**, 583-592.

Uchino, S., and Waga, C. (2013) SHANK3 as an autism spectrum disorder-associated gene. *Brain Dev* **35**, 106-110.

Uruno, T., Liu, J., Zhang, P., Fan, Y., Egile, C., Li, R., Mueller, S.C., and Zhan, X. (2001) Activation of Arp2/3 complex-mediated actin polymerization by cortactin. *Nature cell biology* **3**, 259-266.

Van de Velde, S., Wiater, E., Tran, M., Hwang, Y., Cole, P.A., and Montminy, M. (2019) CREB Promotes Beta Cell Gene Expression by Targeting Its Coactivators to Tissue-Specific Enhancers. *Mol Cell Biol* **39**.

van Woerden, G.M., Hoebeek, F.E., Gao, Z., Nagaraja, R.Y., Hoogenraad, C.C., Kushner, S.A., Hansel, C., De Zeeuw, C.I., and Elgersma, Y. (2009) betaCaMKII controls the direction of plasticity at parallel fiber-Purkinje cell synapses. *Nature neuroscience* **12**, 823-825.

Verpelli, C., Dvoretskova, E., Vicidomini, C., Rossi, F., Chiappalone, M., Schoen, M., Di Stefano, B., Mantegazza, R., Broccoli, V., Bockers, T.M., Dityatev, A., and Sala, C. (2011) Importance of Shank3 protein in regulating metabotropic glutamate receptor 5 (mGluR5) expression and signaling at synapses. *J Biol Chem* **286**, 34839-34850.

Vicidomini, C., Ponzoni, L., Lim, D., Schmeisser, M.J., Reim, D., Morello, N., Orellana, D., Tozzi, A., Durante, V., Scalmani, P., Mantegazza, M., Genazzani, A.A., Giustetto, M., Sala, M., Calabresi, P., Boeckers, T.M., Sala, C., and Verpelli, C. (2016)

Pharmacological enhancement of mGlu5 receptors rescues behavioral deficits in SHANK3 knock-out mice. *Mol Psychiatry*.

Vickers, C.A., Dickson, K.S., and Wyllie, D.J. (2005) Induction and maintenance of late-phase long-term potentiation in isolated dendrites of rat hippocampal CA1 pyramidal neurones. *J Physiol* **568**, 803-813.

Villalobo, A., Gonzalez-Munoz, M., and Berchtold, M.W. (2019) Proteins with calmodulin-like domains: structures and functional roles. *Cell Mol Life Sci* **76**, 2299-2328.

Vyas, Y., and Montgomery, J.M. (2016) The role of postsynaptic density proteins in neural degeneration and regeneration. *Neural Regen Res* **11**, 906-907.

Waga, C., Asano, H., Sanagi, T., Suzuki, E., Nakamura, Y., Tsuchiya, A., Itoh, M., Goto, Y., Kohsaka, S., and Uchino, S. (2013) Identification of two novel Shank3 transcripts in the developing mouse neocortex. *J Neurochem* **128**, 280-293.

Wang, L., Adamski, C.J., Bondar, V.V., Craigen, E., Collette, J.R., Pang, K., Han, K., Jain, A., S, Y.J., Liu, Z., Sifers, R.N., Holder, J.L., Jr., and Zoghbi, H.Y. (2019a) A kinome-wide RNAi screen identifies ERK2 as a druggable regulator of Shank3 stability. *Mol Psychiatry*.

Wang, L., Pang, K., Han, K., Adamski, C.J., Wang, W., He, L., Lai, J.K., Bondar, V.V., Duman, J.G., Richman, R., Tolias, K.F., Barth, P., Palzkill, T., Liu, Z., Holder, J.L., Jr., and Zoghbi, H.Y. (2019b) An autism-linked missense mutation in SHANK3 reveals the modularity of Shank3 function. *Mol Psychiatry*.

Wang, W., Li, C., Chen, Q., van der Goes, M.S., Hawrot, J., Yao, A.Y., Gao, X., Lu, C., Zang, Y., Zhang, Q., Lyman, K., Wang, D., Guo, B., Wu, S., Gerfen, C.R., Fu, Z., and

Feng, G. (2017a) Striatopallidal dysfunction underlies repetitive behavior in Shank3-deficient model of autism. *The Journal of clinical investigation*.

Wang, X., Bey, A.L., Katz, B.M., Badea, A., Kim, N., David, L.K., Duffney, L.J., Kumar, S., Mague, S.D., Hulbert, S.W., Dutta, N., Hayrapetyan, V., Yu, C., Gaidis, E., Zhao, S., Ding, J.D., Xu, Q., Chung, L., Rodriguiz, R.M., Wang, F., Weinberg, R.J., Wetsel, W.C., Dzirasa, K., Yin, H., and Jiang, Y.H. (2016) Altered mGluR5-Homer scaffolds and corticostriatal connectivity in a Shank3 complete knockout model of autism. *Nature communications* **7**, 11459.

Wang, X., Marks, C.R., Perfitt, T.L., Nakagawa, T., Lee, A., Jacobson, D.A., and Colbran, R.J. (2017b) A novel mechanism for Ca(2+)/calmodulin-dependent protein kinase II targeting to L-type Ca(2+) channels that initiates long-range signaling to the nucleus. *J Biol Chem* **292**, 17324-17336.

Wang, X., McCoy, P.A., Rodriguiz, R.M., Pan, Y., Je, H.S., Roberts, A.C., Kim, C.J., Berrios, J., Colvin, J.S., Bousquet-Moore, D., Lorenzo, I., Wu, G., Weinberg, R.J., Ehlers, M.D., Philpot, B.D., Beaudet, A.L., Wetsel, W.C., and Jiang, Y.H. (2011) Synaptic dysfunction and abnormal behaviors in mice lacking major isoforms of Shank3. *Hum Mol Genet* **20**, 3093-3108.

Wang, X., Xu, Q., Bey, A.L., Lee, Y., and Jiang, Y.H. (2014) Transcriptional and functional complexity of Shank3 provides a molecular framework to understand the phenotypic heterogeneity of SHANK3 causing autism and Shank3 mutant mice. *Molecular autism* **5**, 30.

Wasilewska, J., and Klukowski, M. (2015) Gastrointestinal symptoms and autism spectrum disorder: links and risks - a possible new overlap syndrome. *Pediatric Health Med Ther* **6**, 153-166.

Weick, J.P., Groth, R.D., Isaksen, A.L., and Mermelstein, P.G. (2003) Interactions with PDZ proteins are required for L-type calcium channels to activate cAMP response element-binding protein-dependent gene expression. *J Neurosci* **23**, 3446-3456.

Wheeler, D.G., Barrett, C.F., Groth, R.D., Safa, P., and Tsien, R.W. (2008) CaMKII locally encodes L-type channel activity to signal to nuclear CREB in excitation-transcription coupling. *J Cell Biol* **183**, 849-863.

Wheeler, D.G., Groth, R.D., Ma, H., Barrett, C.F., Owen, S.F., Safa, P., and Tsien, R.W. (2012) Ca(V)1 and Ca(V)2 channels engage distinct modes of Ca(2+) signaling to control CREB-dependent gene expression. *Cell* **149**, 1112-1124.

White, R.R., Kwon, Y.G., Taing, M., Lawrence, D.S., and Edelman, A.M. (1998) Definition of optimal substrate recognition motifs of Ca2+-calmodulin-dependent protein kinases IV and II reveals shared and distinctive features. *J Biol Chem* **273**, 3166-3172.

Williams, A.J., and Umemori, H. (2014) The best-laid plans go oft awry: synaptogenic growth factor signaling in neuropsychiatric disease. *Frontiers in synaptic neuroscience* **6**, 4.

Wu, J., Yan, Z., Li, Z., Qian, X., Lu, S., Dong, M., Zhou, Q., and Yan, N. (2016) Structure of the voltage-gated calcium channel Ca(v)1.1 at 3.6 A resolution. *Nature* **537**, 191-196.

Wu, J., Yan, Z., Li, Z., Yan, C., Lu, S., Dong, M., and Yan, N. (2015) Structure of the voltage-gated calcium channel Cav1.1 complex. *Science (New York, NY)* **350**, aad2395.

Wu, Y., and Anderson, M.E. (2014) CaMKII in sinoatrial node physiology and dysfunction. *Front Pharmacol* **5**, 48.

Xu, W., and Lipscombe, D. (2001) Neuronal Ca(V)1.3alpha(1) L-type channels activate at relatively hyperpolarized membrane potentials and are incompletely inhibited by dihydropyridines. *J Neurosci* **21**, 5944-5951.

Yan, Z., Kim, E., Datta, D., Lewis, D.A., and Soderling, S.H. (2016) Synaptic Actin Dysregulation, a Convergent Mechanism of Mental Disorders? *J Neurosci* **36**, 11411-11417.

Yasuda, R., Sabatini, B.L., and Svoboda, K. (2003) Plasticity of calcium channels in dendritic spines. *Nature neuroscience* **6**, 948-955.

Yi, F., Danko, T., Botelho, S.C., Patzke, C., Pak, C., Wernig, M., and Sudhof, T.C. (2016) Autism-associated SHANK3 haploinsufficiency causes Ih channelopathy in human neurons. *Science (New York, NY)* **352**, aaf2669.

Zablotsky, B., Bramlett, M.D., and Blumberg, S.J. (2017) The Co-Occurrence of Autism Spectrum Disorder in Children With ADHD. *J Atten Disord* **24**, 94-103.

Zacchi, P., Antonelli, R., and Cherubini, E. (2014) Gephyrin phosphorylation in the functional organization and plasticity of GABAergic synapses. *Front Cell Neurosci* **8**, 103.

Zalcman, G., Federman, N., and Romano, A. (2018) CaMKII Isoforms in Learning and Memory: Localization and Function. *Frontiers in molecular neuroscience* **11**, 445.

Zamponi, G.W., Striessnig, J., Koschak, A., and Dolphin, A.C. (2015) The Physiology, Pathology, and Pharmacology of Voltage-Gated Calcium Channels and Their Future Therapeutic Potential. *Pharmacol Rev* **67**, 821-870.

Zeng, M., Shang, Y., Guo, T., He, Q., Yung, W.H., Liu, K., and Zhang, M. (2016) A binding site outside the canonical PDZ domain determines the specific interaction between Shank and SAPAP and their function. *Proc Natl Acad Sci U S A* **113**, E3081-3090.

Zhang, F., Hu, Y., Huang, P., Toleman, C.A., Paterson, A.J., and Kudlow, J.E. (2007) Proteasome function is regulated by cyclic AMP-dependent protein kinase through phosphorylation of Rpt6. *J Biol Chem* **282**, 22460-22471.

Zhang, H., Fu, Y., Altier, C., Platzer, J., Surmeier, D.J., and Bezprozvanny, I. (2006) Ca1.2 and CaV1.3 neuronal L-type calcium channels: differential targeting and signaling to pCREB. *The European journal of neuroscience* **23**, 2297-2310.

Zhang, H., Maximov, A., Fu, Y., Xu, F., Tang, T.S., Tkatch, T., Surmeier, D.J., and Bezprozvanny, I. (2005) Association of CaV1.3 L-type calcium channels with Shank. *J Neurosci* **25**, 1037-1049.

Zhang, J., Carver, C.M., Choveau, F.S., and Shapiro, M.S. (2016) Clustering and Functional Coupling of Diverse Ion Channels and Signaling Proteins Revealed by Super-resolution STORM Microscopy in Neurons. *Neuron* **92**, 461-478.

Zhong, H., Sia, G.M., Sato, T.R., Gray, N.W., Mao, T., Khuchua, Z., Huganir, R.L., and Svoboda, K. (2009) Subcellular dynamics of type II PKA in neurons. *Neuron* **62**, 363-374.

Zhou, Y., Kaiser, T., Monteiro, P., Zhang, X., Van der Goes, M.S., Wang, D., Barak, B., Zeng, M., Li, C., Lu, C., Wells, M., Amaya, A., Nguyen, S., Lewis, M., Sanjana, N., Zhang, M., Zhang, F., Fu, Z., and Feng, G. (2015) Mice with Shank3 Mutations

Associated with ASD and Schizophrenia Display Both Shared and Distinct Defects. *Neuron* **89**, 147-162.

Zhu, S., and Gouaux, E. (2016) Structure and symmetry inform gating principles of ionotropic glutamate receptors. *Neuropharmacology* **112**, 11-15.

APPENDIX

A. DEVELOPMENT AND VALIDATION OF A NOVEL PLATE-BINDING ASSAY

Ca^{2+}/calmodulin-dependent protein kinase II (CaMKII) is a multifunctional Ser/Thr kinase with a large interactome. Improved mechanistic understanding of how various CaMKII-associated proteins (CaMKAPs) interact with CaMKII can provide invaluable insight into their biological roles. Previous work by our lab and others has examined the functional relevance of single protein-protein interactions with CaMKII, but the large CaMKII interactome has made the physiological consequences of specific interactions difficult to study. To address this problem, we aim to identify point mutations in CaMKII that disrupt binding interactions with specific CaMKAPs while retaining essentially normal binding to others. In order to identify CaMKII mutants with specific binding deficits, we have designed a medium-throughput screen to selectively disrupt specific interactions. Positive hits from this screen will be further characterized in biochemical, functional, and physiological studies (see Figure 9.1 for final experimental design). This appendix will document the validation process of this plate-binding assay as well as provide preliminary data from the initial screen of point mutants.

The current protocol, as published (Stephenson et al., 2017; Wang et al., 2017b): GST-fusion protein [GST, GST-GluN2B (1260-1309), GST-$Ca_V1.3$ (1-126), GST-β2a (full-length protein), GST-Densin-IN (793-824), and GST-mGlu5 (827-964)] were expressed in *Escherichia coli* and purified essentially as described previously (Robison et al.,

2005a). Wells of glutathione-coated 96-well plates (Thermo Fisher Scientific) were coated with the indicated GST protein (200 pmol in 100 µl binding buffer: 50 mM Tris-HCl, pH 7.5, 200 mM NaCl, 0.1 mM EDTA, 5 mM 2-mercaptoethanol, 0.1% v/v Tween 20, 5 mg/ml BSA) at 4°C overnight and then washed to remove unbound protein. Soluble fractions of HEK293FT cells expressing mApple, mApple-CaMKIIα-WT, or mApple- CaMKIIα-(point mutant) prepared in cold low ionic strength lysis buffer were adjusted to ~150 nM mApple-CaMKIIα subunit concentration (see above). Where indicated, soluble fractions were supplemented with 2.5 mM $CaCl_2$, 1 µM calmodulin, 10 mM $MgCl_2$, and 400 µM ADP (final concentrations). Our previous studies have shown that binding of Ca^{2+}/calmodulin and adenine nucleotides induces conformational changes that fully support binding to many CaMKAPs, such as GluN2B and the densin-IN domain (Robison et al., 2005b; Jiao et al., 2011), without the need for Thr286 autophosphorylation. Soluble fractions were then added to the pre-coated wells of glutathione-coated plate at 4°C for 2 h. The wells were washed in wash buffer (50 mM Tris-HCl, pH 7.5, 150 mM NaCl, 0.5% v/v Triton X-100, and 2.5 mM $CaCl_2$) 2 times and bound mApple-CaMKIIα was detected using a fluorescent plate reader at 592 nm. Data from quadruplicate wells were averaged to provide 1 data point. Analyses were repeated 3 times using independently prepared HEK293 cell-soluble fractions.

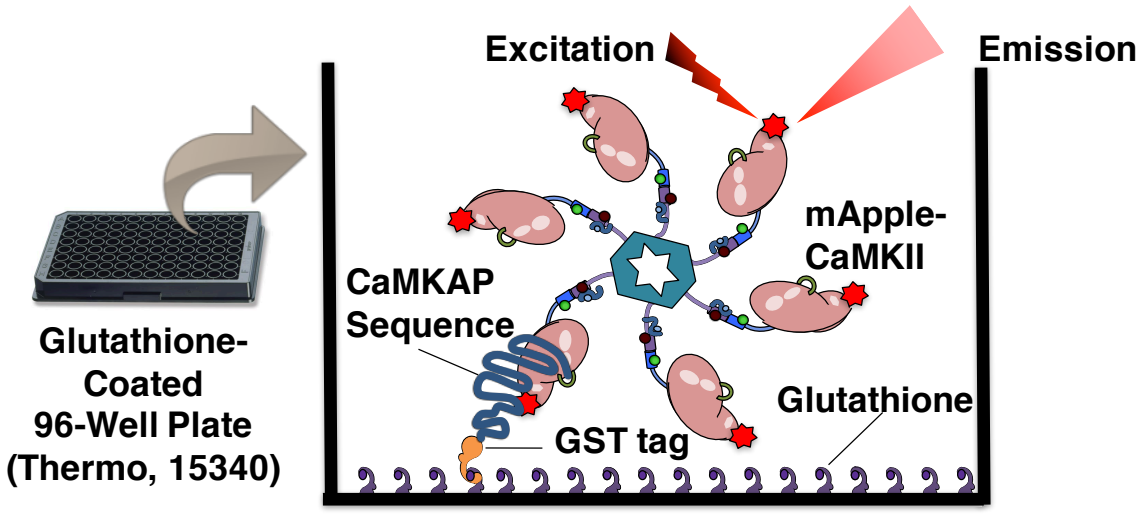

Figure 9.1: Experimental design of fluorescent plate-binding assay.

Diagram of plate-binding assay. Briefly, glutathione-coated 96-well plates are incubated with GST fusion proteins containing canonical CaMKAP sequences. HEK293 cell lysates expressing mApple-tagged CaMKIIα are then incubated in each well and washed to remove unbound protein. Wells are then excited using a fluorescence plate reader to detect bound mApple signal. Emitted mApple signal is then used as a proxy for CaMKII binding.

Initial experiments in this plate-binding assay used GFP-tagged CaMKIIα. We validated that fluorescent signal from GFP-CaMKIIα could be enhanced by the addition of Ca^{2+}/CaM and ADP in cell lysates to activate the kinase and promote binding to GST-GluN2B (Fig 9.2A). In addition, no fluorescence is detected from non-transfected or GFP-expressing cell lysates, and no fluorescence is detected with GST negative control (Figure 9.2B). Fluorescence could be disrupted by the addition of a CaMKII inhibitor peptide, CaMKIIN-tide, to HEK cell lysates (Figure 9.3C). Further studies were conducted

with mApple-tagged CaMKIIα to reduce background fluorescence at wavelengths associated with GFP.

A library of point mutations in the CaMKII catalytic and regulatory domains was generated using site-directed mutagenesis. Point mutations were selected based on the structure of binding sites within the catalytic domain, in an effort to specifically and selectively disrupt binding interactions between CaMKII and CaMKAPs. This initial screen identified a number of mutants that had some disruption in CaMKAP binding (Table 9.1). From these studies, a point mutation of Val102 to Glu (CaMKIIα-V102E) was found to selectively disrupt binding to the NTD of the α1 subunit of $Ca_V1.3$ L-type Ca^{2+} channel. After ensuring proper kinase activity and expression, this mutant was used for functional studies in heterologous cells and primary neurons (Wang et al., 2017b). This exemplifies the future applications of point mutants identified in this screening process.

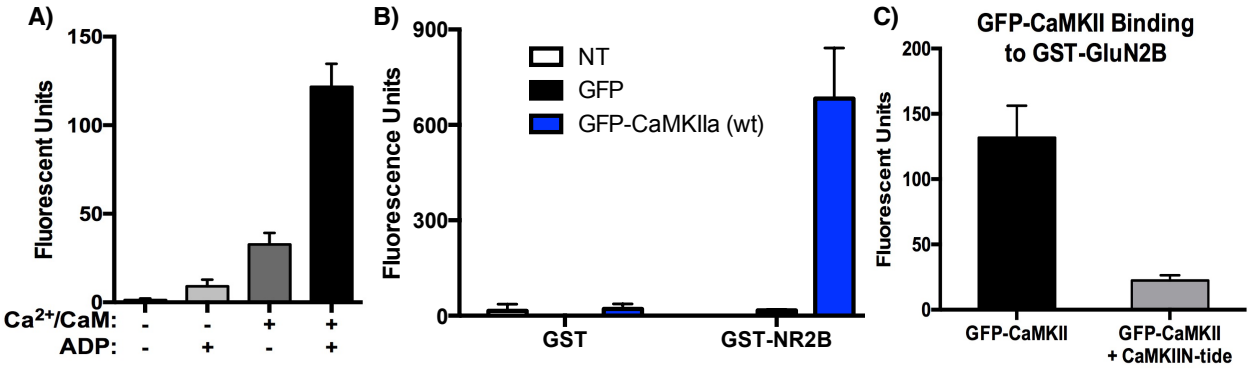

Figure 9.2: Validation of specific CaMKII-binding in assay.

A. CaMKII binding to GluN2B requires calcium/calmodulin (Ca^{2+}/CaM) and adenosine nucleotide binding. Addition of each component individually enhanced fluorescence, while addition of both

substantially increased fluorescence. **B.** Non-transfected (NT) or GFP-transfected HEK293 lysates did not significantly bind to GST-GluN2B, while activated GFP-CaMKII displayed a robust fluorescence. No fluorescence was observed with GST negative control. **C.** Incubation of GFP-CaMKII lysates in the absence or presence of inhibitor peptide CaMKIIN-tide (5 μM), which substantially blocked fluorescence. Panels A. and C. were performed by Christian Marks.

		CaMKII									
		WT	V102E	E109K	S113E	L120E	E121K	I205K	Y210E	W237K	T239E
GST-CaMKAP Fusion Protein:	GST	-	-	-	-	-	-	-	-	-	-
	GluN2B	+	+	-	+	-	+	-	+	+	+
	CaV1.3	+	-	-	+	-	+	-	+	-	+
	Densin-IN	+	+	-	+	-	+	-	+	-	+
	Densin-CTD	+	+	+	+	+	+	+	+	+	+

Table 9.1: Positive hits from original point mutation screen.

Binding interactions are denoted by black (+); no detected binding denoted by red (-).

B. CREB SIGNALING THROUGH GROUP I mGlu RECEPTORS

The transcription factor CREB can be phosphorylated as a result of multiple different signaling cascades. Previous studies have shown that a 30 min DHPG application to cultured neurons can increase CREB phosphorylation, and that this is dependent on Shank3 expression (Verpelli et al., 2011). At 30 min, Group 1 mGlu receptors would have already signaled to release intracellular Ca^{2+} stores (Mao and Wang, 2003). Ca^{2+} influx after this initial peak occurs by extracellular Ca^{2+} influx through NMDA receptors and LTCCs. Therefore, we sought to confirm that DHPG-dependent CREB signaling required LTCCs using a modified stimulation protocol utilized in Chapter VII.

We utilized DIV21 neurons for these studies, since previous reports indicated that more neurons were responsive to DHPG at DIV21 compared to DIV13 (Mao and Wang, 2003). Similar to LTCC-dependent CREB signaling, cultures were incubated in 5K Tyrode's solution for two hours along with inhibitors to NMDA receptors, AMPAR receptors, and voltage-gated sodium channels to prevent action potential firing (Figure 9.3A). Two minutes before stimulation, some cultures were incubated with 10 μM nimodipine to block LTCCs. Cultures were stimulation by the addition of 100 μM DHPG in 5K Tyrode's, 100 μM DHPG with 10 μM nimodipine, or were unstimulated with 5K Tyrode's solution as a negative control. As this signaling occurs beyond the initial Ca^{2+} signal generated by DHPG, we tested multiple time points, up to 30 min (Figure 9.3B). At 90 s, the time point of our LTCC-dependent CREB signaling with depolarization, no significant pCREB signal was observed. At 5 min, a slight increase in pCREB signal in DHPG-stimulated neurons was observed. However, both 10 and 30 min time points had robust pCREB signal, which

was completely blocked by nimodipine. A further comparison of this 30 min time point shows that the application of DHPG results in a robust increase in pCREB signal, which is lost with pre-incubation of the LTCC blocker nimodipine (Two-way ANOVA, n=3 biological replicates, **** $p < 0.0001$) (Figure 9.3C).

These results provide preliminary data that Group I mGlu receptor activation, in the absence of NMDA receptor, AMPA receptor, and sodium channel activity, is able to increase CREB phosphorylation in the nucleus via LTCC Ca^{2+} influx. As mGlu receptors couple to postsynaptic complexes via Homer/Shank interactions, The CaMKII-$Ca_V1.3$-Shank3 multiprotein complex may also play a role in this signaling pathway. Further tests could also pharmacologically determine whether mGlu1 or mGlu5 are the primary receptor activated in this signaling cascade.

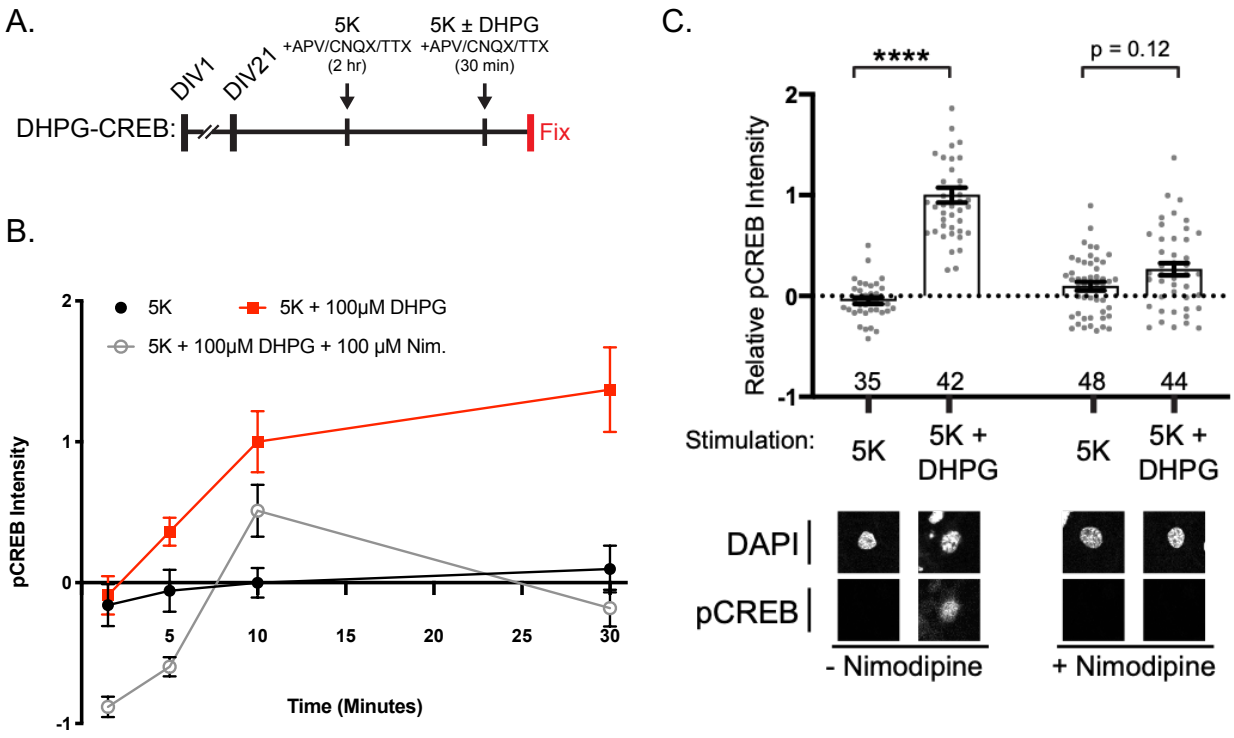

Figure 9.3: DHPG-CREB signaling is dependent on LTCCs.

A. Schematic of experimental protocol. DIV21 neurons were incubated with inhibitors of NMDA- and AMPA-type glutamate receptors and voltage-gated sodium channels (APV, CNQX, and TTX) in 5 mM KCl (5K) Tyrode's solution for 2 hours, and then treated with 5K Tyrode's solution (control) or 5K + 100 μM DHPG (a Group I mGlu receptor agonist) for 30 minutes before fixation. **B.** Time-course of relative pCREB intensity after 90 s, 5 m, 10 m, or 30 m stimulation before fixation. DIV21 neurons were stimulated with 100 μM DHPG in the absence or presence of 10 μM nimodipine, and LTCC blocker. Averages of 16-28 neurons from two biological replicates. **C.** DIV21 neurons were stimulated with 100 μM DHPG in the absence or presence of 10 μM nimodipine. After 30 minutes, pCREB signal is significantly increased in DHPG-treated neurons, which is disrupted in the presence of nimodipine (Two-way ANOVA, ****$p<0.0001$) Scale bar, 5 μm.

C. CHARACTERIZATION OF THE $CA_V1.3$-SHANK3 INTERACTION

Initial characterization of the interaction between $Ca_V1.3$ and Shank3 is described in Section 1. These observations are based from experiments showing that deletion of the very C-terminal amino acids from $Ca_V1.3$ (including the –ITTL PDZ-binding motif) could still bind to GST-Shank3 construct containing the SH3 and PDZ domains, provided CaV1.3 still contained a –PxxP– binding motif (Zhang et al., 2005). However, recent studies solving the atomic structure of the Shank3 SH3 domain have questioned whether this domain can bind typical SH3 ligands such as a –PxxP– motif (Ishida et al., 2018). A similar study using surface plasmon resonance found that the Shank3 SH3 domain could interact with a –PxxP– motif from $Ca_V1.3$, but that it was a weak interaction (Ponna et al., 2017). Moreover, in our studies using mAp-Shank3-ΔPDZ, in which the entire PDZ domain is deleted, we observed no discernable binding of mAp-Shank3-ΔPDZ and HA-$Ca_V1.3$-CTD (Figure 7.1). In theory, the Shank3 SH3 domain and –PxxP– motif in HA-$Ca_V1.3$-CTD should have some detectable interaction. Therefore, we sought to rigorously test the molecular determinants of the $Ca_V1.3$-Shank3 interaction at both the SH3 and PDZ domains.

We expanded our studies in Figure 7.1 to test the specificity of binding between Shank3 and the two neuronal LTCC $\alpha 1$ subunits, $Ca_V1.2$ and $Ca_V1.3$. To complement our HA-CaV1.3-CTD construct, we generated a N-terminal HA-tagged construct encoding the C-terminal domain of $Ca_V1.2$ (HA-$Ca_V1.2$-CTD). We expressed these two proteins with either soluble GFP or GFP-Shank3 in HEK293T cells, and soluble cell lysates were

immunoprecipitated with a GFP antibody (Figure 9.4A). HA-Ca_V1.3-CTD co-immunoprecipitated with GFP-Shank3, but not HA-Ca_V1.2-CTD, confirming that only the PDZ binding motif in CaV1.3 interacts with Shank3 (Zhang et al., 2005).

We then tested the importance of the –ITTL PDZ-binding motif found at the C-terminus of Ca_V1.3. We generated a HA-CaV1.3-CTD construct with a deletion of the –ITTL motif (HA-$_{Ca1}$.3-CTD ΔITTL). We expressed this construct alone or with mAp-Shank3 (WT and ΔPDZ) in HEK293T cells, and soluble cell lysates were immunoprecipitated with a Shank3 antibody (Figure 9.4B). We detected co-immunoprecipitation of HA-Ca_V1.3-CTD with mAp-Shank3-WT but not mAp-Shank3-ΔPDZ, as previous described (Figure 7.1A). However, no co-immunoprecipitation was detected with HA-Ca_V1.3-CTD ΔITTL, suggesting that the putative Shank3 SH3/Ca_V1.3 –PxxP– binding interaction is not able to support co-immunoprecipitation from heterologous cells.

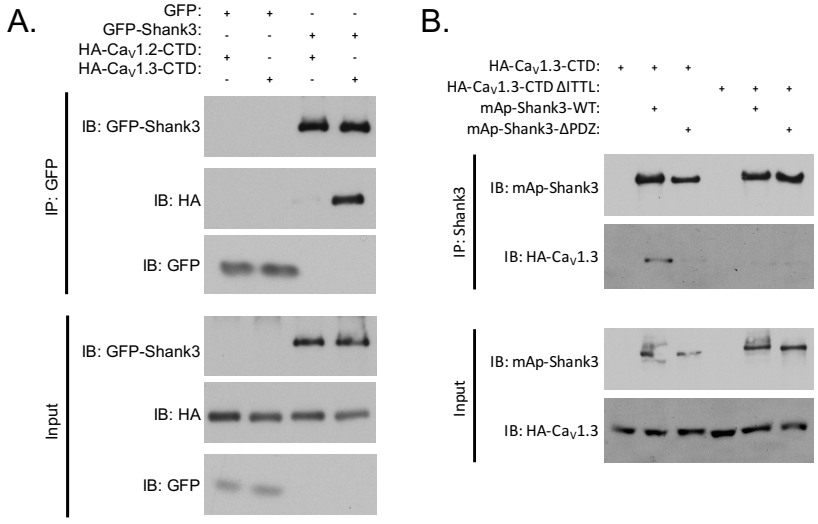

Figure 9.4: Shank3-Ca_V1.3 interaction requires the Shank3 PDZ domain and Ca_V1.3 PDZ-binding motif.

A. Soluble fractions of HEK293T cells expressing GFP or GFP-Shank3 and HA-Ca_V1.2-CTD or HA-Ca_V1.3-CTD were immunoprecipitated using a GFP antibody. Only HA-Ca_V1.3-CTD co-immunoprecipitated with GFP-Shank3. **B.** Soluble fraction of HEK293T cells expressing HA-CaV1.3-CTD (WT or ΔITTL) and mApple-Shank3 (WT or ΔPDZ) were immunoprecipitated using a Shank3 antibody. Co-immunoprecipitation was only consistently detected with HA-CaV1.3-CTD and mAp-Shank3-WT, but not either mutant. Immunoblots are representative of 3-4 biological replicates.

We generated a library of GST-Shank3 fusion proteins from the SH3 domain to the ABI1 binding motif, which lies C-terminal to the PDZ domain (Figure 9.5 A). These truncations also included a deletion of the region N-terminal of the PDZ domain; this non-canonical region has been shown to be important for GKAP binding to the PDZ domain, but no other binding partners tested (Zeng et al., 2016). The previous study reported an interaction between Ca_V1.3 and a Shank3 fragment containing the SH3 domain and this N-terminal region. We hypothesized that this N-terminal region was the potential site of binding, not the SH3 domain.

In our GST pulldown assay, we found that no HA-Ca_V1.3-CTD bound to GST-Shank3 proteins containing the SH3 domain or the SH3 + N-terminal region, a direct contradiction with previous findings (Figure 9.5B). Binding was observed with GST-Shank3 fusion proteins 473-664, 473-664 ΔN-term (543-564), 537-663, and 566-671, all of which contain the PDZ domain. Binding was not consistently detected with GST-Shank3 572-691, even though the PDZ domain is present; this may be due to a short linker of 13 amino acids between the GST tag and the PDZ domain prevented proper binding. Therefore, our preliminary data indicate that any weak interaction between the Shank3 SH3 domain and a –PxxP– binding motif in Ca_V1.3 may not be physiologically relevant.

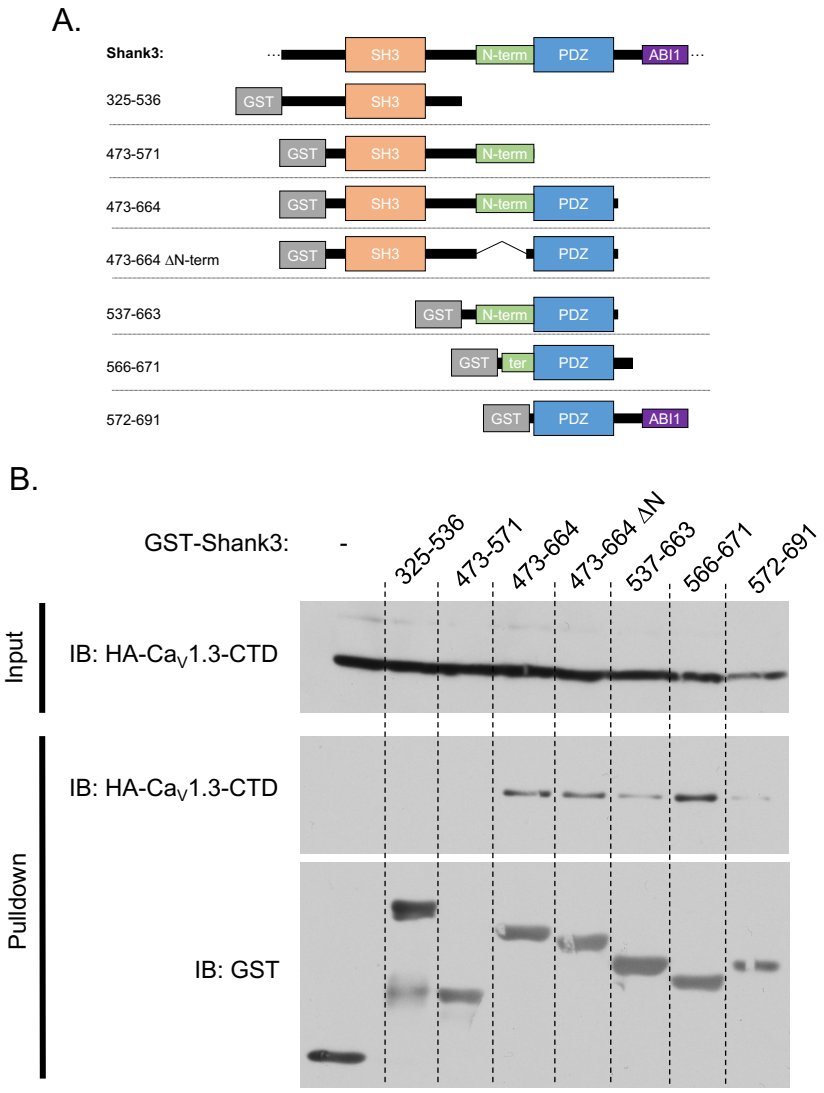

Figure 9.5: No detection of binding between Shank3 SH3 domain and $Ca_V1.3$ CTD.

A. Schematic of GST-Shank3 truncations and deletions generated for this experiment. SH3, aa 473-524; non-canonical N-terminal PDZ extension (N-term), aa 543-564; PDZ, aa 572-663; ABI1 binding motif, aa 677-684. **B.** GST pulldown assay of HA-$Ca_V1.3$-CTD with indicated GST-Shank3. HA-CaV1.3-CTD only binds to GST-fusion proteins that contain the PDZ domain and part of the N-terminal region. Representative of three biological experiments.